Microfluidics to Liquid Phase Non-Catalytic Naphthenic-Aromatic Hydrocarbon Oxidation

By

Yucheng Wu

A thesis submitted in partial fulfillment of the requirements for the degree of

Master of Science

In

Chemical Engineering

Department of Chemical and Materials Engineering

University of Alberta

Abstract

Liquid phase oxidation is industrially important to produce valuable petrochemicals and pharmaceuticals. However, due to the complex nature of free-radical reactions in a non-catalytic oxidation process, it is a challenge to achieve desired selectivity at a high conversion. This study investigates liquid phase non-catalytic oxidation of naphthenic-aromatic hydrocarbon in microfluidic reactors. The interest of the study is to exploit the potential of using microfluidic reactors to manipulate conversion rate and product selectivity. The research consists of two studies. The first study shows using microfluidics reactor, one can achieve order of magnitude of increase from 1:1 to 10:1 in product selectivity compared to that in batch reactor due to increasing gas-liquid interfacial area. Regardless of the reactor type, semi-batch or microfluidics reactor, gas-liquid interfacial area is the most important parameter influencing the oxidation conversion and selectivity. The second study investigated the effect of reactor configuration (size and shape) on liquid phase oxidation of naphthenic aromatic hydrocarbon in two microfluidic reactors with different dimension and flow path geometry. It was observed that reactor dimensions and volume changed the reactor hydrodynamics and influenced the oxygen availability in different ways and affected the conversion and product selectivity differently. The reactor with smaller size had higher oxidation conversion and suppressed the addition product selectivity, whereas large reactor had moderate conversion and enhanced ketone-to-alcohol product selectivity. The contributor to get higher oxygen availability could either be smaller reactor dimension and volume or increased length of the liquid film surrounding the gas bubble. The findings from the thesis could be used to improve design and operation of liquid phase non-catalytic hydrocarbon oxidation in microfluidic reactors to produce desired petrochemicals and pharmaceuticals.

Preface

(Mandatory due to collaborative work)

Chapter 3 of this thesis was accepted to be published in Journal of Flow Chemistry as "Siddiquee M. N., **Wu Y.**, De Klerk. A. and Nazemifard N. The impact of microfluidic reactor configuration on hydrodynamics, conversion and selectivity during indan oxidation". I was responsible for concept formation, performing experiments, data collection, data interpretation and manuscript writing. Muhammad Siddiquee was responsible for concept formation, data interpretation and manuscript writing. Arno de Klerk and Neda Nazemifard acted as the supervisory authors and were involved with concept formation, data analysis and manuscript composition.

Chapter 4 of this thesis was published partly as "Siddiquee M. N., Sivaramakrishnan K., **Wu Y.**, De Klerk. A. and Nazemifard N. A statistical approach dealing with multicollinearity among predictors in microfluidic reactor operation to control liquid-phase oxidation selectivity. *React. Chem. Eng*., **2018**, 3, 972-990.". I was responsible for performing experiments, data collection and data analytics for this paper. Muhammad Siddiquee and Kaushik Sivaramakrishnan were responsible for concept formation, data interpretation and manuscript writing. Arno de Klerk and Neda Nazemifard acted as the supervisory authors and were involved with concept formation, data analysis and manuscript composition.

Acknowledgement

I would like to take the chance to express my greatest gratitude to all people who have supported me during the memorable journey.

In particular, I would like to thank Professor Neda Nazemifard and Dr. Muhammad Siddiquee, who is always willing to provide me guidance when I encounter setbacks and challenges during the research. I am very proud and glad to have the opportunity to work with them.

I would like to extend my thank to:

Kiarash Keshmiri and Amin Karkooti for their insightful advice on my research and career.

Hanrui Zheng for his help on coding which opens the door for me to explore the magic of automation and data analytics.

All my friends for their kindly support and advice.

My family in Shanghai for supporting me during the journey and encouraging me to achieve greatness.

Finally, I would like to give my sincere thank and gratitude to my dear fiancée, Shenglei Huang for her companion and support.

Contents

List of Figures

List of Tables

Chapter 1: Introduction

1.1 Background

The development of microfluidic reactor has gained popularity for chemical synthesis, such as oxidation [1–4], hydrogenation [5, 6], halogenation [7] and bioprocessing [8] in the past two decades. A microfluidic reactor usually has a high surface-to-volume ratio, which brings advantages in mass and heat transfer. In addition, with a small radial diffusion length, the microfluidic reactor can achieve proper mixing between two phases. Furthermore, performing experiments using microfluidic reactor can be considered as a cost-saving and safe approach with expensive and toxic materials because it requires only small amount of chemicals. [4, 9-12]. These characteristics make the microfluidic reactors useful for the study of liquid phase oxidation.

Oxidation, incorporation of oxygen functional group, is one of the key steps to many petrochemicals [13-16] and pharmaceutical products [17-18]. Most of the steps are catalytic that generate huge waste [16, 19-20]. There is some non-catalytic process, but it faces problem to control the product selectivity. Industrially the non-catalytic liquid phase oxidation is performed at low conversion to control the product selectivity [21].

To limit the scope, this study focuses mainly on using microfluidic reactor to investigate non-catalytic liquid phase oxidation which follow a complex free radical process and how reactor design and operation affect the performance.

1.2 Objectives

The objective of the study was to investigate liquid phase oxidation of naphthenic-aromatic hydrocarbon. The specific objectives of the research were as follows:

1. To study the role of oxygen availability on liquid phase oxidation of naphthenic-aromatic hydrocarbon.
2. To compare the microfluidic reactor performance with batch and semi-batch reactor.
3. To study the effect of reactor configuration (size and shape) on liquid phase oxidation of naphthenic aromatic hydrocarbon.

4. To study the effect of temperature on liquid phase oxidation of naphthenic-aromatic hydrocarbon.

1.3 Scope of Work

Two naphthenic-aromatic compounds namely, tetralin and indan, were oxidized pure oxygen in batch reactor, semi-batch reactor, and two microfluidic reactors of different configuration at different operating conditions. The following chapters have been included in the thesis to achieve the listed objectives:

Chapter 2: Literature review. The chapter provides an overview of hydrocarbon oxidation chemistry, microfluidics, and oxidation in microfluidic reactors.

Chapter 3: The impact of microfluidic reactor configuration on hydrodynamics, conversion, and selectivity during indan oxidation. The chapter discusses the liquid phase indan oxidation in two microfluidic reactors of different configuration. The effect of reactor size, reactor shape, and temperature on reactor hydrodynamics, product selectivity and conversion are discussed.

Chapter 4: Tetralin oxidation in microfluidic and batch reactor. The chapter compares the liquid phase tetralin oxidation in batch and microfluidic reactors.

Chapter 5: Conclusions. The chapter provides the main conclusions derived from the research and direction of future works that can be applied to petrochemical and pharmaceutical industry.

1.4 Literature Cited

1. Gemoets HPL, Su Y, Shang M, Hessel V, Luque R, Noël T (2016) Liquid phase oxidation chemistry in continuous flow microreactor. Chem Soc Rev 45:83–117.

2. Hone CA, Kappe CO (2019) The Use of Molecular Oxygen for Liquid Phase Aerobic Oxidations in Continuous Flow. Top Curr Chem 2: 377.

3. Vanoye L, Aloui A, Pablos M, Philippe R, Percheron A, Favre-Réguillon A, de Bellefon C (2013) A safe and efficient flow oxidation of aldehydes with O2. Org Lett 15:5978–5981.

4. Siddiquee MN, Sivaramakrishnan K, Wu Y, De Klerk A, Nazemifard N (2018) A statistical approach dealing with multicollinearity among predictors in microfluidic reactor operation to control liquid-phase oxidation selectivity. React Chem Eng 3:972–990.

5. Sharma S, Yaminia, Das P (2019) Hydrogenation of nitroarenes to anilines in a flow reactor using polystyrene supported rhodium in a catalyst-cartridge. (Cart-Rh@PS) New J Chem 43: 1764–1769.

6. Ifran M, Glasnov TN, Kappe CO (2011) Heterogeneous catalytic hydrogenation reactions in continuous-flow reactors. Chem Sus Chem 4, 300 – 316.

7. Cantillo, D, Kappe, CO (2017) Halogenation of organic compounds using continuous flow and microreactor technology. React Chem Eng 2:7–19.

8. Karande R, Schmid A, Buehler K (2016) Applications of Multiphasic Microreactors for Biocatalytic Reactions. Org Process Res Dev 20:361-370.

9. L. Kiwi-Minsker and A. Renken, Microstructured reactors for catalytic reactions, Catal. Today, 2005, 110, 2–14.

10. J. J. Lerou, A. L. Tonkovich, L. Silva, S. Perry and J. McDaniel, Microchannel reactor architecture enables greener processes, Chem. Eng. Sci. 2010, 65, 380–385.

11. D. Wilms, J. Klos and H. Frey, Microstructured reactors for polymer synthesis: a renaissance of continuous flow processes for Tailor-Made macromolecules? Macromol. Chem. Phys., 2008, 209, 343–356.

12. G. Chen, Q. Yuan, H. Li and S. Li, CO selective oxidation in a microchannel reactor for PEM fuel cell, Chem. Eng. J., 2004, 101, 101–106.

13. Suresh AK, Sharma MM, Sridhar T (2000) Engineering aspects of industrial liquid-phase air oxidation of hydrocarbon. Ind Eng Chem Res 39:3958–3997.

14. De Klerk A (2003) Continuous- mode thermal oxidation of Fischer-Tropsch waxes. Ind Eng Chem Res 42:6545–6548.

15. Siddiquee MN, De Klerk A (2016) In situ measurement of liquid Phase oxygen during oxidation. Ind Eng Chem Res 55:6607–6618.

16. Dimitratos N, Lopez-Sanchez JA, Hutchings GJ (2014) Supported metal nanoparticles in liquid-phase oxidation reactions. In: Duprez D, Cavani F (Eds) Handbook of Advanced Methods and Processes in Oxidation Catalysis: From Laboratory to Industry, Imperial College Press, London 631–678.

17. Snead DR, Jamison TF (2015) A three-minute synthesis and purification of ibuprofen: pushing the limits of continuous-flow processing. Angew Chem Int Ed 54:1521–3773.

18. Gutmann B, Cantillo D, Kappe CO (2015) Continuous-flow technology—A tool for the safe manufacturing of active pharmaceutical ingredients Angew Chem Int Ed 54:6688–6729.

19. C. D. Pina, E. Falletta and M. Rossi, Liquid phase oxidation of organic compounds by supported metal-based catalysts with a focus on gold. In Liquid Phase Oxidation via Heterogeneous Catalysis: Organic Synthesis and Industrial Applications, First Edition; M. G. Clerici and O. A. Kholdeeva, Eds.; Wiley: Hoboken, 2013, 221–262.

20. G. Centi and S. Perathoner, Selective oxidation— industrial. In Encyclopedia of Catalysis; Wiley, 2002.

21. Hermans, J. Peeters and P. A. Jacobs, Autoxidation of Hydrocarbons: From Chemistry to Catalysis, Top Catal. 2008, 50, 124–132.

Chapter 2: Literature Review

2.1 Oxidation Chemistry

2.1.1 Liquid Phase Oxidation

Liquid phase oxidation studies the kinetics and mechanism of the oxidation of hydrocarbons in the liquid phase. Due to the scope limitation, literature focuses on liquid phase oxidation of aromatic hydrocarbon.

2.1.2 Catalytic and Non-Catalytic Aromatic Hydrocarbon Oxidation

As illustrated in **Figure 2.1**, liquid phase aromatic hydrocarbon oxidation could be separated into following 3 groups: (i) non-cleavage of aromatic ring such as formation of 1,4 – benzoquinone through benzene oxidation, (ii) cleavage of aromatic ring such as maleic anhydride formation through benzene oxidation and (iii) formation of oxygenates through hydrogen abstraction from side chain at aromatic ring such as benzoic acid formation through toluene oxidation [1]. Reaction (i) and (ii) require catalyses such as MoO3, V2O5 or catalyst promoter such as oxides or salts of P, Ag, W, Bi, Sn, Cu, Na, B, Ti and Ni.

Reaction (iii) is a non-catalytic oxidation process following free radical oxidation mechanism involving initiation, propagation, and termination [2, 3-5]. A variety of intermediate products, for instance peroxides, alcohols, ketones, acids, esters, and bi-functional compounds [3, 5] are formed during a non-catalytic free radical oxidation. As shown in **Table 2.1**, reaction rate is low during initiation and high during propagation and termination [2, 3].

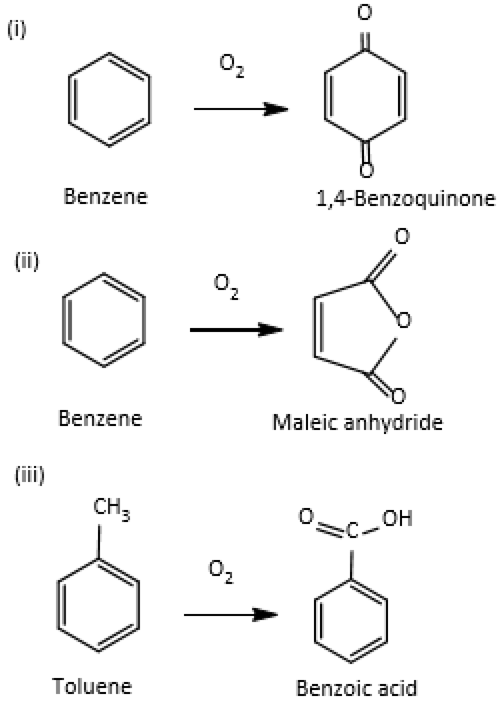

Figure 2.1: Oxidation Routes of Aromatic Hydrocarbons [1]

reaction		activation energy, E_a×10^{-1} (kJ/mol)	pre-exponential factor (A) [b]	reaction rate constant (k_r) [b]
$RH + O_2 \xrightarrow[]{+RH \quad k_i} 2\dot{R} + H_2O_2$	(1)	8.7 × 10^{1}	3.5 × 10^{3} L^2/mol^2. s	7.1 × 10^{-8} L^2/mol^2. s
$R^{\cdot} + O_2 \xrightarrow{k_1} R\dot{O}_2$	(2)	0.0	6.8 × 10^{7} L/mol. s	6.8 × 10^{7} L/mol. s
$R\dot{O}_2 + RH \xrightarrow{k_2} ROOH + R^{\cdot}$	(3)	1.9	2.5 × 10^{4} L/mol. s	120 L/mol. s
$ROOH \xrightarrow{k_3} R\dot{O} + O\dot{H}$	(4)	1.0 × 10^{1}	9.3 × 10^{8} s^{-1}	2.29 × 10^{-4} s^{-1}
$R^{\cdot} + R^{\cdot} \xrightarrow{k_4} R—R$	(5)	1.1	5.5 × 10^{8} L/mol. s	2.5 × 10^{7} L/mol. s
$R\dot{O}_2 + R^{\cdot} \xrightarrow{k_5} ROOR$	(6)	-[a]	-[a]	-[a]
$R\dot{O}_2 + R\dot{O}_2 \xrightarrow{k_6} ROH + R_1COR_2 + O_2$	(7)	1.7 × 10^{-1}	4.2 × 10^{7} L/mol. s	2.6 × 10^{7} L/mol. s

[a] not reported
[b] calculated for the reaction temperature, 150 °C.

Table 2.1: Free radical mechanism of tetralin oxidation [2, 3]

2.1.3 Operating Parameters That Affect Oxidation Rate and Selectivity

Oxidation rate and selectivity are affected by operating parameters such as temperature, pressure, mass transport between phases, local oxygen availability, free radical availability etc. At stage of initiation, free radicals are generated during the reactions between oxygen molecules and hydrocarbons. Oxygen molecules abstract hydrogen from hydrocarbons to form free radicals such as hydroperoxyl radicals and alkyl radicals [3,5]. The oxidation rate is slow due to the breakage of C-H bond. Once the hydrocarbon is activated, the reaction rate increases drastically due to the existence of free radicals, which are prone to forming new bonds because they contain unpaired electrons [2-5]. Therefore, the challenge is to control these operating parameters to achieve desired product selectivity. Both reaction rate and product selectivity are influenced by operating temperature. Local oxygen and free radical availability also play important roles in product selectivity. [2-5]

2.2 Reaction Engineering

2.2.1 Mass transfer & kinetics

In a liquid phase hydrocarbon oxidation with gas phase air or oxygen, mass transfer plays an essential role in reactor design and operation, which is well explained throughout literature. Different models such as penetration, surface renewal and film model [6-9], have been built to describe gas-liquid mass transfer as well as chemical reactions. Film theory is widely applied for describing mass transfer in microfluidic reactors, which assumes a stagnant film with uniform thickness across gas-liquid interface. The mass transfer rate can be described as: [2, 6, 6-10]

$$J_A = k_L a \,(C_{Ai} - C_b) = \frac{D_A}{\delta}\, a \,(C_{Ai} - C_b)$$

in which, J_A is mass transfer rate across gas-liquid interface per unit volume(mol/m^3.s), k_L is the liquid mass transfer coefficient (m/s), D_A is diffusivity of gas in liquid (m^2/s) , δ is the thin film thickness (m), a is gas-liquid interfacial area (m^2/ m^3), C_{Ai} is the concentration of gas at the interface, (mol/ m^3), and C_b is the concentration of gas in bulk liquid (mol/ m^3).

Based on experimental observation as reported in literatures [2, 11], gas-liquid interfacial area is the most important parameter to determine the mass transfer rate. In the case of liquid phase hydrocarbon oxidation with gaseous oxygen, a larger gas-liquid interfacial area increases oxygen mass transfer rate between gas phase and bulk liquid, which ensures higher local oxygen availability in the liquid phase hydrocarbon.

2.3 Microfluidics

There is a rising trend of applying microfluidics in both academia and industry. The current study on hydrocarbon oxidation is mainly investigated using microfluidic reactors. A reduction in the channel size into microscale leads to an increase importance of some properties which is negligible in a macro scale. This section provides an overview of its characteristics, flow regime, advantages, and state-of-art research.

2.3.1 Microfluidic Reactor

A microfluidic device is typically used for controlling fluids which are constrained within channels with internal dimensions or hydrodynamic diameters in the sub-millimetre range [12]. The microfluidic reactor chip is commonly fabricated using materials including polymer, glass, silicon, stainless steel, and ceramics depending on operating temperature, pressure, chemical compatibility and ease of fabrication and integration [13]. For instance, polydimethylsiloxane, also known as PDMS, has been widely applied in biological and chemical microfluidics at mild operating conditions due to its rapid, convenient, inexpensive and fabrication process [14]. There are also tremendous applications using glass and silicon-based microfluidic systems because of their excellent performance in mechanical strength-to-density ratio, temperature characteristics, low cost, and chemical compatibility. In addition, those devices provide convenience for developing catalytic coatings and integration of silicon micro-sensor for temperature, pressure, and flow monitoring [13]. In the current study, glass microfluidic reactors are employed to conduct the hydrocarbon oxidation.

2.3.2 Fluid Dynamics in Microchannels

The flow in a microfluidic device can be single phase (gas or liquid) or multiple phase (gas-liquid, or liquid-liquid). As for the single-phase flow, the fluid dynamics in the microchannel is close to that in a channel with a large diameter. However, for a multiphase flow in the microchannel, the fluid dynamics is different [15].

The gas-liquid flow in the microchannel can have several flow patterns. **Figure 2.2a** shows the flow regime map developed by Triplett et al. [16]. Superficial velocity of a given phase is a hypothetical velocity, which could be expressed as:

$$U_G = Q_G/A$$

$$U_L = Q_L/A$$

Where, U_G is gas superficial velocity in m/s, Q_G is gas flow rate in m^3/s, U_L is the liquid superficial velocity in m/s, Q_L is liquid flow rate in m^3/s, and A is the cross sectional area.

There are five main flow regimes including bubbly flow, slug flow, slug-annular flow, annular flow, and churn flow as shown in **Figure 2.2b.** The transition lines are marked by Gupta et al. [15].

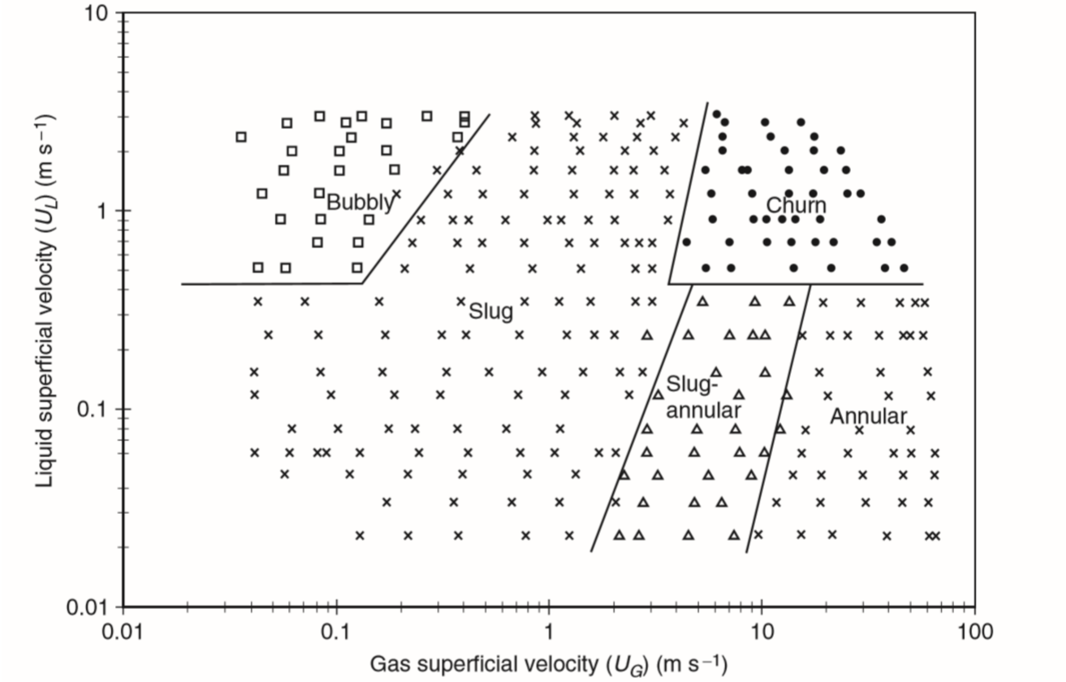

Figure 2.2a: Flow pattern mapped by Triplett et al. and marked by Gupta et al. [15]

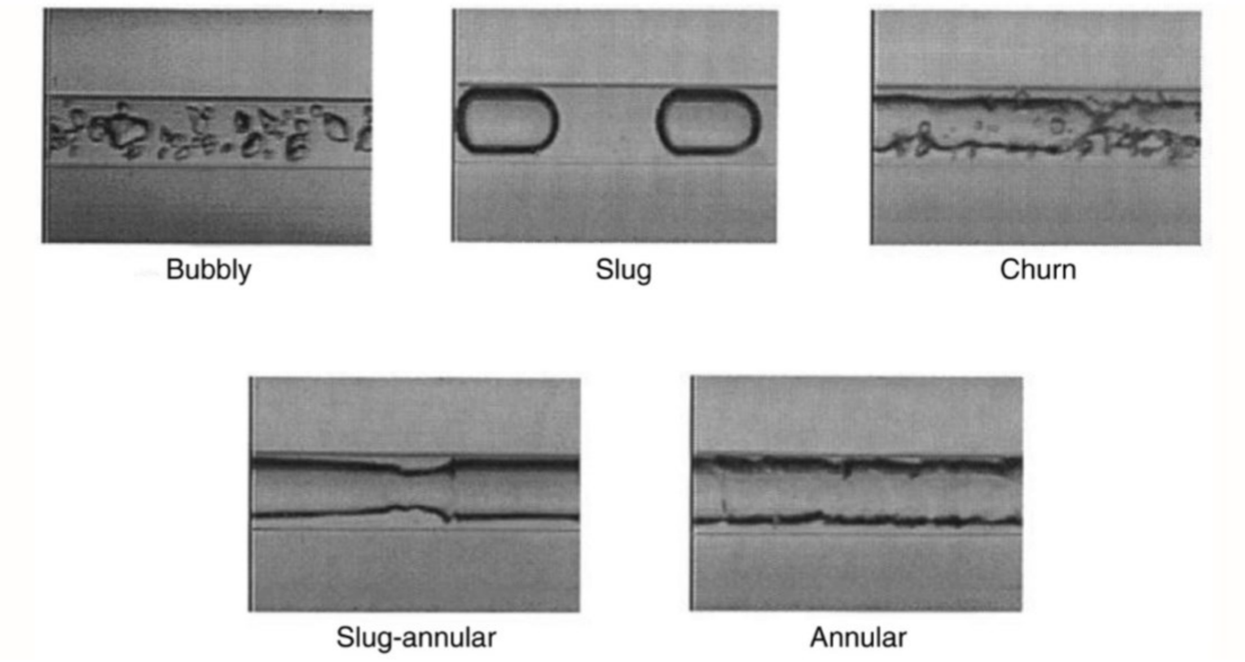
Bubbly
Slug
Churn
Slug-annular
Annular

Figure 2.2b: Typical flow patterns in microchannels observed by Triplett et al. [16]

Gupta et al. has listed five important dimensionless numbers for multiphase flow characterization in microchannels as listed in **Table 2.2** [15].

Name	**Formula**	**Physical Interpretation**
Reynolds number	$\frac{\rho v d}{\mu}$	$\frac{\text{Inertial force}}{\text{Viscous force}}$
Froude number	$\frac{\rho v^2}{\Delta\rho g d}$	$\frac{\text{Inertial force}}{\text{Gravitational force}}$
Bond/ Eötvös number	$\frac{\Delta\rho d^2 g}{\sigma}$	$\frac{\text{Gravitational force}}{\text{Surface tension force}}$
Capillary number	$\frac{\mu v}{\sigma}$	$\frac{\text{Viscous force}}{\text{Surface tension force}}$
Weber number	$\frac{\rho v^2 d}{\sigma}$	$\frac{\text{Inertial force}}{\text{Surface tension force}}$

Table 2.2: Important dimensionless number for multiphase flow characterization in microchannels [15]

Typically, a laminar flow is observed in the microfluidic reactor because it has a low Reynolds number from 0.01 to 100 [17].

2.3.3 Oxidation in Microfluidic Reactor

There is an increasing trend to explore the potential of using microfluidic reactor to conduct non-catalytic liquid phase hydrocarbon oxidation. Advantages of the microfluidic reactors are: (i) improved heat and mass transfer due to the higher surface area-to-volume ratio, (ii) better mixing because of small radial diffusion and internal circulation in liquid slug in case of Taylor flow, (iii) well-defined flow properties, (iv) exact control of gas-liquid ratio, and (v) enhanced safety for using pure oxygen.

Jevtic et al. (2010) has investigated using a capillary reactor on the production of Nylon 6,6 through a non-catalytic liquid phase oxidation of cyclohexane. The results show a conversion of 12% and selectivity of 80%. As a comparison, in industry, a low conversion of 4-5% is maintained to achieve a product selectivity of 80% [18].

Siddiquee et al. (2016) has performed an experimental research using a microfluidic reactor on liquid phase oxidation of tetralin, a naphthenic-aromatic hydrocarbon, at Taylor flow conditions [2]. The study shows a promising 13 times increase in ketone to alcohol selectivity by increasing oxygen availability at a constant conversion compared to the selectivity reported in tetralin oxidation in a batch or semi-batch reactor.

Neuenschwander and Jensen (2014) has performed experiments on non-catalytic liquid phase oxidation of olefin (β-pinene) in a microfluidic reactor. The results show order of magnitude increase in oxyfunctionalization of olefins [19] as compared with that in a batch reactor.

Despite all the above promising advancements in liquid phase oxidation in the microfluidic reactors, the impact of microfluidic reactor configuration and operating temperature on hydrodynamics, conversion, and selectivity during a non-catalytic liquid phase oxidation is not well studied. This void in knowledge suggests further research is required to achieve future commercial applications.

2.4 Literature Cited

1. N. M. Sánchez and A. de Klerk, Autoxidation of aromatics, App. Petro. Res., 2018, 8, 55–78.

2. M. N. Siddiquee, A. de Klerk and N. Nazemifard, Application of microfluidics to enhance gas-liquid mass transfer during selective oxidation of hydrocarbons. React. Chem. Eng., 2016, 1, 418–435.

3. N. M. Emanuel, E. T. Denisov, and Z. K. Maizus, Liquidphase oxidation of hydrocarbons; Plenum Press: New York, 1967.

4. A. K. Suresh, M. M. Sharma and T. Sridhar, Engineering aspects of industrial liquid-phase air oxidation of hydrocarbon, Ind. Eng. Chem. Res., 2000, 39, 3958–3997.

5. A. de Klerk, Continuous- mode thermal oxidation of Fischer-Tropsch waxes, Ind. Eng. Chem. Res., 2003, 42, 6545–6548.

6. P. V. Danckwerts, Gas-Liquid Reactions; McGraw-Hill: New York, 1970.

7. F. Kaštánek, J. Zaharadnǐk, J. Kratochvǐl and J. Čermák, Chemical Reactors for Gas-Liquid Systems, 1st ed.; Ellis Horwood: West Sussex, 1993.

8. E. L. Cussler. Diffusion: Mass Transfer in Fluid Systems, 3rd ed.; Cambridge University Press: Cambridge, 2009.

9. L. K. Doraiswamy and D. Üner, Chemical Reaction Engineering, Beyond the Fundamentals; CRC Press: Boca Raton, 2014.

10. A. K. Suresh, T. Sridhar and O. E. Potter, Autocatalytic oxidation of cyclohexane− mass transfer and chemical reaction. AIChE J., 1988, 34(1), 81–93.

11. M. N. Siddiquee, K. Sivaramakrishnan, Y. Wu, A. de Klerk and N. Nazemifard, A statistical approach dealing with multicollinearity among predictors in microfluidic reactor operation to control liquid-phase oxidation selectivity. React. Chem. Eng., 2018, 3,972–990.

12. P. Tabeling, Introduction to Microfluidics. Oxford, U.K., OUP Oxford, 2005.

13. K. F. Jensen, "Silicon-based microchemical systems: Characteristics and applications." Mrs Bulletin 31(2): 101-107, 2006.

14. G. M. Whitesides, E. Ostuni, S. Takayama, X. Jiang and D. E. Ingber. "Soft Lithography in Biology and Biochemistry." Annual Review of Biomedical Engineering 3(1): 335-373, 2001.

15. R. Gupta, D. F. Fletcher and B. S. Haynes, "Taylor Flow in Microchannels: A Review of Experimental and Computational Work." The Journal of Computational Multiphase Flows 2(1): 1-31, 2010.

16. K. A. Triplett, S. M. Ghiaasiaan, S. I. Abdel-Khalik and D. L. Sadowski, "Gas-liquid two-phase flow in microchannels part I: Two-phase flow patterns." International Journal of Multiphase Flow 25(3): 377-394, 1999.

17. H. Song, J. D. Tice and R. F. Ismagilov, "A Microfluidic System for Controlling Reaction Networks in Time." Angewandte Chemie International Edition 42(7): 768-772, 2003.

18. R. Jevtic, P. A. Ramachandran and M. P. Dudukovic. Capillary reactor for cyclohexane oxidation with oxygen, Chem. Eng. Res. Des., 2010, 88, 255–62.

19. U. Neuenschwander and K. F. Jensen, Olefin autoxidation in flow, Ind. Eng. Chem. Res., 2014, 53(2), 601–608.

Chapter 3: The impact of microfluidic reactor configuration on hydrodynamics, conversion, and selectivity during indan oxidation

In this chapter we discuss the effect of reactor configuration (size and shape) and temperature on liquid phase oxidation of indan, a naphthenic-aromatic hydrocarbon. The work has been accepted to be published as a paper on Journal of Flow Chemistry.

Abstract

Conversion and product selectivity of liquid phase autoxidation of hydrocarbons are affected by numbers of operating conditions, but foremost oxygen availability and temperature. The objective of this study was to understand the impact of reactor configuration on hydrodynamics, conversion, and selectivity. The experiments were performed by using oxygen and indan (a highly reactive naphthenic-aromatic hydrocarbon) in two microfluidic reactors of different dimensions and cross-section geometries, (Reactor A: 62.5 µL of irregular shape and Reactor B: 1000 µL of rectangular shape) at 100-160 °C temperatures and 300 kPa absolute pressures maintaining slug (Taylor) flow. It was found that reactor configuration influenced the hydrodynamics and oxygen availability that consequently changed the conversion and product selectivity in different ways. At constant temperature, pressure and near constant conversion of 12 wt/wt %, Reactor A showed mostly primary products, in contrast, Reactor B showed secondary products, addition products, and primary product having higher ketone-to-alcohol ratio (13:1) than the Reactor A (4.5:1). Overall, Reactor A showed higher indan conversion and suppressed addition product selectivity, whereas Reactor B showed moderate indan conversion and enhanced ketone-to-alcohol ratio (13:1) from the typical ketone-to-alcohol ratio of 1:1.The main contributor in Reactor A to get higher local oxygen availability (gas-liquid interfacial area) was the smaller reactor dimension and liquid slug size whereas the length of the liquid film surrounding the gas bubble was the main contributor for Reactor B to obtain the higher oxygen availability. Comparison of the rate of oxygen consumption and the rate of oxygen transformation ensured the presence of adequate oxygen within the liquid slug and also validated the assumption of using Fick's law to describe the oxygen transport from the gas phase to liquid phase. The understanding

A version of this chapter was accepted to be published as "The impact of microfluidic reactor configuration on hydrodynamics, conversion and selectivity during indan oxidation" on Journal of Flow Chemistry

from the study can be applied in design and operation of industrial units to control the conversion and product selectivity of a complex free radical system.

3.1 Introduction

The study of chemistry in miniaturized flow reactors became very popular for a wide range of chemical synthesis processes, such as oxidation [1–4], hydrogenation [5, 6], halogenation [7] and bioprocessing [8]. Advantages of the miniaturized reactors are: (i) improved heat and mass transfer due to the higher surface area-to-volume ratio, (ii) better mixing because of small radial diffusion and internal circulation in liquid slug in case of Taylor flow, (iii) well-defined flow properties, (iv) exact control of gas-liquid ratio, and (v) enhanced safety for using pure oxygen [1, 9 – 11]. All these characteristics make the microfluidic reactors useful for the study of liquid phase oxidation.

Liquid phase oxidation is an industrially important process to produce many petrochemicals [12 –15] and pharmaceutical products [16–17]. The key challenge of this free radical process involving initiation, propagation, and termination reactions is to control the product selectivity. A few operating conditions affect the product selectivity during liquid phase autoxidation of hydrocarbons, but foremost temperature in combination with oxygen availability [9, 12–14]. Selectivity in the propagation step is influenced by oxygen availability in relation to the free radical concentration and the oxidation reaction can easily become oxygen transfer limited, because the reaction between alkyl radical and oxygen is very fast [9, 12, 18]. Operation at low conversion is commonly practiced in industry to control the product selectivity.

Indan oxidation, as shown in **Figure 3.1**, was selected for this study. Naphthenic-aromatic compounds are important classes of hydrocarbon available in coal, oilsands bitumen and conventional petroleum. The naphthenic-aromatic compounds are susceptible to oxidation, because hydrogen abstraction from the benzylic carbon results in a free radical that is resonance stabilized [19–20].

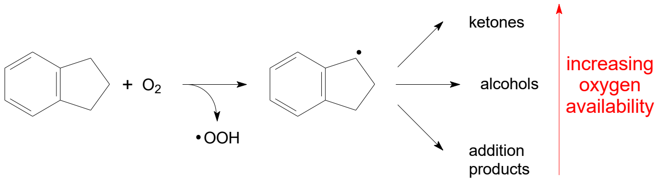

Figure 3.1: Indan oxidation, showing hydrogen abstraction by oxygen and the impact of subsequent oxygen availability on primary product selectivity.

The primary products following on hydrogen abstraction by oxygen are ketones, alcohols and addition products (**Figure 3.1**). When the oxygen availability is high, it is likely that the free radical intermediate will be oxidized, but when oxygen availability is low, the probability is increased that two free radical intermediates will combine. Naphthenic-aromatic compounds with a 5-membered naphthenic ring, such as indan, is more susceptible to addition reactions than those with a 6-membered naphthenic ring, such as tetralin. This difference in propensity for addition product formation is due to the inability of the 5-membered ring on repeated hydrogen transfer to form an aromatic like a 6-membered ring. Indan was therefore more sensitive to reflect changes in oxygen availability during oxidation and better suited for discriminating between conditions in the microfluidic reactors used in this study.

The influence of reaction hydrodynamics on oxidation selectivity was reported in a previous study [9]. It showed that the ketone-to-alcohol selectivity ratio in primary oxidation products could be manipulated independent of conversion by changing reactor hydrodynamics. The microfluidic reactor had a rectangular shape cross-section with 1000 μL of reactor volume. This configuration was also employed as one of the reactors in this study (Reactor B in **Table 3.1**). How the microfluidic reactor design would affect the hydrodynamic parameters pertinent to oxidation selectivity control was not determined.

Table 3.1: Specification of reactors used in this study

Specification	Reactor A	Reactor B
Reactor volume (μL)	62.5	1000
Material	Glass	Glass
Channel cross section	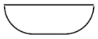	
Mixing channel depth (μm)	85	1240
Mixing channel width (μm)	220	161
Mixing channel length (μm)	532	536
Reactor channel depth (μm)	85	1240
Reactor channel width (μm)	370	391
Reactor channel length (μm)	1912	1488

The primary objectives of this study were i) to investigate how the reactor hydrodynamics would change with reactor size and shape and ii) how changes in hydrodynamics influenced the oxygen availability that controlled oxidation selectivity. A secondary objective was to study the effect of temperature, which would increase the reaction rate and thereby make the reaction selectivity more sensitive to differences in oxygen availability.

The experiments were performed by using oxygen and indan in two glass microfluidic reactors (**Table 3.1**) of different dimensions and volumes, (Reactor A: 62.5 μL of irregular shape and Reactor B: 1000 μL of rectangular shape). The operating conditions were 100-160 °C, 300 kPa absolute pressure, with flow conditions maintaining slug (Taylor) flow at different gas-to-liquid ratios.

3.2 Experimental

3.2.1 Materials

A list of chemicals used in the chapter is provided in **Table 3.2**.

Table 3.2: List of chemicals used in this study

Name	CASRN [a]	Formula	Purity (wt %)		Supplier
			supplier [b]	analysis [c]	
indan	496-11-7	C_9H_{10}	95	96.68	Aldrich
1-indanol	6351-10-6	$C_9H_{10}O$	98		Aldrich
1-indanone	83-33-0	C_9H_8O	≥99		Aldrich
1 ,2-Indandione	16214-27-0	$C_9H_6O_2$	97		Sigma-Aldrich
1 ,3-Indandione	606-23-5	$C_9H_6O_2$	97		Sigma-Aldrich
hexachlorobenzene	118-74-1	C_6Cl_6	99	99.10	Supleco
chloroform	67-66-3	$CHCl_3$	99.1	98.03	Fisher Scientific

[a] CASRN = Chemical Abstracts Services Registry Number.
[b] This is the purity of the material guaranteed by the supplier.
[c] This is the purity based on peak area obtained by GC-FID analysis.

Indan, a five-member ring naphthenic-aromatic hydrocarbon, was selected as the model hydrocarbon. The model oxidized products 1-indanone (ketone), 1-indanol (alcohol), indan-1,2-dione, and 1,3-indandione (diketone) were used for the product identification by GC-FID (gas chromatography with a flame ionization detector). Chloroform (98%, HPLC grade, Fischer Scientific) was used as a solvent and hexachlorobenzene (99%, analytical standard, Supleco) was used as an internal standard in sample preparation for GC analysis. Extra-dry oxygen (99.6 % molar purity), and nitrogen (99.999 % molar purity) were purchased from Praxair Inc., Canada and used as an oxidizing agent and used to control back pressure, respectively. The properties of oxygen and indan for all the experimental conditions were used in hydrodynamic parameter calculation and are reported in **Table 3.3**.

Table 3.3: Properties of oxygen and indan at experimental conditions

	Indan				Oxygen			
Temperature (°C)	Density (kg/m^3)	Surface tension (N/m)	Dynamic Viscosity (Pa.s)	Kinematic Viscosity (m^2/s)	Density (kg/m^3)	Dynamic Viscosity (Pa.s)	Kinematic Viscosity (m^2/s)	D_A (m^2/s)
25	953.64	3.41E-2	1.37E-3	1.43E-6	3.99	2.05E-5	5.14E-6	2.73E-9
100	890.39	2.57E-2	5.48E-4	6.15E-7	3.18	2.43E-5	7.65E-6	1.46E-8
120	872.69	2.35E-2	4.73E-4	5.42E-7	3.02	2.53E-5	8.37E-6	2.07E-8
130	863.69	2.24E-2	4.44E-4	5.14E-7	2.94	2.57E-5	8.75E-6	2.43E-8
140	854.56	2.14E-2	4.19E-4	4.91E-7	2.87	2.62E-5	9.12E-6	2.83E-8
150	845.30	2.04E-2	3.99E-4	4.72E-7	2.80	2.66E-5	9.51E-6	3.27E-8
160	835.91	1.94E-2	3.81E-4	4.56E-7	2.74	2.71E-5	9.90E-6	3.75E-8

3.2.2 Equipment

Two glass microfluidic reactors (Reactor A and Reactor B) of different dimensions and volumes were used to perform experiments and were purchased from Dolomite (Dolomite Microfluidics, Charlestown, MA, USA). The dimensions and channel cross-section of the reactors are summarized in **Table 3.1** and the more details of reactors are provided in Supplemental Information. Irregular shape Reactor A (62.5μl) had a mixing channel of depth=85 μm, width= 220 μm, length= 532 mm and a reaction channel of depth=85 μm, width= 370 μm, length= 1912 mm. The hydraulic diameter of the reaction channel of the Reactor A was $d_H = 1.4\times10^{-4}$ m. Rectangular reactor (Reactor B) had a mixing channel of depth = 1240 μm, width = 161 μm, length = 536 mm and reaction channel of depth = 1240 μm, width = 391 μm, length = 1844 mm. The hydraulic diameter of the reaction channel of the Reactor B was $d_H = 6.0\times10^{-4}$ m.

The experimental setup (**Figure 3.2**) consisted of a microfluidic reactor, a syringe pump (Harvard Apparatus, USA), gas cylinders (O_2 and N_2), gas flow meter (Swagelok, Canada), pressure bomb (Swagelok, Canada), and backpressure regulator (Swagelok, Canada). Indan was injected into the microfluidic reactor at the desired flowrates by using a syringe pump equipped with a 5 mL syringe (Model: 1005TLL, Hamilton Co., USA). A Heidolph MR Hei-Standard hot plate (Model: 505-20000-01-2, Heldolph Instruments, Germany) and a surface mounted thermocouple (Model: CO 1, Cement-on Thermocouple, Omega Engineering, Inc., USA) were used to control the system temperature in the microfluidic reactor. The reactor was mounted on an aluminum block (built at University of Alberta Machine Shop) with thermal adhesive (Dow Corning Corporation, Midland, MI, USA) to ensure better heat transfer between the hot plate and the reactor. A Flea3FL3-U3-13E4M camera (Point Grey Research Inc., Canada) was placed above the reactor to capture the images of gas bubbles and liquid slugs during the experiment. A Fiber–Lite lamp (Model: 3100, Dolan-Jenner Industries, Inc., USA) was used to improve lighting. PTFE tubing, 1/16″ OD × 0.8 mm ID (Dolomite Microfluidics, Charlestown, MA, USA) were used to connect the reactor with the syringe pump, gas flow meter, and pressure bomb.

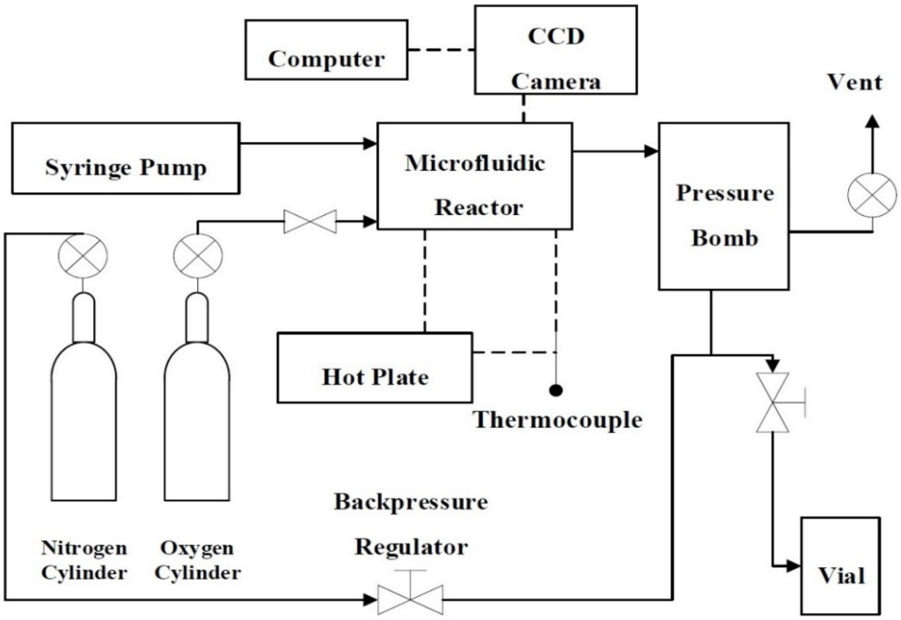

Figure 3.2: Schematic of microfluidic experiment Setup

3.2.3 Procedure

The experiments were performed at different indan injection rates and at different temperatures (100 to 160 °C) maintaining a system pressure of 300 kPa absolute. Taylor flow regime was maintained during the experiment in which liquid slugs (indan) were separated by elongated oxygen bubbles (**Figure 3.3**). In each experiment, indan was loaded into a 5ml syringe, which was then mounted on the syringe pump with flow rate being set to a desired value (2, 3, 5, 7 and 10 µl/min). The reactor was heated to a desired experimental temperature by a hot plate and the system was pressurized to 300 kPa by flowing oxygen and nitrogen as shown in **Figure 3.2**. The co-feed of oxygen and indan resulted a Taylor flow in the reactor by manipulating backpressure using a backpressure regulator and nitrogen. The gas-liquid flow was monitored using a digital camera mounted above the reactor and images of slug and bubble size were captured during the experiment for further analysis of hydrodynamic properties. Flow was continued for twenty minutes at the reaction conditions. The heat supply was disconnected, and the system was then depressurized. The oxidized sample was collected from the pressure vessel and stored in a glass vial for the further product content analysis by using GC-FID. After each experiment, the system was flushed with acetone and indan separately.

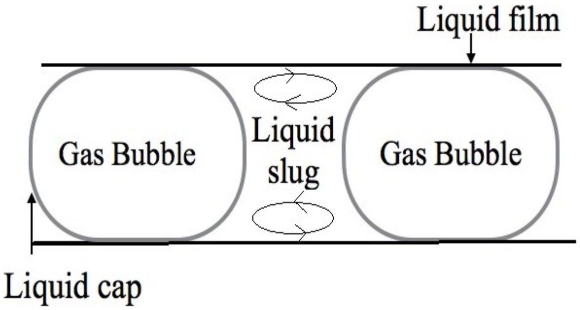

Figure 3.3: Sketch of a typical Taylor (slug) flow in which liquid can circulate within liquid slug

3.2.4 Analyses

The collected oxidized sample was quantitatively analyzed by using a gas chromatograph with a flame ionization detector (GC-FID). An Agilent CP 8858 GC system was equipped with a capillary column (VF-200 MS capillary column, 30 m × 250 µm × 0.25 µm). Nitrogen was used as the carrier gas with flow rate of 1 mL per minute. The initial oven temperature was set at 75°C and held for 0.5 minute. The temperature was then raised to 325 °C at a rate of 20 °C/min and held for 5 minutes. The inlet heater temperature was set at 250 °C and split ratio was 100:1.

Typical oxidation products formation is explained in **Figure 3.1.** Oxidation of indan yielded oxygenates can also be classified as primary, secondary and addition products as described previously [19]. Primary products included mono-ketone of indan (1-indanone or 2-indanone) and mono-alcohol of indan (1-indanol or 2-indanol). Secondary products produced from the oxidation of primary products contained more than one ketone and/or alcohol functional groups, such as indan-1, 2-dione and 1, 3-indandione. Addition products were characterized with the compound containing at least a dimer with/ without different functional groups. GC-FID was calibrated by using response factor of indan, 1-indanol, 1-indanone, indan-1, 2-dione and 1, 3-indandione. A typical GC-FID chromatogram is provided in **Figure 3.4**. Response factors of the products are listed in **Table 3.4**.

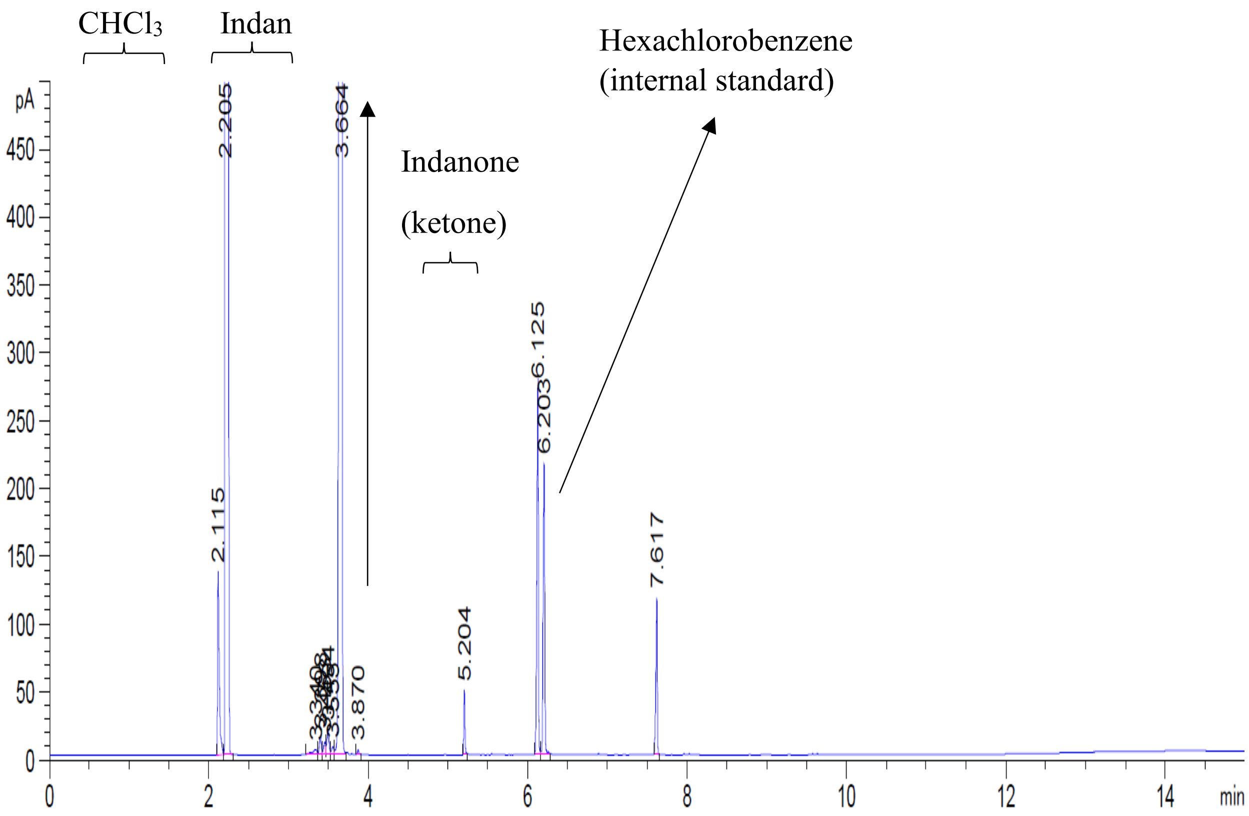

Figure 3.4: A typical GC-FID chromatogram of Indan and its oxidized products

Table 3.4. Response factors of the studied chemicals.

Compound Name	Retention Time (minute)	Response Factor
Heptane	2.23	1.00
$CHCl_3$	2.21	0.06
Hexachlorobenzene	7.62	0.31
Indan	3.66	0.88
1-indanol	5.20	0.79
1-indanone	6.20	0.83
1,3-indandione	7.04	0.58
Indan-1,2-dione	8.13	0.67

3.2.5 Calculations

Hydrodynamic properties for each experiment were calculated from captured images of the Taylor flow in the microfluidic reactor as described in previous study [9].

3.2.5.1 Size of liquid slug and gas bubble and Velocity Calculations

The length of liquid slugs L_S and gas bubble L_G were calculated from captured images using MATLAB (version 2018b). The code is included in **Appendix A**.

For calibration, a ruler was placed between the camera and the microfluidic reactor shown in **Figure 3.5**. The unit length l was measured by dividing length over pixel. The average value in the current study was 2.95×10^{-5}m/pixel with a standard deviation of 2.17×10^{-7}m/pixel.

The size of gas bubble and liquid slug was calculated respectively from images captured **Figure 3.6(a)** and **Figure 3.6(b)**.

The velocity of gas bubble and liquid slug could be calculated by dividing position change ΔL over the time between selected frame shown in **Figure 3.7**. The green bubble shown the target liquid/gas at the first frame. The purple bubble shown the target liquid/gas at the 15th frame. The frequency of camera is 60 hz.

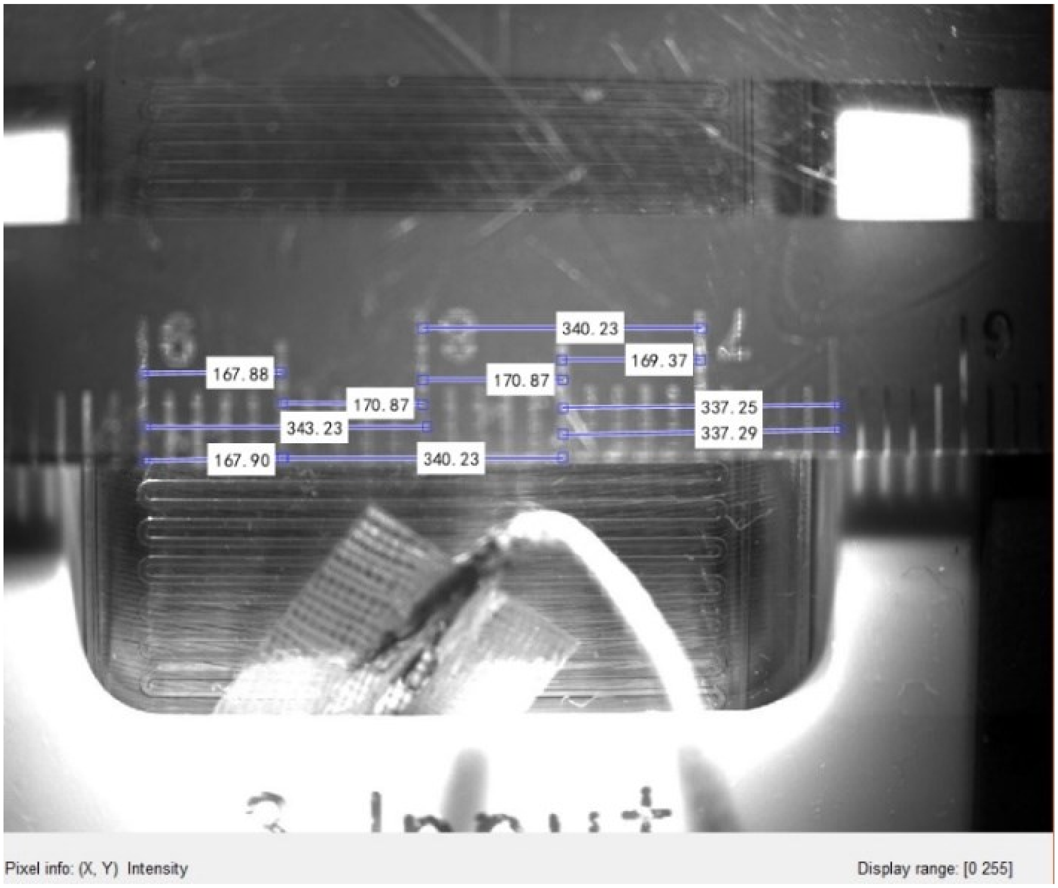

Figure 3.5: Ruler calibration of size measurement using MATLAB version 2018b

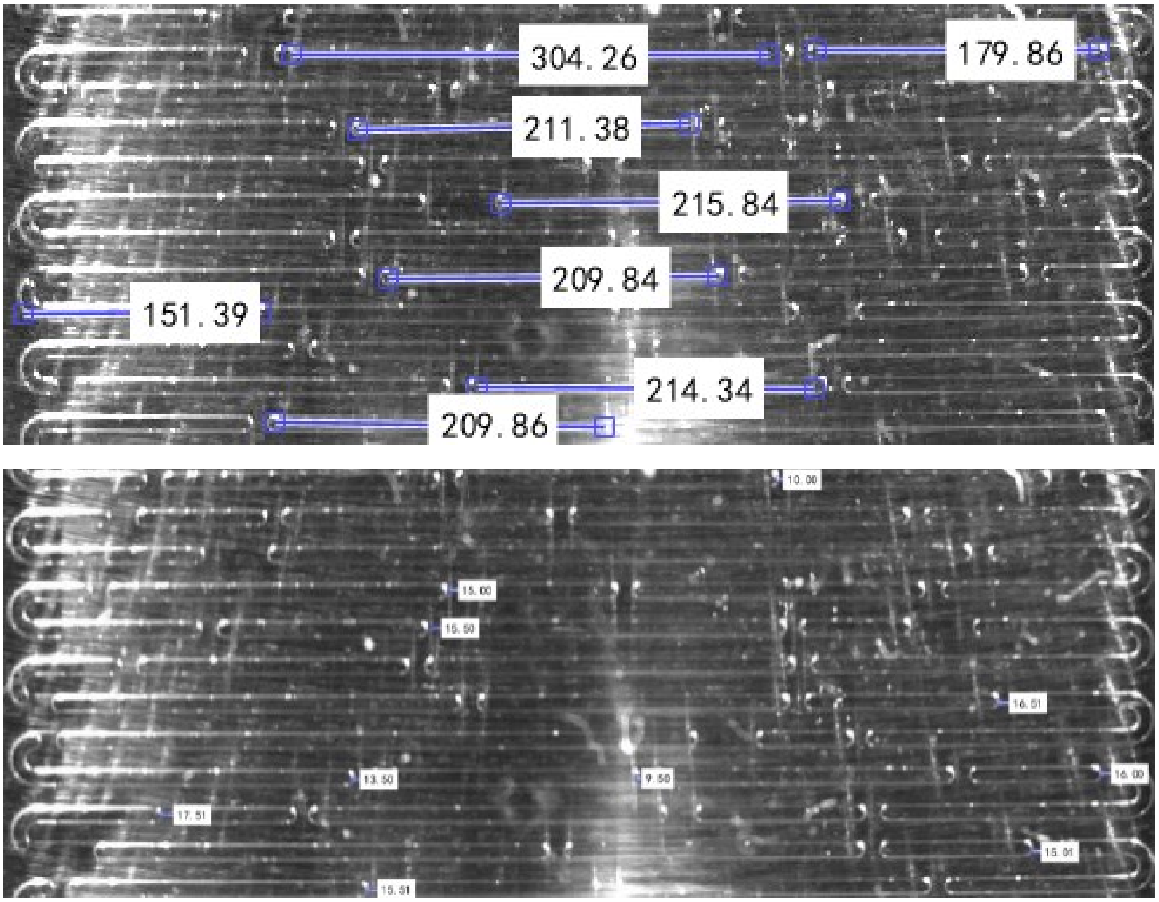

Figure 3.6: (a) Measurement of gas bubble length L_G (b) Measurement of liquid slug length L_S

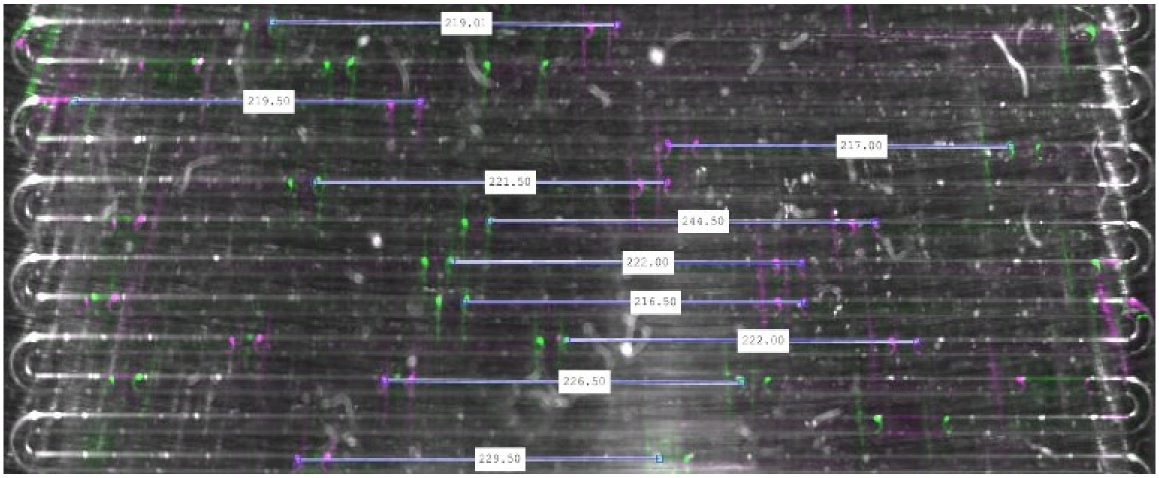

Figure 3.7: Measurement of position change of liquid slugs over a specific period ΔL

3.2.5.2 Hydrodynamic Properties

Following hydrodynamic properties for each experiment were calculated from captured images of the Taylor flow in the microfluidic reactor:

(a) Surface area of gas bubble (S_G) : Reactor A had an irregular channel geometry as shown in Figure 2(a). The surface area of bubble was calculated with following equations:

$$S_G = PL_{G,actual} + 4\pi {r_{cap}}^2 \tag{i}$$

$$L_{G,actual} = L_G - r_{cap} \tag{ii}$$

Where, P is the perimeter of the cross-section. For Reactor A:

$$\mathrm{P} = 0.5\pi\mathrm{d} + 2(\mathrm{w} - \mathrm{h}) \tag{iii}$$

Here, S_G is the surface area of the gas bubble, L_G is the lengths of the gas bubble measured using method provided in Supplemental Information, and w and h are the width and depth of the reactor channel, respectively.

Because there was no empirical equations found for the radius of cap approximation in this meniscus-shape reaction channel, for simplification, it was resembled as a reactor with a rectangular shape cross section with w=370 μm and h=85μm. The radius of the cap was then approximated as:

$$r_{cap} = \frac{w+h}{4} \tag{iv}$$

For Reactor B, the surface area was also calculated using Equation (i). But the perimeter of Reactor B was calculated as follows:

$$\mathrm{P} = 2(w + \mathrm{h}) \tag{v}$$

Where, w is the width of the reactor channel

h is the height of the reactor channel

(b) Volume of liquid slug (V_L): For Reactor A the volume of liquid slug was calculated using following equation:

$$V_L = AL_S + 2Ar_{cap} - \left(\frac{4}{3}\right)\pi {r_{cap}}^3 \tag{vi}$$

Where, A is the cross-sectional area of the reactor channel. For Reactor A,

$$A = 0.5\pi h^2 + (w - 2h)h \quad \text{(vii)}$$

For Reactor B, the volume of liquid slug was also calculated using Equation (vi). But the cross-sectional area A of the reactor channel was:

$$A = wh \quad \text{(vii)}$$

(c) Gas-liquid interfacial area (*a*): For Reactors A and B, the gas-liquid interfacial area was calculated using following equation:

$$a = S_G/V_L \quad \text{(viii)}$$

(d) Hydraulic diameter (d_H): The hydraulic diameter for reactor A and B was calculated using following equation:

$$d_H = \frac{4A}{P} \quad \text{(ix)}$$

Where, A is the cross-sectional area of the reactor, P is the wetted perimeter of the cross section

(e) Superficial velocity: Superficial liquid slug velocity, U_L and gas bubble velocity, U_G: these were calculated from the distance travelled by the slug and bubble in a particular time. Two phase superficial velocity (U_{TP}) was calculated as follows:

$$U_{TP} = \varepsilon_G U_G + (1 - \varepsilon_G)U_L \quad \text{(x)}$$

Where, the volume fraction of gas bubble: $\varepsilon_G = \frac{V_G}{V_G + V_L}$ (xi)

V_L is the volume of liquid slug

V_G is the volume of gas bubble:

(f) Residence time: The average residence time for each experiment was calculated from the two-phase superficial velocity (U_{TP}) and the reactor length.

(g) The thickness of the liquid thin film surrounding a gas bubble, δ: this was calculated from the captured images and using the correlations provided by Yun et al. (2010) for a rectangular microchannel as follows [21]:

$$\frac{\delta_{\max}}{D_h} = 0.39\, We^{0.09} \quad \text{(xii)}$$

$$\frac{\delta_{\min}}{D_h} = 0.02\, We^{0.62} \quad \text{(xiii)}$$

Here, Weber number, $We = \frac{D_H U_T^2 \rho_l}{\sigma_l}$ (xiv)

D_H is the hydraulic diameter of the channel (m)

$\delta_{\max}$ and $\delta_{\min}$ are the maximum and minimum thicknesses of the liquid film (m), respectively.

U_{TP} (m/s) is the two phase superficial gas velocity, ρ_l is the density of liquid and σ_l is the surface tension of liquid (N/m).

w and h are the width and depth of the reactor channel, respectively.

For Reactor A, there was no empirical equations found for this meniscus-shape reaction channel, for simplification, it was resembled as a reactor with a rectangular shape cross section with w=370 µm and h=85µm.

(h) Volumetric mass transfer coefficient, $k_L a$ (s^{-1}): this was calculated using film theory[1, 9]:

$$k_L = \frac{D_A}{\delta} \quad \text{(xv)}$$

Here, D_A is the diffusivity of oxygen in indan, δ is the thickness of liquid film surrounding the oxygen bubble.

3.2.5.3 Conversion and Selectivity Calculation

Conversion and selectivity were calculated with MATLAB version 2018b code (**Appendix B**) from the GC-FID results obtained as follows:

(a) Product selectivity: this was calculated from the relative peak area of the products:

$$\text{Product selectivity (\%)} = \frac{\text{relative peak area of specific product}}{\text{sum of relative peak area of all the products}} \times 100$$

Ketone-to-alcohol selectivity in primary oxidation products was calculated from the relative peak areas of ketones and alcohols in primary oxidation products.

(b) The conversion of indan could be calculated from disappearance of indan or formation of products. The weight percentage of each compound was calculated using following equation:

$$\text{Conversion} = \frac{W_0 - W_i}{W_o} \times 100$$

Where, w_0 = Initial weight % of model compounds

w_i =weight percentage of model compounds

$$W_i = \frac{A_i W_{HCB} RF_{HCB}}{A_{HCB} RF_i}$$

w_{HCB}= weight percentage of Hexachlorobenzene

A_i= peak area of compound

A_{HCB}= peak area of Hexachlorobenzene

RF_i= response factor of compound with respect to Heptane

` RF_{HCB}= response factor of hexachlorobenzene with respect to Heptane

(c) Conversion Rate Calculation

Conversion rate (mol/s) was calculated as follows:

$$Conversion\ Rate = Conversion \times \frac{V_s \times A \times \rho_s}{MW_s}$$

Where, V_s = velocity of the liquid slug

A = cross-sectional area of the reactor (m^2)

ρ_s = density of the liquid slug at experimental condition (kg/m^3)

MW_s = molecular weight of liquid slug (kg/mol)

3.2.5.4 Flame Ionization Detector (FID) Response Factor

A flame ionization detector is used to conduct quantitative analysis of organic compounds whose response factor vary. Therefore, it is essential to determine the response factor for each compound in the oxidation. The response factor was calculated based on the Dietz-method [27]:

$$\text{Response Factor (RF)} = \frac{(area\ of\ compound)(mass\ of\ standard)}{(mass\ of\ compound)(area\ of\ standard)}$$

3.2.5.5 Diffusion Coefficient Calculation

The oxygen diffusivity in indan was calculated using Diaz et al. (1987) Correlation [28].

$$(D_A)_{\mathrm{T}} = 4.996 \times 10^3 \times (D_{AB})_{\mathrm{T}=25\,^\circ\mathrm{C}} \times e^{-2539/\mathrm{T}}$$

Where, $(D_{AB})_{\mathrm{T}=25\,^\circ\mathrm{C}} = 6.02 \times 10^{-5} \times \frac{v_B^{0.36}}{\mu_B^{0.61} v_A^{0.64}}$

$(D_A)_{\mathrm{T}}$ = diffusion coefficient of oxygen in indan at specific temperature (cm^2/s)

$(D_{AB})_{\mathrm{T}=25\,^\circ\mathrm{C}}$ = diffusion coefficient of oxygen in indan at 25 °C (cm^2/s)

T = experiment temperature (K)

μ_B = viscosity of indan (cp)

v_A = molar volume of oxygen at normal boiling point temperature cm^2/gmol

v_B = molar volume of indan at normal boiling point temperature cm^2/gmol

3.2.5.6 Mass Transfer Coefficient Calculation

Volumetric mass transfer coefficient was calculated using Vandu et al. (2005) method as following [29]:

$$k_L a = k_{L,cap} a_{cap} + k_{L,film} a_{L,film}$$

Where, $k_{L,cap} = 2\sqrt{\frac{2DV_b}{\pi^2 d_c}}$

$k_{L,film} = 2\sqrt{\frac{D}{\pi t_{film}}}$

D = liquid phase diffusivity

d_c = capillary inner diameter

t_{film} = contact time of gas bubble and liquid thin film

V_b= bubble velocity

3.3 Results

3.3.1 Constant Temperature Oxidation

Reactor hydrodynamics changed the local oxygen availability that influenced the conversion and product selectivity during liquid phase oxidation. It was previously found that the most important variable in microfluidic reactors affecting oxygen availability was gas–liquid interfacial area [4]. If this holds true for all microfluidic reactor configurations, then at constant temperature and pressure, the local oxygen availability could be manipulated by the gas–liquid interfacial area and is related to the hydrodynamic behavior of the microfluidic reactor.

3.3.1.1 Measured Reactor Hydrodynamics

Indan oxidation was performed both in the Reactor A (62.5 µL) and Reactor B (1000 µL) at different indan injection rates (2 – 10 µL/min) at 300 kPa absolute and 150 °C to investigate the role of reactor hydrodynamics in conversion and product selectivity. **Table 3.5** reported the measured hydrodynamic parameters and gas-liquid interfacial area (oxygen availability).

Table 3.5: Hydrodynamic properties and oxygen availability during indan oxidation in microfluidic reactors at 300 kPa pressure absolute and 150 °C at different indan injection rates using oxygen as oxidizing agent.

reactors	series	Flow rate (µL/min)	experimental [a]						
			length of liquid slug, $L_S \times 10^4$ (m)	length of gas bubble, $L_G \times 10^4$ (m)	liquid slug velocity, $U_S \times 10^2$ (m/s)	bubble velocity, $U_G \times 10^2$ (m/s)	two-phase superficial velocity, $U_{TP} \times 10^2$ (m/s)	residence time (min)	gas-liquid interfacial area, $a \times 10^{-4}$ (m^2/m^3)
Reactor A (62.5 µL)	A	2	2.9 ± 0.2	94.4 ± 6.8	2.4 ± 0.2	2.4 ± 0.2	2.4 ± 0.2	1.5 ± 0.1	78.0 ± 8.2
	B	3	4.3 ± 0.4	93.0 ± 2.8	2.3 ± 0.2	2.3 ± 0.2	2.3 ± 0.2	1.6 ± 0.2	55.6 ± 4.7
	C	5	5.3 ± 0.5	61.7 ± 4.7	1.9 ± 0.2	1.9 ± 0.2	1.9 ± 0.2	2.0 ± 0.3	30.6 ± 3.4
	D	7	7.1 ± 0.4	27.1 ± 1.4	1.8 ± 0.2	1.8 ± 0.2	1.8 ± 0.2	2.0 ± 0.2	10.8 ± 1.2
	E	10	8.4 ± 0.6	26.1 ± 1.8	1.5 ± 0.2	1.5 ± 0.2	1.5 ± 0.2	2.5 ± 0.3	8.4 ± 0.9
Reactor B (1000 µL)	F	2	11.6 ± 1.5	331.7 ±31.8	2.2 ± 0.4	2.2 ± 0.4	2.2 ± 0.4	1.6 ± 0.3	14.3 ± 1.4
	G	3	17.2 ± 1.6	191.0 ±23.8	2.1 ± 0.4	2.1 ± 0.4	2.1 ± 0.4	1.7 ± 0.4	7.0 ± 1.1
	H	5	31.0± 3.1	113.8 ±13.1	2.0 ± 0.4	2.0 ± 0.4	2.0 ± 0.4	1.8 ± 0.5	2.7 ± 0.4
	I	7	35.0 ± 4.4	96.0 ± 13.2	1.8 ± 0.3	1.8 ± 0.3	1.8 ± 0.3	2.0 ± 0.4	2.0 ± 0.5

	J	10	36.6 ± 0.1	88.2 ± 9.2	1.7 ± 0.3	1.7 ± 0.3	1.7 ± 0.3	2.1 ± 0.4	1.8 ± 0.2

[a] Based on 60 different slugs and gas bubbles of each series of experiments

In both cases (Reactor A and Reactor B), the length of the liquid slug increased with the indan injection rates, but the size of the slug varied with reactor size. In case of the Reactor A, the liquid slug was increased from 2.9×10^{-4} m to 8.4×10^{-4} m whereas liquid slug size was increased from 11.6×10^{-4} m to 36.6×10^{-4} m in case of Reactor B. Variation of liquid injection rates resulted a decrease in gas bubble size, from 94.4×10^{-4} m to 26.1×10^{-4} m (62.5 µL reactor) and from 331.7×10^{-4} m to 88.2×10^{-4} m (Reactor B). The variation of liquid slug and gas bubble size obtained at 2 µL/min indan resulted maximum gas-liquid interfacial areas, *a*, that were substantially different for the two configurations, namely, 78×10^{4} m^2/m^3 (Reactor A) and 14.3×10^{4} m^2/m^3 (Reactor B).

The two-phase superficial velocity (U_{TP}) was decreased with increasing indan injection rates in both reactor categories. The maximum U_{TP} (**Table 3.5**) were 2.4×10^{-2} m/s and 2.2×10^{-2} m/s, respectively, for the Reactor A (62.5 µL) and Reactor B (1000 µL) that were observed at the indan injection rate of 2 µL/min. The residence time of the indan-oxygen in the reactor were different due to the change of U_{TP} with the indan injection rates. The residence time were varied in the range of 1.5 – 2.5 min (Reactor A) and 1.6 – 2.1 min (Reactor B), i.e. the residence times were in the same range for the two configurations.

3.3.1.2 Calculated Reactor Hydrodynamics

The film thickness surrounding the gas bubble varies and the reactor corner would have the maximum liquid film thickness. The maximum and minimum liquid film thicknesses surrounding a gas bubble were calculated, based on Equations (xii) and (xiii) in the Supporting Information. For the Reactor A (62.5 µL), the maximum and minimum film thickness were 0.3×10^{-4} m and 1.1×10^{-6} m, respectively (**Table 3.6**). In contrast, 1.5×10^{-4} m and 5.4×10^{-6} m were the maximum and minimum film thicknesses, respectively, for the Reactor B (**Table 3.6**). The film thickness for Reactor B was consistently larger than that in Reactor A, but the difference was less than double the thickness in Reactor A.

Table 3.6: Calculated hydrodynamic properties and mass transfer coefficients during indan oxidation using oxygen as oxidizing agent in microfluidic reactors at 300 kPa pressure absolute and 150 °C at different indan injection rates.

reactors	series	flow rate (μL/min)	calculated [a]			calculated [a]		
			film thickness, $\delta_{min}\times10^{6}$ (m)[b]	mass transfer coefficient, $k_L\times10^{2}$ (m/s)[c]	liquid side volumetric mass transfer coefficient, $k_La\times10^{-3}$ (s^{-1})	film thickness, $\delta_{max}\times10^{4}$ (m)[d]	mass transfer coefficient, $k_L\times10^{4}$ (m/s)[c]	liquid side volumetric mass transfer coefficient, $k_La\times10^{-1}$ (s^{-1})
Reactor A (62.5 μL)	A	2	$1.1 \pm 1.1\times10^{-3}$	$3.2 \pm 3.3\times10^{-3}$	24.8 ± 2.5	$0.3 \pm 3.6\times10^{-3}$	$10.8 \pm 1.2\times10^{-1}$	84.6 ± 8.5
	B	3	$1.1 \pm 1.8\times10^{-3}$	$3.2 \pm 5.3\times10^{-3}$	17.7 ± 1.4	$0.3 \pm 5.7\times10^{-3}$	$11.0 \pm 2.0\times10^{-1}$	61.0 ± 4.8
	C	5	$1.1 \pm 2.1\times10^{-3}$	$3.2 \pm 6.2\times10^{-3}$	9.7 ± 1.0	$0.3 \pm 6.5\times10^{-3}$	$11.4 \pm 2.5\times10^{-1}$	34.7 ± 3.2
	D	7	$1.1 \pm 1.7\times10^{-3}$	$3.2 \pm 5.2\times10^{-3}$	3.5 ± 0.4	$0.3 \pm 5.4\times10^{-3}$	$11.4 \pm 2.1\times10^{-1}$	12.3 ± 1.3
	E	10	$1.1 \pm 1.7\times10^{-3}$	$3.0 \pm 5.3\times10^{-3}$	2.7 ± 0.3	$0.3 \pm 5.3\times10^{-3}$	$11.8 \pm 2.2\times10^{-1}$	10.0 ± 1.0
Reactor B (1000 μL)	F	2	$5.4 \pm 1.5\times10^{-2}$	$0.7 \pm 2.0\times10^{-3}$	1.0 ± 0.09	$1.5 \pm 4.7\times10^{-2}$	$2.5 \pm 7.8\times10^{-2}$	3.6 ± 0.4
	G	3	$5.4 \pm 1.9\times10^{-2}$	$0.7 \pm 2.6\times10^{-3}$	0.5 ± 0.08	$1.5 \pm 5.9\times10^{-2}$	$2.5 \pm 1.0\times10^{-1}$	1.8 ± 0.3
	H	5	$5.4 \pm 2.0\times10^{-2}$	$0.7 \pm 2.7\times10^{-3}$	0.1 ± 0.02	$1.5 \pm 6.0\times10^{-2}$	$2.6 \pm 1.1\times10^{-1}$	0.5 ± 0.1
	I	7	$5.4 \pm 1.5\times10^{-2}$	$0.7 \pm 2.0\times10^{-3}$	0.2 ± 0.03	$1.5 \pm 4.6\times10^{-2}$	$2.6 \pm 8.2\times10^{-2}$	0.5 ± 0.1
	J	10	$5.4 \pm 1.5\times10^{-2}$	$0.7 \pm 2.0\times10^{-3}$	0.1 ± 0.02	$1.5 \pm 4.4\times10^{-2}$	$2.6 \pm 8.2\times10^{-1}$	0.5 ± 0.1

[a] Based on 60 different slugs and gas bubbles of each series of experiments

[b] Minimum film thicknesses were calculated based on the correlation provided for Taylor flow in a rectangular channel [9]

[c] Based on film theory and $k_L = D_A/\delta$ [1, 9]

[d] Maximum film thicknesses were calculated based on the correlation provided for Taylor flow in a rectangular channel [9]

The variation of the film thickness and gas-liquid interfacial area (*a*) resulted the change in liquid side volumetric mass transfer coefficient (k_La). Based on the minimum and maximum film thickness, k_La were 24.8×10^{3} (s^{-1}) and 84.6×10^{1} (s^{-1}), respectively for the Reactor A (**Table 3.6**). Whereas for the reactor B (1000 μL), k_La were 1.0×10^{3} (s^{-1}) and 3.6×10^{1} (s^{-1}), respectively, based on the minimum and maximum film thickness. These calculated values indicated that oxygen availability in the liquid phase in Reactor A would be higher than in Reactor B at the same inlet flow conditions.

3.3.1.3 Conversion and Selectivity

Indan oxidation was performed in both the Reactor A (62.5 µL) and Reactor B (1000 µL) at different indan injection rates (2–10 µL/min) at 300 kPa absolute and 150 °C to investigate the effect on conversion and selectivity. Conversion and product selectivity for the oxidation of indan with oxygen at different hydrodynamic conditions in Reactor A and Reactor B are reported in **Table 3.7**.

Table 3.7: Conversions and product selectivity of indan oxidized in microfluidic reactors at 300 kPa pressure absolute and 150 °C at different indan injection rates using oxygen as oxidizing agent.

reactors	series	flow rate (µL/min)	conversion [a]		product selectivity [a]			
			conversion wt/wt %	conversion rate $\times 10^6$ (mol/s)	primary	secondary	addition	ketone/alcohol [b]
Reactor A (62.5 µL)	A	2	28.0 ± 4.6	1.4 ± 0.2	97.5 ± 0.4	2.5 ± 0.4	0.0 ± 0.0	6.3 ± 0.5
	B	3	25.0 ± 7.5	1.2 ± 0.4	98.5 ± 0.1	1.5 ± 0.1	0.0 ± 0.0	6.1 ± 0.5
	C	5	22.5 ± 3.4	0.9 ± 0.1	98.9 ± 0.5	1.1 ± 0.5	0.0 ± 0.0	5.9 ± 0.5
	D	7	13.3 ± 2.2	0.5 ± 0.1	98.9 ± 0.1	1.1 ± 0.1	0.0 ± 0.0	6.9 ± 0.6
	E	10	12.8 ± 3.9	0.4 ± 0.1	99.0 ± 0.3	0.9 ± 0.2	0.1 ± 0.1	4.5 ± 0.5
Reactor B (1000 µL)	F	2	11.5 ± 1.5	8.9 ± 1.2	91.4 ± 1.2	6.6 ± 0.2	2.0 ± 1.0	13.0 ± 1.0
	G	3	8.9 ± 1.1	6.5 ± 0.8	91.6 ± 1.9	6.3 ± 1.2	2.1 ± 0.7	11.0 ± 1.0
	H	5	5.8 ± 0.8	4.1 ± 0.6	94.4 ± 0.8	4.2 ± 0.6	1.4 ± 0.1	9.1 ± 0.6
	I	7	4.2 ± 0.6	2.6 ± 0.4	94.0 ± 0.6	2.9 ± 0.2	3.1 ± 0.4	7.0 ± 0.4
	J	10	3.9 ± 0.4	2.3 ± 0.2	91.5 ± 4.0	2.3 ± 0.2	6.2 ± 3.7	6.7 ± 0.2

[a] *Calculated based on the GC-FID relative peak area of triplicate runs of each experiment*

[b] Ketone-to-alcohol ratio in primary oxidation products that *calculated based on the GC-FID relative peak area of triplicate runs*

Indan conversion was increased with increasing liquid phase residence time (decreasing indan injection rate) for both reactors. But conversion was much higher in Reactor A (62.5 µL) compared to the conversion obtained at corresponding indan injection rate in Reactor B (1000 µL). Maximum indan conversion was found at 2 µL/min indan injection rate; 28 wt/wt % (Series A in Reactor A) and 11.5 wt/wt % (Series F in Reactor B).

The product selectivity was noticeably different for the two configurations. No addition products were noticed at the maximum oxygen availability in Reactor A (62.5 µL reactor) even at very high conversion. Whereas some addition products were noticed in case of Reactor B (1000 µL reactor). The ketone-to-alcohol selectivity in case of Reactor A was about constant in spite of changing conversion, but in contrast, the ketone-to-alcohol selectivity changed with conversion in case of reactor B.

3.3.2 Variable Temperature Oxidation

Temperature affects oxidation rate and thereby conversion and selectivity during liquid phase oxidation, which is why it was kept constant in **Section 3.1**. When temperature is increased at otherwise similar conditions, the oxidation rate will be increased if oxygen remains available in the liquid phase. As the oxidation rate increases, mass transport of oxygen from the gas phase to the liquid phase becomes increasingly important, because the rate of oxygen consumption in the liquid phase is also higher. Varying temperature, while keeping other parameters constant, is a way to explore the impact of the microfluidic reactor configuration on gas–liquid mass transport, using not only conversion, but also selectivity as indirect measures of how reactor configuration affects oxygen availability in the liquid phase. Even at constant flow rate, hydrodynamic properties changed somewhat with temperature as physical properties of the reactants changed with temperature, such as density, viscosity, and surface tension.

3.3.2.1 Change of Hydrodynamic Parameters with Temperature

In order to investigate the role of temperature on reactor hydrodynamic parameters, indan oxidation was performed in both the 62.5 µL (Reactor A) and 1000 µL microfluidic reactors (Reactor B) at different temperatures (100–160 °C) and 300 kPa absolute at the indan injection rate of 7 µL/min. **Table 3.8** lists the measured hydrodynamic parameters and gas–liquid interfacial-area.

Table 3.8: Hydrodynamic properties and oxygen availability during indan oxidation in microfluidic reactors at 300 kPa pressure absolute and different temperatures at 7 µL/min indan injection rate using oxygen as oxidizing agent.

reactors	series	temperature (°C)	experimental [a]						
			length of liquid slug, $L_S \times 10^4$ (m)	length of gas bubble, $L_G \times 10^4$ (m)	liquid slug velocity, $U_S \times 10^2$ (m/s)	bubble velocity, $U_G \times 10^2$ (m/s)	two-phase superficial velocity, $U_{TP} \times 10^2$ (m/s)	residence time (min)	gas-liquid interfacial area, $a \times 10^{-4}$ (m^2/m^3)
Reactor A (62.5 μL)	K	100	7.9 ± 0.7	24.1 ± 1.4	1.6 ± 0.3	1.6 ± 0.3	1.6 ± 0.3	2.3 ± 0.0	8.4 ± 1.1
	L	120	7.4 ± 0.5	23.6 ± 2.4	1.6 ± 0.3	1.6 ± 0.3	1.6 ± 0.3	2.3 ± 0.0	8.7 ± 0.8
	M	130	7.6 ± 0.9	23.2 ± 3.1	1.7 ± 0.3	1.7 ± 0.3	1.7 ± 0.3	2.1 ± 0.0	8.4 ± 1.3
	N	140	7.2 ± 0.4	24.6 ± 4.1	1.8 ± 0.4	1.8 ± 0.4	1.8 ± 0.4	2.0 ± 0.1	9.2 ± 1.7
	O	150	7.1 ± 0.4	27.1 ± 1.4	1.8 ± 0.2	1.8 ± 0.2	1.8 ± 0.2	2.0 ± 0.2	10.8 ± 1.2
	P	160	6.9 ± 0.5	28.0 ± 2.7	2.0 ± 0.4	2.0 ± 0.4	2.0 ± 0.4	1.9 ± 0.1	11.0 ± 1.6
Reactor B (1000 μL)	Q	100	35.7 ± 5.2	94.2 ± 6.8	1.3 ± 0.2	1.3 ± 0.2	1.3 ± 0.2	2.7 ± 0.5	2.0 ± 0.3
	R	120	38.3 ± 4.8	92.6 ± 3.1	1.4 ± 0.2	1.4 ± 0.2	1.4 ± 0.2	2.7 ± 0.6	1.8 ± 0.2
	S	130	34.8 ± 3.2	91.2 ± 9.7	1.4 ± 0.2	1.4 ± 0.2	1.4 ± 0.2	2.6 ± 0.5	1.9 ± 0.3
	T	140	35.3 ± 4.5	91.7 ± 4.3	1.7 ± 0.3	1.7 ± 0.3	1.7 ± 0.3	2.1 ± 0.4	1.9 ±0.2
	U	150	35.0 ± 4.4	96.0 ± 13.2	1.8 ± 0.3	1.8 ± 0.3	1.8 ± 0.3	2.0 ± 0.4	2.0 ± 0.5
	V	160	34.4 ± 5.0	94.4 ± 5.9	1.9 ± 0.3	1.9 ± 0.3	1.9 ± 0.3	1.9 ± 0.4	2.0 ± 0.3

[a] Based on 60 different slugs and gas bubbles of each series of experiments

As shown in **Table 3.8**, only a small variation in hydrodynamic parameters were observed for both the reactors A and B.

In case of Reactor A (62.5 μL), length of the liquid slug (L_S) varied between 6.9×10^{-4} m to 7.9×10^{-4} m, and the length of the gas bubbles (L_G) varied between 23.2×10^{-4} m to 28.0×10^{-4} m resulting gas-liquid interfacial area (*a*) in the range of 8.4×10^4 m^2/m^3 to 11.0×10^4 m^2/m^3. Reactor B (1000 μL) showed larger liquid slugs (L_S) and gas bubbles (L_G) than in Reactor A. L_S varied in the range of 35.7×10^{-4} m to 38.3×10^{-4} m and gas bubbles (L_G) varied between 91.2×10^{-4} m to 96.0×10^{-4} m. But gas-liquid interfacial area (*a*) was approximately constant for the reactor B (~ 2×10^4 m^2/m^3). The two-phase velocity (U_{TP}) and the residence time were changed as a result of the variation of the liquid slug, bubble size, and change in physical properties with temperature. In case of Reactor A, U_{TP} varied in the range of 1.6×10^{-2} m/s to 2.0×10^{-2} m/s resulting residence times between 1.9 min to 2.3 min. The minimum residence time (1.9 min) was observed at 160 °C and maximum residence time was 2.3 min that was resulted at 100 °C. In

Reactor B (1000 μL), U_{TP} varied in the range of 1.3×10^{-2} m/s to 1.9×10^{-2} m/s resulting the maximum residence time of 2.7 min and minimum residence time of 1.9 min.

3.3.2.2 Change of Calculated Reactor Hydrodynamics with Temperature

Reactor B showed higher film thickness compared to the film thickness calculated for the Reactor A (**Table 3.9**). The minimum film thicknesses were almost identical for all test conditions at 5.4×10^{-6} m (Reactor B) and 1.1×10^{-6} m (Reactor A). The maximum film thickness were ~0.3 × 10^{-4} m and ~1.4×10^{-4} m, respectively for Reactor A and Reactor B.

Table 3.9: Calculated hydrodynamic properties and mass transfer coefficients during indan oxidation using oxygen as oxidizing agent in microfluidic reactors at 300 kPa pressure and different temperatures at 7 μL/min indan injection rate.

			calculated [a]			calculated [a]		
reactors	series	temperature (°C)	film thickness, $\delta_{min}\times10^{6}$ (m)[b]	mass transfer coefficient, $k_L\times10^{2}$ (m/s)[c]	liquid side volumetric mass transfer coefficient, $k_La\times10^{-3}$ (s^{-1})	film thickness, $\delta_{max}\times10^{4}$ (m)[d]	mass transfer coefficient, $k_L\times10^{4}$ (m/s)[c]	liquid side volumetric mass transfer coefficient, $k_La\times10^{-1}$ (s^{-1})
Reactor A (62.5 μL)	K	100	$1.1 \pm 3.0\times10^{-4}$	$2.0 \pm 0.6\times10^{-3}$	1.7 ± 0.2	$0.3 \pm 0.9\times10^{-2}$	$7.5 \pm 2.3\times10^{-2}$	6.3 ± 0.8
	L	120	$1.1 \pm 2.6\times10^{-4}$	$2.4 \pm 0.6\times10^{-3}$	2.1 ± 0.2	$0.3 \pm 0.8\times10^{-2}$	$8.7 \pm 2.4\times10^{-2}$	7.5 ± 0.7
	M	130	$1.1 \pm 2.6\times10^{-4}$	$2.8 \pm 0.7\times10^{-3}$	2.3 ± 0.4	$0.3 \pm 0.8\times10^{-2}$	$10.0\pm 2.7\times10^{-2}$	8.3 ± 1.4
	N	140	$1.1 \pm 6.3\times10^{-4}$	$3.2 \pm 1.9\times10^{-3}$	3.0 ± 0.5	$0.3 \pm 2.0\times10^{-2}$	$11.5\pm 7.6\times10^{-2}$	10.6 ± 1.9
	O	150	$1.1 \pm 1.7\times10^{-3}$	$3.2 \pm 5.2\times10^{-3}$	3.5 ± 0.4	$0.3 \pm 5.4\times10^{-2}$	$11.4 \pm2.1\times10^{-1}$	12.3 ± 1.3
	P	160	$1.1 \pm 5.9\times10^{-4}$	$3.7 \pm 2.0\times10^{-3}$	4.0 ± 0.5	$0.3 \pm 1.9\times10^{-2}$	$13.5 \pm8.0\times10^{-2}$	14.4 ± 2.0
Reactor B (1000 μL)	Q	100	$5.4 \pm 1.5\times10^{-2}$	$0.4 \pm 1.1\times10^{-3}$	$0.08 \pm1.2\times10^{-2}$	$1.4 \pm 4.2\times10^{-2}$	$1.5 \pm 4.7\times10^{-2}$	$0.3 \pm 4.8\times10^{-2}$
	R	120	$5.4 \pm 1.7\times10^{-2}$	$0.5 \pm 1.2\times10^{-3}$	$0.09 \pm1.0\times10^{-2}$	$1.4 \pm 4.8\times10^{-2}$	$1.8 \pm 6.2\times10^{-2}$	$0.3 \pm 4.3\times10^{-2}$
	S	130	$5.4 \pm 1.5\times10^{-2}$	$0.6 \pm 1.5\times10^{-3}$	$0.11 \pm1.6\times10^{-2}$	$1.4 \pm 4.3\times10^{-2}$	$2.1 \pm 6.5\times10^{-2}$	$0.4 \pm 6.4\times10^{-2}$
	T	140	$5.4 \pm 1.5\times10^{-2}$	$0.6 \pm 1.8\times10^{-3}$	$0.12 \pm1.7\times10^{-2}$	$1.5 \pm 4.6\times10^{-2}$	$2.3 \pm 7.2\times10^{-2}$	$0.5 \pm 6.1\times10^{-2}$
	U	150	$5.4 \pm 1.5\times10^{-2}$	$0.7 \pm 2.0\times10^{-3}$	$0.15 \pm3.1\times10^{-2}$	$1.5 \pm 4.6\times10^{-2}$	$2.6 \pm 8.2\times10^{-2}$	$0.5 \pm 1.1\times10^{-1}$
	V	160	$5.4 \pm 1.7\times10^{-2}$	$0.8 \pm 2.5\times10^{-3}$	$0.16 \pm2.1\times10^{-2}$	$1.5 \pm 5.1\times10^{-2}$	$2.8 \pm 9.9\times10^{-2}$	$0.6 \pm 9.0\times10^{-2}$

[a] Based on 60 different slugs and gas bubbles of each series of experiments

[b] Minimum film thicknesses were calculated based on the correlation provided for Taylor flow in a rectangular channel [9, 21]

[c] Based on film theory and $k_L = D_A/\delta$ [1,9]

[d] Maximum film thicknesses were calculated based on the correlation provided for Taylor flow in a rectangular channel [9, 21]

The variation of the film thicknesses and gas-liquid interfacial area (*a*) resulted the change in liquid side volumetric mass transfer coefficient (k_La). For Reactor A, based on the minimum film thickness, k_La varied between 1.7×10^3 s^{-1} and 4.0×10^3 s^{-1}, and based on the maximum film thickness, k_La varied between 6.3×10^1 s^{-1} and 14.4×10^1 s^{-1}. For Reactor B, based on the minimum film thickness, k_La varied between 7.8×10^1 s^{-1} and 1.6×10^2 s^{-1}, and based on the maximum film thickness, k_La varied between 3.0 s^{-1} and 6.0 s^{-1}.

3.3.2.3 Change of Conversion and Selectivity with Temperature

Conversion and selectivity changed with temperature (100 to 160 °C) for the oxidation performed at indan injection rate of 7 µL/ min at 300 kPa absolute (**Table 3.10**).

Table 3.10: Conversions and product selectivity of indan oxidation using oxygen as oxidizing agent in microfluidic reactors at 300 kPa pressure and different temperatures at 7 µL/min indan injection rate.

reactors	series	temperature (°C)	conversion [a]		product selectivity [a]			
			conversion wt/wt %	conversion rate $\times 10^6$ (mol/s)	primary	secondary	addition	ketone/alcohol [b]
Reactor A (62.5 µL)	K	100	1.2 ± 0.4	0.04 ± 0.01	97.1 ± 0.5	2.9 ± 0.5	0.0 ± 0.0	3.3 ± 0.6
	L	120	1.1 ± 0.2	0.04 ± 0.01	96.4 ± 0.6	3.6 ± 0.6	0.0 ± 0.0	4.8 ± 0.3
	M	130	2.0 ± 0.2	0.07 ± 0.01	98.1 ± 0.1	1.9 ± 0.1	0.0 ± 0.0	5.1 ± 0.5
	N	140	5.7 ± 0.7	0.21 ± 0.03	97.6 ± 0.1	1.4 ± 0.2	1.0 ± 0.6	6.7 ± 0.9
	O	150	13.3 ± 2.2	0.49 ± 0.08	98.9 ± 0.1	1.9 ± 0.1	0.0 ± 0.0	6.9 ± 0.6
	P	160	15.2 ± 1.1	0.62 ± 0.04	97.7 ± 0.5	1.1 ± 0.1	1.2 ± 0.4	4.5 ± 0.2
Reactor B (1000 µL)	Q	100	0.7 ± 0.0	0.4 ± 0.0	99.2 ± 0.5	0.8 ± 0.5	0.0 ± 0.0	2.5 ± 0.4
	R	120	1.0 ± 0.2	0.6 ± 0.1	99.0 ± 0.6	1.0 ± 0.6	0.0 ± 0.0	2.6 ± 0.9
	S	130	1.9 ± 0.1	1.1 ± 0.1	98.6 ± 0.1	1.4 ± 0.1	0.0 ± 0.0	2.8 ± 0.5
	T	140	3.6 ± 0.4	2.3 ± 0.2	98.7 ± 0.1	1.3 ± 0.2	0.0 ± 0.0	3.7 ± 0.1
	U	150	4.2 ± 0.6	2.6 ± 0.4	94.0 ± 0.6	2.9 ± 0.2	3.7 ± 0.6	7.0 ± 0.4
	V	160	6.0 ± 0.5	4.2 ± 0.4	93.4 ± 0.2	1.2 ± 0.1	5.4 ± 0.2	4.4 ± 0.4

[a] *Calculated based on the GC-FID relative peak area of triplicate runs of each experiment*

[b] Ketone-to-alcohol ratio in primary oxidation products that *calculated based on the GC-FID relative peak area of triplicate runs*

In both cases, conversion increased with temperature. In the case of Reactor A (62.5 μL), conversion increased from 1.2 wt/wt % at 100 °C to 15. 2 wt/wt% at 160 °C, whereas conversion increased from 0.7 wt /wt % to 6.0 wt/wt % for the oxidation performed in Reactor B (1000 μL).

Product selectivity also changed with temperature. Very little amount of addition product (~ 1 wt %) was noticed at 160 °C in Reactor A (62.5 μL reactor) at the conversion level of 15.2 wt/wt %. Whereas approximately 4 to 5 wt % of addition products were found at 150 to 160 °C in case of Reactor B (1000 μL reactor). Ketone-to-alcohol ratio remained in the range 2.5 to 7.5 but changed with temperature. For both the reactors, ketone-to-alcohol ratio increased with temperature from 100 to 150 °C, but the ketone-to-alcohol ratio dropped in both cases at 160 °C.

3.4 Discussion

3.4.1 Impact of Reactor Configuration on Hydrodynamics

Reactor configuration plays an important role to control the reactor hydrodynamics. Both the reactor size and shape influence the reactor hydrodynamics and discussed separately:

3.4.1.1 Role of Reactor Size on Reactor Hydrodynamics

Miniaturized reactor, as discussed in Introduction (Section 1), has advantages such as higher surface-to-volume ratio, and well-defined flow properties [1, 9 – 11]. Generally, smaller the reactor size higher the surface-area-to volume ratio. It would enhance higher gas-liquid interfacial area in slug flow conditions.

In this study, two miniaturized reactors of different dimensions (**Table 3.1**) were used: 62.5 μL (Reactor A) and 1000 μL (Reactor B). The Reactor A would have higher gas-liquid interfacial area compared to the reactor B. It reflected in the results of gas-liquid interfacial area (a) shown in **Tables 3.5 and 3.8.** Maximum gas-liquid interfacial area (*a*) for reactor A was 78.0 × 10^4 m^2/m^3 and for reactor B, and maximum gas-liquid interfacial area (*a*) for reactor B was14.3 × 10^4 m^2/m^3.

Moreover, smaller reactor sizes ensure better operational control over gas-liquid slug flow. It was also reflected on the formation of liquid slugs and gas bubbles (Tables 3.5 and 3.8). Reactor A ensured smaller liquid slugs of 2.9×10^{-4} m (**Table 3.5**, Series A), whereas in case of Reactor B the length of the liquid slug for the same conditions was 11.6×10^{-4} m (**Table 3.5**, Series F). Better operational control also ensured shorter gas bubbles (94.4×10^{-4} m) in smaller reactor (Reactor A) compared to gas-bubble length (331.7×10^{-4} m) obtained in Reactor B (**Table 3.5**). As the length of the gas bubble enhance the liquid film formation surrounding the gas bubbles, length of the liquid film in case of Reactor B would be higher compared to Reactor A. Liquid film formation would also increase with depth of the reactor and Reactor A (depth = 1240 μm) would have higher liquid film compared to the reactor A (depth = 85 μm). Variation in the formation of liquid slug, liquid film, and gas bubbles also resulted the variation in two-phase superficial velocity, and residence time.

Hence, the change in reactor size changed the formation of liquid slug, liquid film, and gas bubbles which resulted the variation in gas-liquid interfacial area, two-phase superficial velocity, and residence time. Reactors A and B contributed to the most important parameter, gas-liquid interfacial area (a) differently. For the Reactor A, reactor size was the more dominant to obtain the higher gas-liquid interfacial area (a). In contrast, the liquid film surrounding the gas-bubble played a significant role to obtain the gas-liquid interfacial area for Reactor B. It would have some impacts on oxygen availability and hence on oxidative conversion and product selectivity that have discussed in **Section 3.3**.

3.4.1.2 Role of Reactor Shape on Reactor Hydrodynamics

Reactor shape would also influence the reactor hydrodynamics. The reactor shape could change the shape of the liquid slug, gas bubble and more importantly mixing of oxygen within the liquid.

Two microfluidic reactors of different shapes (**Table 3.1**) were used in this study: irregular (half-elliptical) shape (Reactor A: 62.5 μL) and rectangular shape (Reactor B: 1000 μL). Reactor A has smoother bottom and two edges on top side, but rectangular shape Reactor B has four edges. Each edge would have more liquid compared to the liquid film as sketched in **Figure 3.8**. Moreover, reactor dimensions would also affect the amount of liquid within each edge. Higher dimension would have more liquid in each edge (Reactor B) compared to the smaller depth (Reactor A). Yun et al. (2010) investigated the slug flow formation in rectangular reactor and confirmed the maximum thickness (liquid in edge) and minimum thickness (film surrounding the gas bubbles) and proposed empirical relations to determine the maximum and minimum thicknesses. Our previous study of liquid phase oxidation in microfluidic reactor in a rectangular channel also confirmed the maximum and minimum thicknesses [9]. The results shown in Tables 4 and 7 confirmed maximum and minimum thicknesses and these were different for the Reactor A and Reactor B. Hence, partially smooth edges and smaller reactor dimension of Reactor A ensured more homogenous mixing of oxygen and liquid indan. But the four edges of rectangular channel and the larger liquid slug size would result inhomogeneity within the liquid edges.

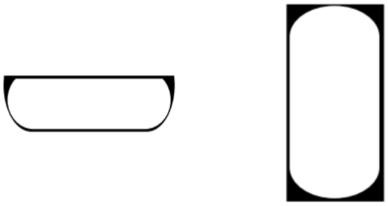

(i) Reactor: A (ii) Reactor: B

Figure 3.8: Illustration of liquid present in the edges at slug flow conditions: (i) irregular (half-elliptical) shape Reactor A and (ii) rectangular shape Reactor B.

Therefore, reactor shape would result the inhomogeneity of gas-liquid mixing within the edges of the reactors that would change the oxygen availability differently and change the oxidative conversion and product selectivity.

3.4.2 Role of Oxygen Availability on Conversion and Product Selectivity

As discussed in the previous section, the reactor size and shape influence the reactor hydrodynamic parameters differently and it would ensure oxygen availability differently. Some parts of the liquid slug (liquid film) had very high oxygen level, but other parts might not have enough oxygen availability. The variation of oxygen availability would influence oxidative conversion and product selectivity.

Due to the variation of the residence time for the different indan injection rates, conversion rates were calculated **(Table 3.10**) and plotted with oxygen availability (**Figures 3.9 and 3.10**). Conversion rates were increased with increasing gas-liquid interfacial area. The maximum conversion rates were 8.9×10^{-6} mol/s (Reactor B) and 1.4×10^{-6} mol/s (Reactor A). Conversion rate was slightly higher in reactor B compared to the Reactor A. But overall conversion was higher in reactor A compared to the reactor B.

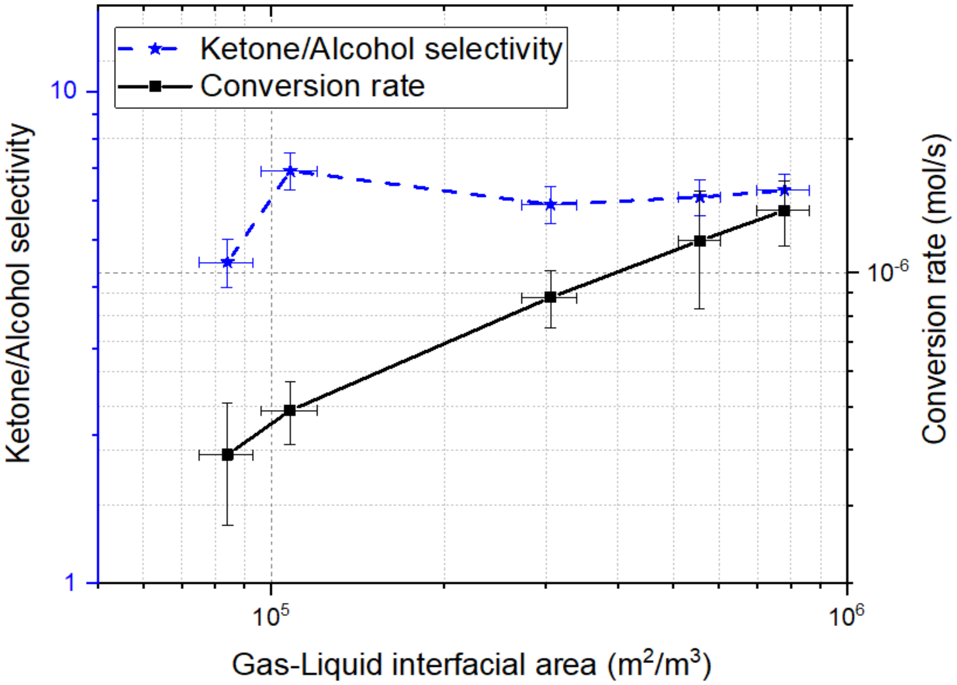

Figure 3.9: Role of oxygen availability during indan oxidation in slug flow condition in a Reactor A (62.5 µL) microfluidic reactor at 150 °C and 300 kPa absolute.

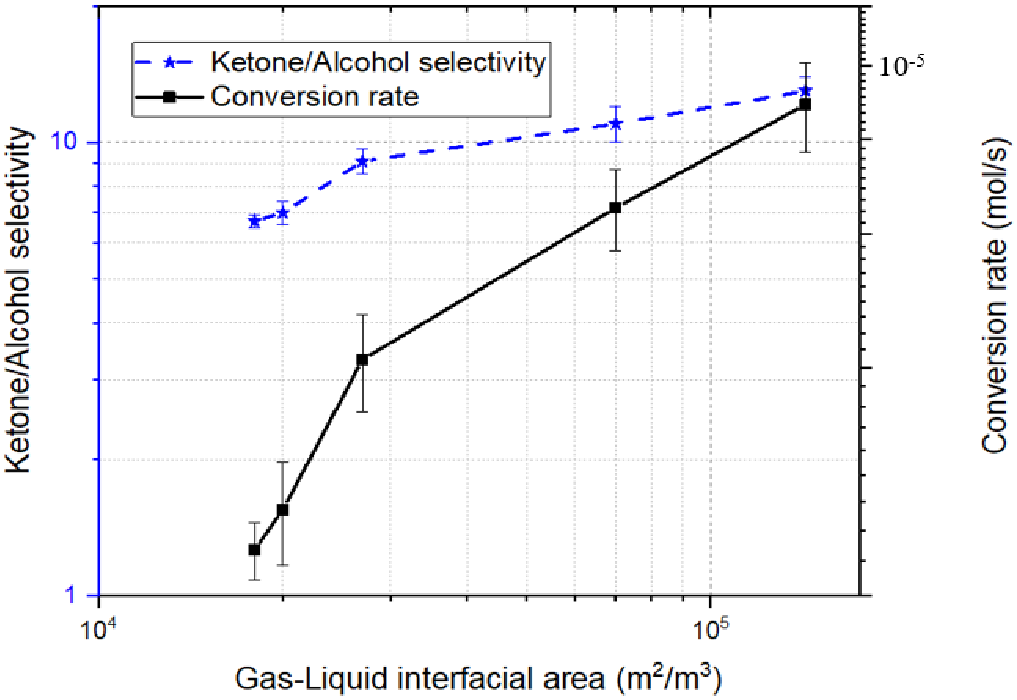

Figure 3.10: Role of oxygen availability during indan oxidation in slug flow condition in a Reactor B (1000 µL) microfluidic reactor at 150 °C and 300 kPa absolute.

Product selectivity was also changed due to the variation of oxygen availability. No addition product was noticed at the maximum oxygen availability in Reactor A (62.5 µL reactor) even at very high conversion. Whereas some addition products were noticed in case of Reactor B (1000 µL reactor). The ketone-to-alcohol selectivity in case of Reactor A was about constant in spite of changing conversion and oxygen availability (**Figure 3.9**). In contrast, the ketone-to-alcohol selectivity was enhanced with oxygen availability in case of reactor B (**Figure 3.10**). The maximum ketone-to-alcohol selectivity in primary oxidation products were higher in Reactor B (13:1, series F) compared to the Reactor A (6.3:1, Series A).

The reactors showed near constant conversion of 12 wt/wt% (Series E: Reactor A and Series F: Reactor B). At this conversion level, variation in product selectivity was also observed. Reactor A (62.5 µL reactor) showed mostly primary product with ketone-to-alcohol ratio of 4.5:1. In contrast, Reactor B (1000 µL reactor) showed secondary products, addition products, and primary product having higher ketone-to-alcohol ratio (13:1) than the Reactor A (4.5:1).

The five-member ring indan is reactive. The oxidation of indan follows the complex free radical oxidation mechanism of hydrocarbon involving initiation, propagation and termination and it is well described in literature [9, 13, 22-24]. During initiation step free radical (R˙) is formed from hydrocarbon (R-H), in propagation step the free radical reacts with oxygen to form peroxy radicals (ROO˙) which react with another hydrocarbon (R-H) to form hydroperoxide (ROOH) and another free radical (R˙). Depending on the temperature and oxygen availability different products are formed such as alcohol (R-OH), ketone (R=O), diketone (O=R=O) and dimer (R-R) in termination steps. Conversion was calculated from the amount of hydrocarbon (R-H) is participated in the reaction whereas selectivity is calculated from the product formation. For many industrial applications, it is important to reduce the addition (dimer) product selectivity and increased the ketone-to-alcohol selectivity. These two aspects are discussed separately.

3.4.2.1 Role of oxygen availability on Addition Product Selectivity

Figure 3.11 illustrate the typical addition (dimer) product formation of indan. Oxidation of indan is preferentially occurred at α-position from aromatic nucleus. Oxygen abstract H-from α-position and it could form indene by hydrogen disproportion (II) or it could form peroxy radicals (III) or both depending on the local oxygen availability. Once it formed the indene (II), the C-H bond at α-position from both the olefinic group and aromatic nucleus became more susceptible for H-abstraction and formed free radicals that could lead the addition product formation. Moreover, free radical formed could facilitate the further indan conversion. It would explain why oxidative conversion of indan was high and why it would have addition product selectivity.

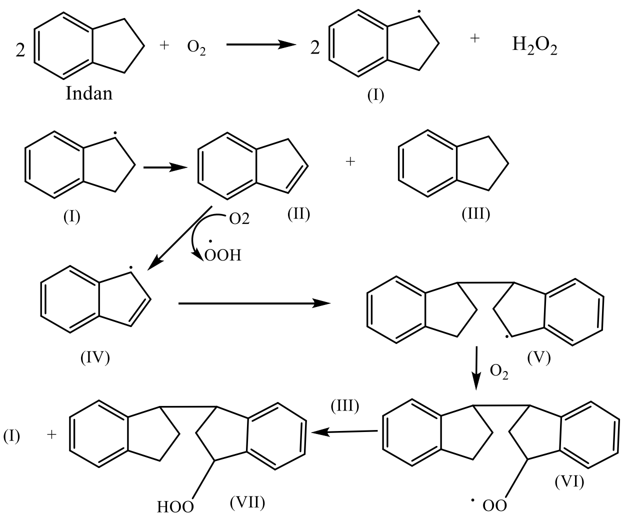

Figure 3.11: Illustration of typical addition product formation during indan oxidation.

Small reactor (Reactor A) efficiently reduced addition product selectivity. No addition products were observed in case of small reactor even at higher conversion of indan (~ 28 wt/wt %) (**Series A, Table 3.7**). At near constant conversion of 12 wt/wt% addition product selectivities were 0.1 wt/wt % (Series E: Reactor A) and 2.0 wt/wt% (Series F: Reactor B). It can be explained by few factors such as the higher gas-liquid interfacial area, smaller liquid slug size (L_S), higher two-phase velocity (U_{TP}), smoother reactor shape and the smaller reactor volume. All these factors ensured higher oxygen availability, efficient mixing in the liquid slug and surrounding liquid film. In contrast, Reactor B had higher depth (1240 μm), larger liquid slug, and importantly the corner of the reactor contained more liquid. Overall, some parts of the liquid slug (liquid film) had very high oxygen level, but other parts might not have enough oxygen availability. It could lead the addition products of 2 wt% at the conversion level of 11.5 wt/wt % (**Series F, Table 3.7**). This level of conversion of indan was reported to produce about 11 wt % of addition products during autoxidation at 130 °C at near atmospheric pressure in 6 hours in a semi-batch reactor [19]. Although the Reactor B (1000 μL) showed 2 wt% of addition product selectivity, it was much less than the corresponding addition product selectivity obtained in semi-batch reactor.

Overall, microfluidic reactor reduced the addition product selectivity. Size and shape of the microfluidic reactor affected the oxygen availability differently and hence changed the addition product selectivity differently.

3.4.2.2 Role of oxygen availability on Ketone-to-Alcohol Selectivity

Alcohol and ketone are the two main primary products in liquid phase oxidation of hydrocarbons. Typically, ketone-to-alcohol ratio in primary oxidation product is 1:1 [9, 13, 22]. But ketone-to-alcohol selectivity in primary oxidation products could change with oxygen availability and hence with the reactor hydrodynamics.

Ketone-to-alcohol selectivity in primary oxidation product was much higher (13:1) in Reactor B (**Series F**, **Table 3.7**) compared to Reactor A (6.3:1, **Series A, Table 3.7**). At near constant conversion of 12 wt/wt% ketone-to-alcohol selectivities were 4.5:1(Series E: Reactor A) and 13:1 (Series F: Reactor B). It can be explained by the corresponding conversion level during the operation. As the conversion level increased, more free radicals generated and it required more oxygen to react with alkoxy radical ($R^{\cdot}$) to produce ketone compared to alcohol (Reaction (i)). Moreover, oxygen was also required to oxidize the alcohol (Reaction (ii)) to form ketone [9, 26]. As the conversion level was much higher in Reactor A, it produced more alcohol compared to ketone and hence reduced the ketone-to-alcohol selectivity. Length of liquid film surrounding the gas bubbles was higher in case of Reactor B. It ensured the very high oxygen availability which could result the higher ketone-to-alcohol ratio (13:1).

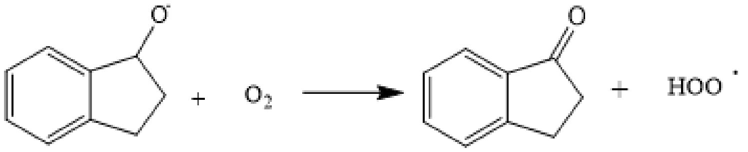

Reaction (i)

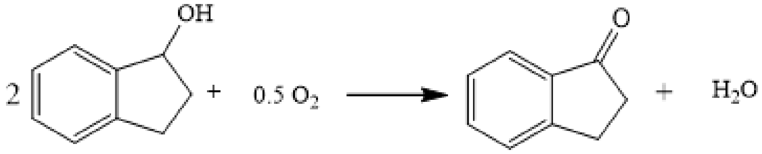

Reaction (ii)

In both reactors, ketone-to-alcohol selectivity was decreased at temperature 160 °C (Series P and Series V). It was also presented in **Figures 3.12 and 3.13.** It can be explained by the decomposition of peroxide (Reaction (iii)) formed at temperature above 150 °C [9, 22]. It would increase the free radical content and require more oxygen to produce ketone. Enough local oxygen availability would lead the formation of ketone (Reaction (i)) or in case of oxygen starvation it could form alcohol reacting with another indan molecule (Reaction (iv)).

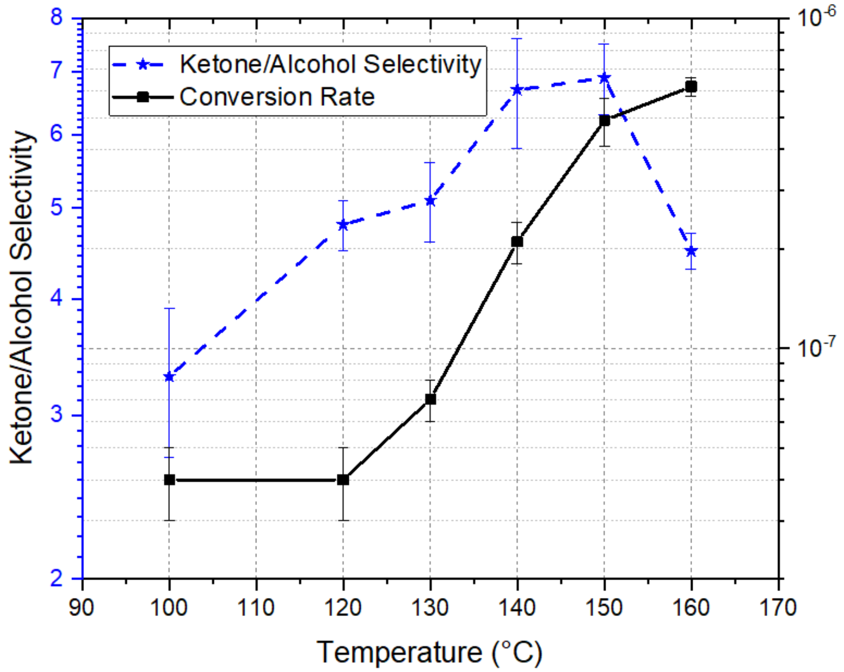

Figure 3.12: Effect of temperature on indan oxidized in slug flow condition in a Reactor A (62.5 µL) microfluidic reactor at 300 kPa absolute and indan injection rate of 7 µL/min.

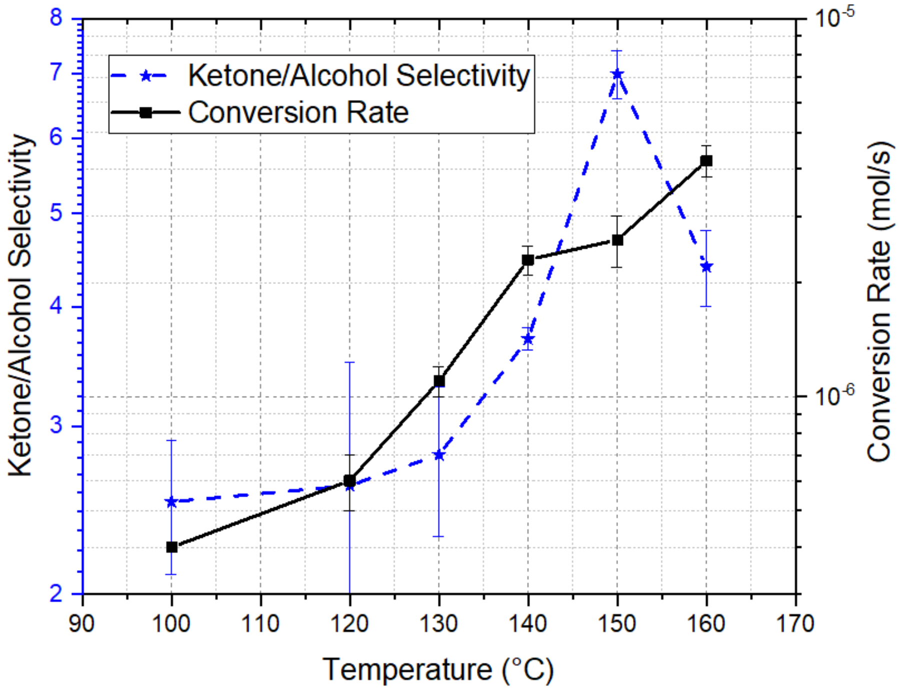

Figure 3.13: Effect of temperature on indan oxidized in slug flow condition in a Reactor B (1000 µL) microfluidic reactor at 300 kPa absolute and indan injection rate of 7 µL/min.

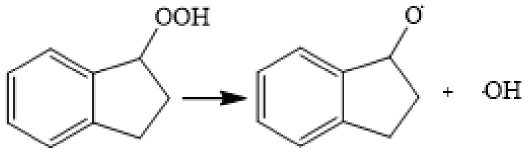

Reaction (iii)

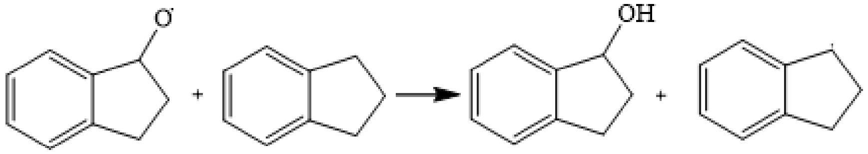

Reaction (iv)

Overall, dimension and shape of microfluidic reactors affected the oxygen availability differently and changed the ketone-to-alcohol selectivity differently.

3.4.3 Role of Reactor Hydrodynamics on Oxygen Consumption and Oxygen Replenishment

Reactor configuration influences the reactor hydrodynamic parameters that ensure oxygen availability differently which would eventually change the oxygen consumption and oxygen transportation from gas to liquid.

As described in previous Section oxygen consumed during the oxidation process and depending on the local oxygen availability product selectivity would change. Extend of oxygen consumption depends on the conversion rate and product selectivity. Increasing oxygen consumption results decrease in oxygen level in the liquid slug and increase in concentration gradient between gas phase and liquid phase. As a result, oxygen replenishment (oxygen transport) from gas phase to the liquid phase would occur. It is important to compare the rate of oxygen consumption and the rate of oxygen replenishment to ensure the presence of adequate oxygen in the liquid. Moreover, it would also confirm the assumption of using Fick's law to describe the oxygen transport in slug flow conditions.

Table 3.11 shows the rate of oxygen consumption and the rate oxygen replenishment during indan oxidation with oxygen in microfluidic reactor A (Series A-E) and reactor B (Series F-J) at 300 kPa pressure absolute and 150 °C at different indan injection rates. In all cases regardless of the minimum and maximum film thickness, oxygen consumptions were much lower compared to the maximum oxygen transportation (replenishment) rate. It ensured the presence of adequate oxygen within the liquid slug. It also validated the assumption of using Fick's law to describe the oxygen transport from the gas phase to liquid phase.

Table 3.11: Rate of oxygen consumption and oxygen replenishment during indan oxidation in microfluidic reactors at 300 kPa pressure absolute and 150 °C at different indan injection rates using oxygen as oxidizing agent.

reactors	series	flow rate (μL/min)	Oxygen consumption rate[a] (mol/m^3. s)	Maximum oxygen replenishment rate[b] (mol/m^3. s)	
				Based on minimum film thickness × 10^{-4}	Based on maximum film thickness × 10^{-2}
Reactor A (62.5 μL)	A	2	28.2	211.5	721.6
	B	3	21.6	150.8	520.3
	C	5	14.9	82.7	296.0
	D	7	10.0	29.9	104.9
	E	10	7.5	23.0	85.3
Reactor B (1000 μL)	F	2	28.5	8.8	30.7
	G	3	26.9	4.3	15.3
	H	5	18.8	1.2	4.3
	I	7	19.9	1.3	4.5
	J	10	27.7	1.2	4.3

[a] *Calculated based on the conversion & selectivity data (Table 5) considering one O for alcohol formation, two O for ketone formation (one for oxygen incorporation and another one for water formation with two hydrogen radicals), and four O for secondary product (mostly diketone) formation, five O for addition product having two functional groups*

[b] *Calculated by multiplying* liquid side volumetric mass transfer coefficient, $k_L a$, (Table 4) and maximum oxygen concentration (85.3 mol/m^3) in the gas bubbles considering zero oxygen level in liquid

Propagation and termination steps of the liquid phase oxidation are usually considered as mass transfer limited as the reaction rates of free radical reactors are very high [9, 12, 14, 22]. But the ensuring enough oxygen in the liquid slug confirmed that oxygen transportation was not limited, in other word there was not oxygen starvation in the liquid slug. The identical observation was also noted in *in situ* monitoring of oxygen transport in indan [14]. Still, little amount of addition (dimerized) product formation in the presence of adequate oxygen was formed. It could be due to the free radical cage effect.

3.4.4 Effect of Temperatures on Oxygen Availability, Conversion and Product Selectivity

The effect of temperature study was the secondary goal which would increase the reaction rate and thereby make the reaction selectivity more sensitive to differences in oxygen availability.

As anticipated, conversion rate was also increased with temperature for both the reactors (**Figures 3.12 and 3.13**). Maximum indan conversion rate were 4.2×10^{-6} mol/s (Reactor B) and 0.62×10^{-6} mol/s (Reactor A). Addition product selectivity was also varied with reactor size and temperature. For example, Series P (Reactor A at 160 °C) and Series V (Reactor B at 160 °C) showed the 1.2 wt% and 5.4 wt% of addition product selectivity, respectively. At temperature above 150 °C, the free radical content in the system increased due to break down of some peroxides formed during the oxidation [9, 19]. In addition to the explanation of the variation of oxygen availability in both reactors, the enhancement of free radical contents would also facilitate the addition product formation. However, as mentioned in last paragraph, oxygen availability ensured in microfluidic reactors suppressed addition product formation (dimerization) despite the high conversion.

The rate of oxygen consumption and the rate oxygen replenishment were also tabulated (**Table 3.12**) for the indan oxidation with oxygen in microfluidic reactor A (Series K-P) and reactor B (Series Q-V) at 300 kPa pressure absolute and different temperatures at 7 μL/min indan injection rate. As like previous case, regardless of the minimum and maximum film thickness, oxygen consumptions were much lower compared to the maximum oxygen transportation (replenishment) rate. It also ensured the presence of adequate oxygen within the liquid slug even at higher conversion rates. Moreover, assumption of using Fick's law to describe the oxygen transport from the gas phase to liquid phase was also valid for the higher conversion rates.

Table 3.12: Rate of oxygen consumption and oxygen replenishment during indan oxidation in microfluidic reactors at 300 kPa pressure absolute and different temperatures at 7 μL/min indan injection rate using oxygen as oxidizing agent.

reactors	series	temperature (°C)	Oxygen consumption rate[a] (mol/m^3. s)	Maximum oxygen replenishment rate (mol/m^3. s)	
				Based on minimum film thickness × 10^{-4}	Based on maximum film thickness × 10^{-2}
Reactor A (62.5 µL)	K	100	6.6	14.5	53.7
	L	120	8.0	17.9	63.9
	M	130	5.3	19.6	70.8
	N	140	9.4	25.6	90.4
	O	150	11.9	29.9	104.9
	P	160	15.0	34.1	122.8
Reactor B (1000 µL)	Q	100	2.4	0.7	2.8
	R	120	2.1	0.8	2.8
	S	130	3.2	0.9	3.4
	T	140	3.8	1.1	3.8
	U	150	19.2	1.3	4.5
	V	160	22.0	1.4	5.0

[a] *Calculated based on the conversion & selectivity data (Table 8) considering one O for alcohol formation, two O for ketone formation (one for oxygen incorporation and another one for water formation with two hydrogen radicals), and four O for secondary product (mostly diketone) formation, five O for addition product having two functional groups*

3.4.5 Implications of Current Research

This study shows how the engineering can be applied to control the oxidative conversion and product selectivity of a complex free radical system. The understanding from the study could be used in design and operation of liquid phase oxidation to produce fine chemicals and pharmaceuticals via oxidative pathway [9, 16, 17]. Although dimer formation via free radical addition has the detrimental impact on product selectivity, one could also view it as a potentially useful synthetic route using oxygen to produce dimers from saturated hydrocarbons under mild conditions. Moreover, the knowledge can also be applied for other free radical system to produce fuels and chemicals.

3.5 Conclusions

Liquid phase autoxidation of indan, a five-member ring naphthenic-aromatic hydrocarbon, was investigated in two microfluidic reactors to understand the impact of reactor configuration on hydrodynamics, conversion, and selectivity. The key observations and conclusions are as follows:

(a) Reactor configuration (dimensions and shape) changed the reactor hydrodynamics and influenced the oxygen availability in different ways and affected the conversion and product selectivity differently. Reactor A (62.5 μL, irregular shape) showed higher indan conversion and suppressed the addition product selectivity very well, whereas Reactor B (1000 μL, rectangular shape) showed moderate indan conversion and enhanced the ketone-to-alcohol ratio (13:1) from the typical ketone-to-alcohol ratio of 1:1.

(b) At constant temperature, pressure and near constant conversion of 12 wt/wt %, Reactor A (62.5 μL reactor) showed almost no addition products (0.1 wt/wt %), very little secondary products (0.9 wt/wt %) and mostly primary products (99 wt/wt %) with ketone-to-alcohol ratio of 4.5:1. In contrast, Reactor B (1000 μL reactor) showed secondary products (6.6 wt/wt %), addition products (2 wt/wt %), and primary product (91.4 wt/wt %) having higher ketone-to-alcohol ratio (13:1) than the Reactor A (4.5:1).

(c) The most important parameter that ensured oxygen availability was the gas-liquid interfacial area (*a*) and it manifested itself differently in reactors A and B. In case of Reactor A, the main contributor to get higher oxygen availability was the smaller reactor dimension and volume whereas the length of the liquid film surrounding the gas bubble was the main contributor to obtain the higher oxygen availability in Reactor B.

(d) Smaller liquid slug size, higher two-phase velocity (U_{TP}), smoother reactor shape and the smaller reactor volume ensured higher oxygen availability in the liquid slug and in the surrounding liquid film in case of reactor A.

(e) Comparison of the rate oxygen consumption and the rate of oxygen transformation ensured that oxygen consumption was much lower compared to the maximum oxygen transportation (replenishment) rate. It confirmed the presence of adequate oxygen within the liquid slug. It also validated the assumption of using Fick's law to describe the oxygen transport from the gas phase to liquid phase. Change in temperatures also showed similar results.

(f) The oxygen availability increased the concentration of oxygen centered free radical ($RO^{\cdot}$ or $ROO^{\cdot}$) and produced more oxygen containing functional groups and decreased the concentration of stable carbon centered free radical ($R^{\cdot}$) of naphthenic-aromatic compounds. It reduced the risk of addition product formation via hydrogen disproportion. The higher ketone formation over alcohol was due to the reaction of oxygen with oxygen center free radicals ($RO^{\cdot}$ or $ROO^{\cdot}$) and/or with alcohol (R-OH) formed during the oxidation.

(g) The study demonstrated how engineering could be used to control the chemistry. The understanding from the study could be used in design and operation of liquid phase oxidation to produce fine chemicals and pharmaceuticals.

3.6 Acknowledgements

This work was supported by the Natural Sciences and Engineering Research Council of Canada (NSERC).

3.7 Nomenclatures

a	gas-liquid interfacial area, (m^2/m^3)
D_A	diffusivity of oxygen in tetralin (m^2/s)
D_H	hydraulic diameter
FID	flame ionization detector
GC	gas chromatography
h	depth of the reactor, (m)
k_L	mass transfer coefficient; $k_L = D_A/\delta$, (m/s)
k_La	overall mass transfer coefficient, (s^{-1})
L_G	length of gas bubble, (m)
L_s	length of liquid slug, (m)

PTFE	Poly tetra fluoro ethylene
RTD	residence time distribution
S_G	surface area of gas bubble, (m^2)
U_G	superficial gas bubble velocity, (m/s)
U_L	superficial liquid slug velocity, (m/s)
U_{TP}	two phase superficial velocity, (m/s)
Vg	volume of gas bubble, (m^3)
V_L	volume of liquid slug, (m^3)
w	width of the reactor, (m)

Greek letters

δ	thickness of liquid film, (m)
ε_G	volume fraction of gas bubble
ρ_G	density of gas, (kg/m^3)
ρ_S	density of liquid, (kg/m^3)

Subscripts

b	bulk
G	gas
L	liquid
TP	two-phase

3.8 Literature Cited

1. Gemoets HPL, Su Y, Shang M, Hessel V, Luque R, Noël T (2016) Liquid phase oxidation chemistry in continuous flow microreactor. *Chem Soc Rev* 45:83–117.
2. Hone CA, Kappe CO (2019) The Use of Molecular Oxygen for Liquid Phase Aerobic Oxidations in Continuous Flow. Top Curr Chem 2: 377.
3. Vanoye L, Aloui A, Pablos M, Philippe R, Percheron A, Favre-Réguillon A, de Bellefon C (2013) A safe and efficient flow oxidation of aldehydes with O_2. Org Lett 15:5978–5981.
4. Siddiquee MN, Sivaramakrishnan K, Wu Y, De Klerk A, Nazemifard N (2018) A statistical approach dealing with multicollinearity among predictors in microfluidic reactor operation to control liquid-phase oxidation selectivity. React Chem Eng 3:972–990.
5. Sharma S, Yaminia, Das P (2019) Hydrogenation of nitroarenes to anilines in a flow reactor using polystyrene supported rhodium in a catalyst-cartridge. (Cart-Rh@PS) New J Chem 43: 1764–1769.
6. Ifran M, Glasnov TN, Kappe CO (2011) Heterogeneous catalytic hydrogenation reactions in continuous-flow reactors. Chem Sus Chem 4, 300 – 316.
7. Cantillo, D, Kappe, CO (2017) Halogenation of organic compounds using continuous flow and microreactor technology. React Chem Eng 2:7–19.
8. Karande R, Schmid A, Buehler K (2016) Applications of Multiphasic Microreactors for Biocatalytic Reactions. Org Process Res Dev *20:361-370.*
9. Siddiquee MN, De Klerk A, Nazemifard N (2016) Application of microfluidics to enhance gas-liquid mass transfer during selective oxidation of hydrocarbons. React Chem Eng 1:418–435.
10. Hartman RL, McMullen JP, Jensen KF (2011) Deciding whether to go with the flow – evaluating the merits of flow reactors for synthesis. Angew Chemie Int Ed 50:7502–7519.
11. Leclerc A, Alame M, Schweich D, Pouteau P, Delattreb C, de Bellefon C (2008) Gas–liquid selective oxidations with oxygen under explosive conditions in a micro-structured reactor. Lab Chip 8:814–817.
12. Suresh AK, Sharma MM, Sridhar T (2000) Engineering aspects of industrial liquid-phase air oxidation of hydrocarbon. Ind Eng Chem Res 39:3958–3997.

13. De Klerk A (2003) Continuous- mode thermal oxidation of Fischer-Tropsch waxes. Ind Eng Chem Res 42:6545–6548.
14. Siddiquee MN, De Klerk A (2016) *In situ* measurement of liquid Phase oxygen during oxidation. Ind Eng Chem Res 55:6607–6618.
15. Dimitratos N, Lopez-Sanchez JA, Hutchings GJ (2014) Supported metal nanoparticles in liquid-phase oxidation reactions. In: Duprez D, Cavani F (Eds) Handbook of Advanced Methods and Processes in Oxidation Catalysis: From Laboratory to Industry, Imperial College Press, London 631–678.
16. Snead DR, Jamison TF (2015) A three-minute synthesis and purification of ibuprofen: pushing the limits of continuous-flow processing. Angew Chem Int Ed 54:1521–3773.
17. Gutmann B, Cantillo D, Kappe CO (2015) Continuous-flow technology—A tool for the safe manufacturing of active pharmaceutical ingredients *Angew Chem Int Ed 54:*6688–6729.
18. Hobbs CC, Drew EH, Van't Hof HA, Mesich FG, Onore MJ (1972) Mass transfer rate-limitation effects in liquid-phase oxidation. Ind Eng Chem Prod Res Develop 11:220–225.
19. Siddiquee MN, De Klerk A (2014) Hydrocarbon addition reactions during low temperature autoxidation of oilsands bitumen. Energy Fuels 28:6848–6859.
20. Siddiquee MN, De Klerk A (2015) Heterocyclic addition reactions during low temperature autoxidation. Energy Fuels 29*:*4236–4244.
21. Yun J, Lei Q, Zhang S, Shen S, Yao K (2010) Slug flow characteristics of gas-miscible liquids in a rectangular microchannel with cross and T-shaped junctions. Chem Eng Sci 65:5256–5263.
22. Emanuel MN, Denisov ET, Maizus ZK (1967) Liquid-phase oxidation of hydrocarbons. Plenum Press, New York.
23. Sheldon RA, Kochi JK (1981) Metal-Catalyzed Oxidations of Organic Compounds. Academic Press, New York.
24. Twigg GH (1954) The mechanism of liquid-phase oxidation. Chem Eng Sci Suppl 8:5–16.
25. Jiayu L, Wanghua C, Liping C, Yingtao T, Xin S (2012) Thermal decomposition analysis and safety study on di-tert-butyl peroxide. Procedia Eng 43:312–317.

26. Tolman CA, Druliner JD, Nappa MJ, Herron N (1989) Alkane oxidation studies in du Pont's central research department. In: Hill CL (ed) Activation and Functionalization of Alkanes, Wiley, New York.
27. Dietz WA (1967) Response factors for gas chromatographic analyses. J Chromatogr Sci 5: 68-71.
28. Diaz M, Vega A, Coca J (1987) Correlation for the estimation of gas-liquid diffusivity. Chem Eng Com 52: 271-281.
29. Vandu CO, Liu H, Krishna R (2005) Mass transfer from Taylor bubbles rising in single capillaries. Chem Eng Sci 60: 6430-6437.

Chapter 4: Comparative Study of Tetralin Oxidation in Microfluidic and Batch Reactor

In this chapter, we discuss the comparison of liquid phase oxidation of Tetralin, a naphthenic-aromatic hydrocarbon in microfluidic and batch reactor. The work is part of a published paper "A statistical approach dealing with multicollinearity among predictors in microfluidic reactor operation to control liquid-phase oxidation selectivity" on Reaction Chemistry and Engineering.

Abstract

Liquid phase oxidation in a microfluidic reactor is advantageous to manipulate conversion rate and product selectivity. At constant temperature and pressure, the parameters that affect the outputs are gas-liquid interfacial area (*a*), length of oxygen gas bubble (L_G), length of liquid slug (L_S), two-phase superficial velocity (U_{TP}) and liquid flowrate to the reactor (Q). The objective of this study was to compare the oxidation conversion rate and product selectivity obtained in tetralin oxidation in microfluidic and batch reactor. The study shows using microfluidics reactor, one can achieve order of magnitude of increase in product selectivity compared to that in batch reactor due to increasing gas-liquid interfacial area.

4.1 Introduction

Liquid phase oxidation of hydrocarbons is industrially important to produce petrochemicals [1–3]. The main challenge of the non-catalytic free radical oxidation is to achieve good product selectivity. Industrially the non-catalytic liquid phase oxidation is performed at low conversion to control the product selectivity, for example, oxidation of cyclohexane [4]. Oxidation product selectivity depends on conversion, temperature, and oxygen availability in the liquid phase [5–8]. Liquid phase oxidation follows initiation, propagation, and termination steps. Once the free radical (R·) is formed during the initiation step, it reacts with local oxygen or other free radicals very fast following zero order kinetics [5,9]. Oxygen transfer to the liquid phase and oxygen

A version of this chapter was published partly as "A statistical approach dealing with multicollinearity among predictors in microfluidic reactor operation to control liquid-phase oxidation selectivity. React. Chem. Eng., 2018, 3, 972-990.".

availability in the liquid phase are critically important to control the product selectivity. Microfluidic reactor, also known as microreactor, is advantageous to ensure higher local oxygen availability. The main advantages of such a miniaturized reactor are: (i) the higher surface-area-to volume ratio that facilitate the improved mass and heat transfer in the liquid phase; (ii) the exact control of the gas to liquid ratio in the reactor that facilitate the manipulation of gas-liquid interfacial area; and (iii) the well-defined flow properties in the microstructure reactor [5,10,11]. These advantages caused the microfluidic reactor to receive attention in the study of liquid phase oxidation. The flow regime in a microchannel depends on the relative gas and liquid properties, flow rates and channel geometry. The five main flow regimes are: bubble, slug, churn, slug annular and annular [5,12,13]. Slug flow, also known as Taylor flow, has its unique hydrodynamic characteristics, where two adjacent liquid slugs are separated by the gas bubbles and are connected only via a thin liquid film [5,10–13]. This thin liquid film contributes to create a higher gas-liquid interfacial area and hence improves oxygen availability. Taylor flow also has a Marangoni effect within the liquid slug, which is the mass transfer along the gas-liquid interface driven by gradient of the surface tension. The convection caused by Marangoni effect is beneficial not only to ensure local oxygen availability by proper mixing but also to bring the surface active oxygenates to the liquid phase to prevent over oxidation at the gas-liquid interface [5,10,11]. Of the parameters that influence oxygen availability, it was not clear which ones affect it the most, in a hydro-dynamically complex Taylor flow system. Oxygen availability at a constant pressure depended on several parameters such as gas-liquid interfacial area (a) based on unit cell volume (volume of gas bubble and liquid slug), the film attached to the wall, length of liquid slug (L_S), length of gas bubble (L_G), two-phase superficial velocity (U_{TP}), and liquid flowrate to the reactor (Q) [5]. Small changes in the design of the microfluidic reactor and its operation could dramatically affect the relationship between these different parameters. Mass transfer in Taylor flow can be explained well by the Film Theory [5,10]. The gaseous component, oxygen in our case, is transferred to the liquid phase where it is consumed during the reaction. Works on mass transport at Taylor flow conditions have been well documented in literature, but the most cases focused on simulation and/or experiments considering water as the liquid at ideal conditions (no gas consumption) [11–17]. Few liquid phase oxidation studies at Taylor flow conditions are reported which dealt mainly with conversion enhancement, but mass transfer characteristics were not discussed [18–22]. In our previous oxidation study, a qualitative description of the mass transport effects on oxidative conversion and product selectivity was provided [5]. However, the quantitative dependency of the parameters affecting the mass transport, oxidative conversion and product selectivity were not deeply analyzed.

4.2 Experimental

4.2.1 Materials

Tetralin, 1,2,3,4-tetrahydronaphthalene (99 % purity, Sigma-Aldrich, Canada), was used to perform experimental validation of the regression model. 1,2,3,4-tetrahydro-1-naphthol (alcohol of tetralin) and α-tetralone (ketone of tetralin) were used to identify the products by using an GC-MS (gas chromatography-mass spectrometry). The internal standard in GC-FID (gas chromatography with a flame ionization detector) analysis for conversion calculation was hexachlorobenzene (99 %, analytical standard, Supleco). Chloroform (98 %, HPLC grade, Fischer Scientific) was used as a solvent for GC-MS and GC-FID analyses. Extra dry oxygen (99.6 molar purity) was purchased from Praxair Inc., Edmonton, Canada and was used as an oxidizing agent. Nitrogen (99.999 molar purity) was purchased from Praxair Inc., Edmonton, Canada and used inert to control backpressure.

Properties of oxygen and tetralin for all the reported conditions are reported in **Table 4.1**.

Table 4.1: Physicochemical properties of tetralin and oxygen at different experimental conditions

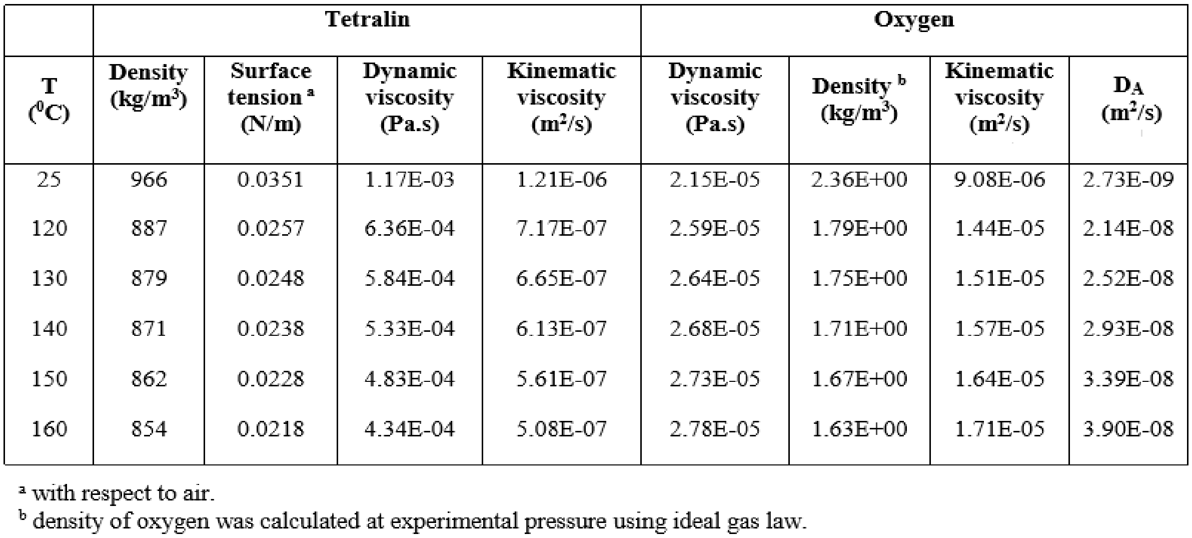

	Tetralin				**Oxygen**			
T (^{0}C)	**Density (kg/m^3)**	**Surface tension ^{a} (N/m)**	**Dynamic viscosity (Pa.s)**	**Kinematic viscosity (m^2/s)**	**Dynamic viscosity (Pa.s)**	**Density ^{b} (kg/m^3)**	**Kinematic viscosity (m^2/s)**	**D_A (m^2/s)**
25	966	0.0351	1.17E-03	1.21E-06	2.15E-05	2.36E+00	9.08E-06	2.73E-09
120	887	0.0257	6.36E-04	7.17E-07	2.59E-05	1.79E+00	1.44E-05	2.14E-08
130	879	0.0248	5.84E-04	6.65E-07	2.64E-05	1.75E+00	1.51E-05	2.52E-08
140	871	0.0238	5.33E-04	6.13E-07	2.68E-05	1.71E+00	1.57E-05	2.93E-08
150	862	0.0228	4.83E-04	5.61E-07	2.73E-05	1.67E+00	1.64E-05	3.39E-08
160	854	0.0218	4.34E-04	5.08E-07	2.78E-05	1.63E+00	1.71E-05	3.90E-08

[a] with respect to air.
[b] density of oxygen was calculated at experimental pressure using ideal gas law.

4.2.2 Equipment and Procedure

4.2.2.1 Oxidation in a Microfluidic Reactor

A glass rectangular microfluidic reactor (Dolomite Microfluidics, Charlestown, MA, USA) was used in this study to validate the predicted conversion and selectivities. The reactor volume was 1000 μl having a mixing channel of depth=1240 μm, width= 161 μm, length= 536 mm and a reaction channel of depth=1240 μm, width= 391 μm, length= 1844 mm). It had three inlet ports and one outlet port. Oxygen and tetralin were injected into the reactor using fluid input 1 and fluid input port 2, respectively, and port 3 was blocked. The hydraulic diameter of the reaction channel was d_H=6.0×10^{-4} m and aspect ratio of the reaction channel of width/depth was 0.32.

The microfluidic experimental setup (**Figure 4.1**) consisted of a microfluidic reactor (Dolomite Microfluidics, Charlestown, MA, USA), syringe pump (KDS-210, KD Scientific, USA), oxygen and nitrogen gas cylinders (Praxair Inc., Edmonton, Canada), pressure transducer (Swagelok, Canada), gas flow meter (Swagelok, Canada), pressure bomb (Swagelok, Canada), and backpressure regulator (Swagelok, Canada), Heidolph MR Hei-Standard hot plate (Model: 505-20000-01-2, Heldolph Instruments, Germany), a surface mounted thermocouple (Model: CO 1, Cement-on Thermocouple, Omega Engineering, Inc., USA), a Flea3FL3-U3-13E4M camera (Point Grey Research Inc., Canada), a Fiber–Lite lamp (Model: 3100, Dolan-Jenner Industries, Inc., USA), and PTFE tubing, 1/16″ OD x 0.8 mm ID (Dolomite Microfluidics, Charlestown, MA, USA).

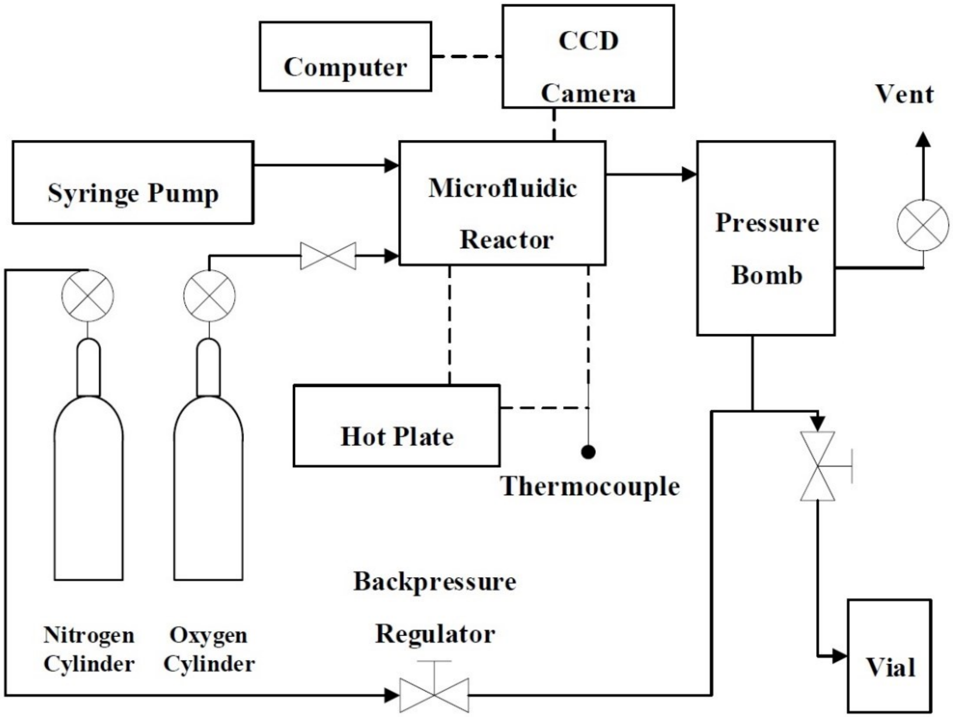

Figure 4.1: Schematic of microfluidic experiment Setup

Oxidations were performed maintaining Taylor flow conditions at 150 °C and an average pressure of 90 kPa gauge to control product selectivity. In Taylor flow conditions, tetralin slugs were separated by elongated oxygen bubbles. The detail experimental procedure of oxidation in microfluidic reactor was provided in Chapter 3. Briefly, in a typical experiment, tetralin was loaded into a five mL syringe and the system was pressurized to 90 kPa gauge by flowing oxygen through the system. Tetralin was then allowed to flow through the system at a specific flowrate (2, 4, 7 or 12 μL/min) by using a syringe pump. The co-feed of tetralin and oxygen and application of backpressure using a backpressure regulator and nitrogen gas facilitated the gas-liquid slug formation. A digital camera mounted above the microfluidic reactor was used to monitor the flow patterns of the gas and liquid during the experiment. The experiments were conducted for twenty minutes. The system was then depressurized and the oxidized tetralin was collected from the pressure vessel using a needle valve and stored for the instrumental analyses. Acetone was used to flush the reactor after each experiment followed by nitrogen flow to dry the system. Experiment was repeated three times and liquid slugs and gas bubbles of different sizes were obtained. Hydrodynamic parameters, mass transfer characteristics and oxygen availability were calculated by taking ten different slugs and gas bubbles from each experiment. The liquid phase products from each experiment was analyzed by a gas chromatograph and oxidative conversion and product selectivity were calculated from the triplicate gas chromatographic analyses.

4.2.2.2 Oxidation in a Batch Reactor

The oxidation was performed in a batch reactor at different gas-liquid interfacial area (*a*) to understand the effect of gas-liquid interfacial area (*a*) without two-phase velocity (U_{TP}). A 25-ml batch reactor (**Figure 4.2**) was used to conduct the experiments. The reactor, manufactured from 316 standard stainless steel and Swagelok fittings and tubing, was equipped with a thermocouple and a pressure gauge to monitor the operating temperature and pressure, respectively. Four different amounts of tetralin (2, 5, 10 and 15 ml) were first charged into the batch reactor, and then oxygen was introduced into the reactor to obtain four different gas-liquid interfacial areas (*a*). The operating temperature and the operating pressure were at 150 °C and 191 kPa respectively. The reactor was then submerged into a temperature controlled preheated sand-bath heater (Model: FSB-3, Omega Engineering, Inc., USA) to control the oxidation temperature. Residence times were 75 s, 100s and 135 s after reaching internal temperature within 1 °C of the heater temperature. The heat-up time required to reach an internal temperature within 1 °C of the heater temperature was six minutes. At the end of oxidation, the reactor was removed from sand bath heater and allowed to cool for 10 minutes. The reactor surface was cleaned to remove the sand. The reactor was then depressurized, and liquid oxidation products were collected for chromatographic analyses to calculate oxidative conversion and product selectivity.

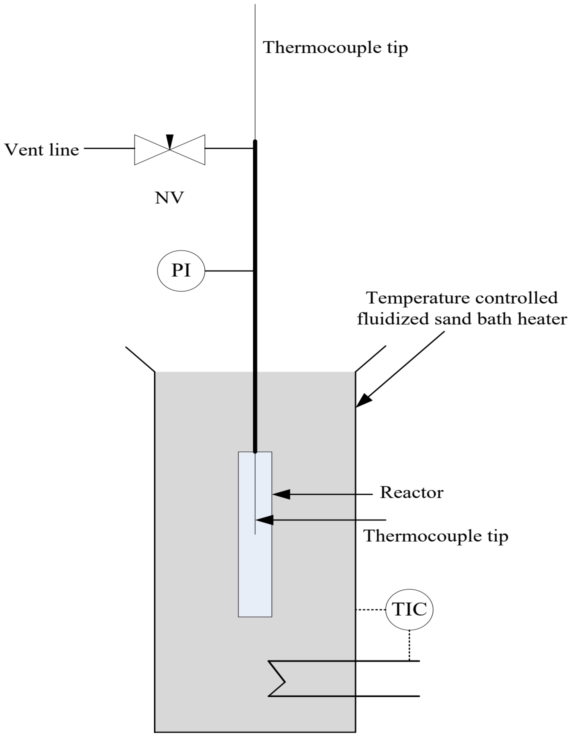

Figure 4.2: Batch reactor setup used in oxidation experiments

4.2.2.3 GC Analyses

An Agilent GC-FID (Agilent 7890A GC system) equipped with DB-5 MS column 30 m × 0.25 mm × 0.25 µm column was used for quantitative analysis. The injector temperature of GC was 250 °C and the split ratio was 10:1. Helium was used as a carrier gas which flowed through column at a constant flowrate of 2 mL/min during the experiments. Oven temperature was varied throughout the experiments. Initially, the oven temperature was 75 °C which was kept constant for 0.5 minutes and then temperature was raised from 75 °C to 325 °C at a rate of 20 °C/min, and finally, the temperature was kept constant at 325 °C for 5 minutes. HPLC grade chloroform was used for sample preparation and hexachlorobenzene was used as an internal standard.

Oxidation products were classified as primary (alcohol and ketones of tetralin), secondary (products contain more than one ketone and/or alcohol functional groups) and addition products (products contain at least a dimer having different functional groups).

GC-FID chromatograms of tetralin oxidized at 150 °C in a microfluidic reactor are shown in **Figure 4.3** to illustrate the ketone-to-alcohol selectivity in primary oxidation product.

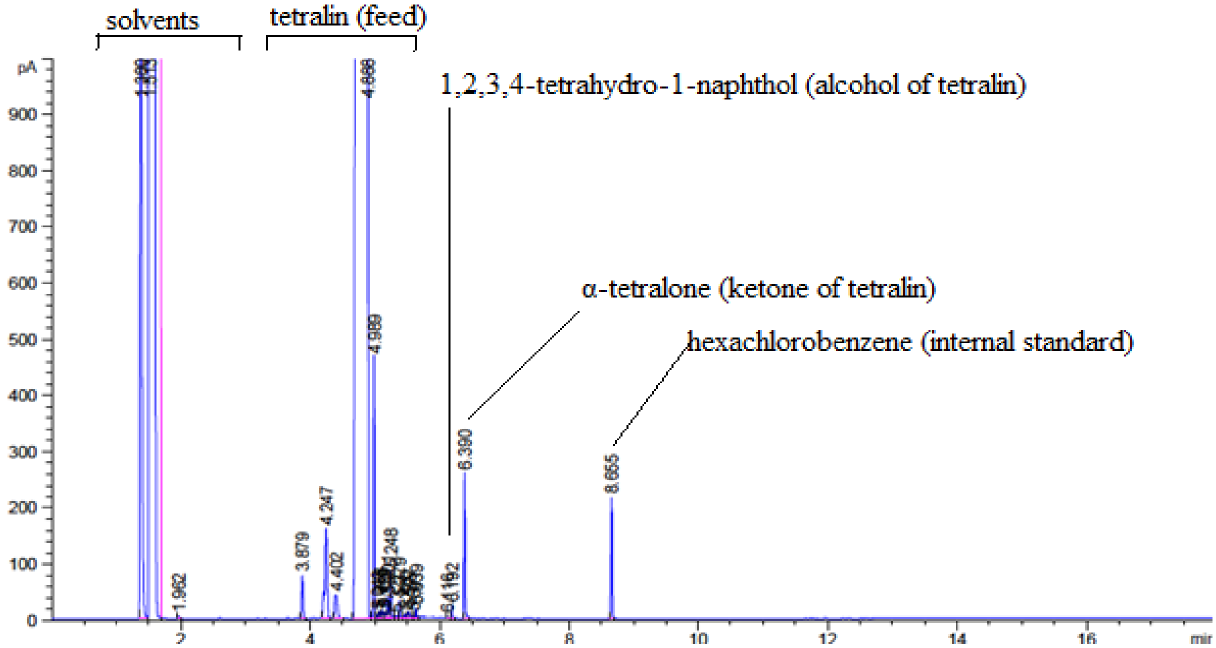

Figure 4.3: Typical GC-FID chromatogram of tetralin oxidized at 150 °C in a microfluidic reactor at gas-liquid interfacial area

4.2.3 Calculations

Different hydrodynamic parameters and mass transfer coefficients were calculated from the images captured during experiments in microfluidic reactor.

(d) a (gas liquid interfacial area per unit liquid slug volume) was calculated from the dimension of the rectangular channel reactor (h × w) and image analysis of gas bubbles and liquid slugs.

Surface area of gas bubble: $S_G = 2\left(wL_{G,actual} + hL_{G,actual}\right) + 4\pi\left((w+h)/4\right)^2$ (i)

$$L_{G,actual} = L_G - (w+h)/2 \qquad \text{(ii)}$$

Volume of liquid slug: $V_L = whL_S + wh[(w+h)/2] - (4/3)\pi[(w+h)/4]^3$ (iii)

Gas liquid interfacial area per unit liquid slug volume, $a = S_G/V_L$ (iv)

Here, S_G is the surface of the gas bubble, L_G and L_S are the lengths of the gas bubble and liquid slug respectively, and w and h are the width and depth of the reactor channel, respectively.

Approximated radius of the cap of liquid slug, $r_{cap}= (w+h)/4$ (v)

Since geometry formed by the two liquid caps is not a complete sphere the approximation was made.

(e) U_L (superficial liquid slug velocity) and U_G (gas bubble velocity) were calculated from the distance travelled by the slug and bubble in a particular time. Two phase superficial velocity (U_{TP}) was calculated as follows:

$$U_{TP} = \varepsilon_G U_G + (1-\varepsilon_G)U_L \qquad \text{(vi)}$$

Here, the volume fraction of gas bubble: $\varepsilon_G = \frac{V_G}{V_G+V_L}$ (vii)

V_L is the volume of liquid slug was calculated according to equation (v).

V_G is the volume of gas bubble:

$$V_G = whL_{G,actual} + (4/3)\pi((w+h)/4)^2 \qquad \text{(viii)}$$

(f) Average residence time: The two-phase superficial velocity (U_{TP}) was divided by the reactor length to calculate the average residence time.

(g) δ (liquid film thickness surrounding a gas bubble) by using the correlations provided by Yun et al. (2010) for a rectangular microchannel reactor as follows [17]:

$$\frac{\delta_{\max}}{D_h} = 0.39\, We^{0.09} \qquad \text{(ix)}$$

$$\frac{\delta_{\min}}{D_h} = 0.02\, We^{0.62} \qquad \text{(x)}$$

Here, Weber number, $We = \frac{D_h U_T^2 \rho_l}{\sigma_l}$ (xi)

Hydraulic diameter of the channel (m), $D_h = 2[wh/(w+h)]$ (xii)

$\delta_{\max}$ and $\delta_{\min}$ are the maximum and minimum thicknesses of the liquid film (m), respectively.

U_{TP} (m/s) is the two-phase superficial gas velocity, ρ_l is the density of liquid and σ_l is the surface tension of liquid (N/m).

w and h are the width and depth of the reactor channel, respectively.

(h) $k_L a$ (volumetric mass transfer coefficient, s^{-1}) was calculated from k_L and a. Film theory was applied to calculate k_L [5, 23] as follows:

$$k_L = \frac{D_A}{\delta} \qquad \text{(xiii)}$$

Here, D_A is the diffusivity of oxygen in tetralin, δ is the thickness of liquid film surrounding the oxygen bubble.

$k_{L(max)}a$ and $k_{L(min)}a$ were based on the equations (ix) and (x), respectively.

(i) Gas-liquid interfacial area (a) in batch reactor was calculated by dividing the cross-sectional area of the batch reactor by volume of liquid used in the reactor.

Calculation of conversion and product selectivity from GC analysis:

(j) Product selectivity was obtained from the relative peak area of the products as follows [5]:

$$\text{Product selectivity (\%)} = \frac{\text{relative peak area of specific product}}{\text{sum of relative peak area of all the products}} \times 100 \qquad \text{(xiv)}$$

Ketone-to-alcohol selectivity in primary oxidation products was calculated by dividing ketone selectivity and alcohol selectivity.

(k) Tetralin conversion was calculated by using GC-FID response factor. Response factors of the products are listed in **Table 4.2**.

Table 4.2: FID response factors of various compounds

Compound Name	Retention Time (minute)	Response factor (RF)
Heptane	1.72	1.00 ± 0.00
$CHCl_3$	1.52	0.09 ± 0.01
Hexachlorobenzene	8.67	0.32 ± 0.01
Tetralin	4.90	1.08 ± 0.01
1,2,3,4-tetrahydro-1-naphthol	6.35	0.82 ± 0.02
alpha-tetralone	6.51	0.84 ± 0.01

For the conversion less than 1 (wt/wt %), the tetralin conversion was calculated based on the formation of products. A conversion factor was calculated using the data obtained from oxidation of tetralin with air conducted in a semi-batch reactor (**Table 4.3**) [5] Conversion factor was multiplied by sum of relative peak areas of product area to get the conversion. Conversion factor was selected based on the sum of product area.

Table 4.3: Conversion data for oxidation of tetralin with air at 130 °C conducted in a semi-batch reactor.[5]

Time	conversion	sum of oxidized products	conversion factor
30 min	0.8	214.8	0.0035
1 hr	1.1	643.3	0.0017
2 hr	2.1	1128.1	0.0019
4 hr	4.5	2922.5	0.0015
6 hr	6.9	4628.7	0.0015

4.4 Results and Discussion

4.4.1 Analyzing Data to validate the results obtained from previous study

In a microfluidic reactor of rectangular geometry, liquid is presented as the thin film attached to the wall and as the liquid slug (**Figure 4.3**). Of these, the film attached to the wall has more contribution in gas-liquid interfacial area calculation comparing to the liquid present in the slug. In previous study, typically, gas-liquid interfacial area was in the order of 10^5 m^2/m^3 for film attached to the wall and in the order of 10^3 m^2/m^3 for the liquid slug (Experiment A: **Table 4.4**). Although it was not possible to calculate the separate contribution of liquid film itself in conversion rate and selectivity (sample collected at the end of the experiment and analyzed by GC), it would have great influence on the outputs. The experimental data in previous study for tetralin oxidation in a microfluidic reactor is listed in **Table 4.4**.

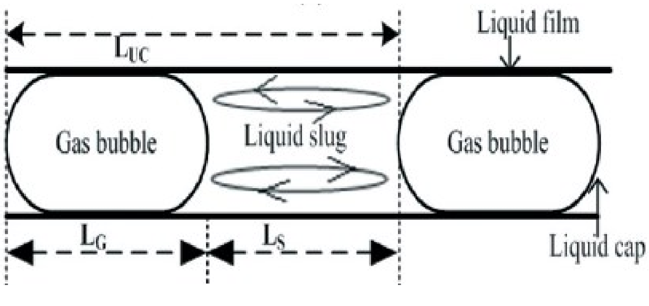

Figure 4.4: Typical Taylor flow (slug flow) in a microfluidic reactor representing to represent length of gas (oxygen) bubble (L_G), length of liquid (tetralin) slug (L_S), unit cell length (L_{UC}), liquid film and liquid cap. Liquid can circulate within the liquid slug (Marangoni effect). [5]

Table 4.4: Experimental data for tetralin oxidation in a microfluidic reactor. [a]

Series	T (^{0}C)	Q[b] (μL/min)	L_S (m)	L_G (m)	U_{TP} (m/s)	t_R (min)	a (m^2/m^3)	k_La (s^{-1})	Conversion rate (mol/s)	Selectivity [c]
A	150	1	0.0016	0.21	0.026	1.5	300000	1900	5.95×10^{-07}	14
B	150	3	0.0027	0.098	0.021	1.8	150000	960	1.40×10^{-07}	7
C	150	5	0.0049	0.051	0.02	2	62000	390	1.03×10^{-07}	1.6
D	150	10	0.0043	0.011	0.016	2.4	16000	100	5.99×10^{-08}	1.3
E	150	15	0.0049	0.004	0.011	3.5	5400	34	5.14×10^{-08}	1.3

[a] Data obtained from our previous study [5]

[b] Inlet tetralin flowrate into the reactor

[c] Ketone-to-alcohol selectivity in primary oxidation products

Table 4.5 reported the measured length of gas bubble, gas-liquid interfacial area, conversion, conversion rate and production selectivity of liquid phase oxidation of tetralin in the microfluidics reactor.

Table 4.5: Experimental data of the tetralin oxidation in a microfluidic reactor at 150°C and 191 kPa.

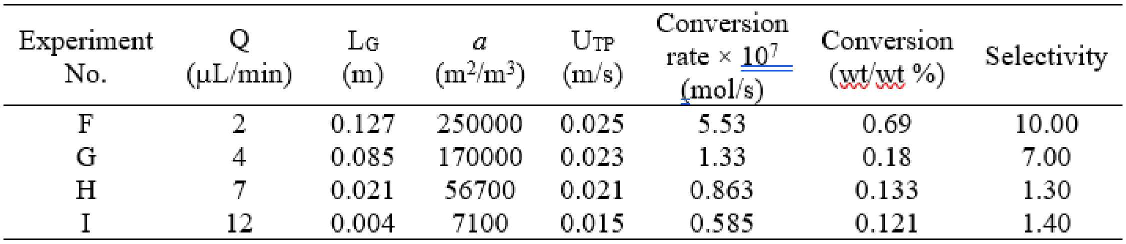

Experiment No.	Q (μL/min)	L_G (m)	a (m^2/m^3)	U_{TP} (m/s)	Conversion rate × 10^7 (mol/s)	Conversion (wt/wt %)	Selectivity
F	2	0.127	250000	0.025	5.53	0.69	10.00
G	4	0.085	170000	0.023	1.33	0.18	7.00
H	7	0.021	56700	0.021	0.863	0.133	1.30
I	12	0.004	7100	0.015	0.585	0.121	1.40

In previous study, the injection rate is ranging from 1 μL/min to 15 μL/min. The conversion rate decreases from 5.95×10^{-7} mol/s to 0.514×10^{-7} mol/s and length of bubble decreases from

0.21m to 0.004m. Gas-liquid interfacial area decreases from 300000 m^2/m^3 to 5400 m^2/m^3. The product selectivity (ketone to alcohol ratio) decreases from 14 to 1.3.

In current study, as tetralin feed rate increases from 2 µL/min to 12 µL/min, the conversion rate decreases from 5.53×10^{-7} mol/s to 0.585×10^{-7} mol/s. Length of gas bubble decreases from 0.127m to 0.004m. Gas-liquid interfacial area decreases from 250000 m^2/m^3 to 7100 m^2/m^3. The product selectivity (ketone to alcohol ratio) decreases from 10 to 1.4. The value of conversion rate, length of gas bubble, gas-liquid interfacial area, and ketone to alcohol ratio is aligned with the result obtained from previous study.

4.4.2 Analyzing Batch Reactor Data to Understand the Effect of Interfacial area

The oxidation conducted in the batch reactor at different gas-liquid interfacial area (*a*) to analyze the role of gas-liquid interfacial area (*a*) in the absence of liquid and gas velocity. Four Different interfacial areas (*a*) were obtained by using 2, 5, 10 and 15 ml tetralin while keeping the reactor volume (25 ml) and oxygen pressure constant.

Table 4.6 shows the conversion and selectivity of tetralin oxidized at 150 °C and 191 kPa in a batch reactor. The gas-liquid interfacial area (*a*) were 173, 69, 35, 23 m^2/m^3, respectively, for the 2, 5, 10 and 15 ml of tetralin. The conversion rates were in the range of $1.6 \times 10^{-7} – 5.2 \times 10^{-7}$ mol/s which could be considered as near constant within the experimental error. The selectivity was changed in the range of 1.55 to 2.33. The highest selectivity (2.33) was obtained at the interfacial area of 173 m^2/m^3 and the lowest selectivity (1.55) was achieved at 23 m^2/m^3 where conversion rates were 4.2×10^{-7} mol/s (Experiment J: **Table 4.6**) and 5.2×10^{-7} mol/s (Experiment S: **Table 4.6**), respectively. The conversion rates were near constant, but the selectivity was different. It indicated the role of gas-liquid interfacial (*a*) to change the selectivity in the absence of two-phase velocity (U_{TP}).

Table 4.6: Conversion and selectivity for the tetralin oxidation in a batch reactor at 150 °C and 191 kPa with different gas-liquid volume and residence time.

experiment No.	volume of tetralin (ml)	gas interfacial area (m^2/m^3)	residence time (s)	conversion (wt/wt %)	conversion rate × 10^7 (mol/s)	selectivity (ketone-to-alcohol in primary oxidation products)
J	2	173	75	0.24	4.18	2.33
K	2	173	100	0.19	2.48	2.33
L	2	173	135	0.16	1.55	2.27
M	5	69	75	0.10	4.35	2.00
N	5	69	100	0.13	4.24	2.14
O	5	69	135	0.12	2.90	1.95
P	10	35	75	0.05	4.35	1.64
Q	10	35	100	0.07	4.57	1.76
R	10	35	135	0.07	3.39	1.79
S	15	23	75	0.04	5.22	1.55
T	15	23	100	0.05	4.90	1.65
U	15	23	135	0.05	4.35	1.78

By comparing the conversion rate of the batch reactor with microfluidic reactor in the range of $1.6 \times 10^{-7} – 5.2 \times 10^{-7}$ mol/s, selectivity was in the range 7 – 10 (in microfluidic reactor, **Table 4.5**) whereas in the batch reactor it varied within 1.55 to 2.33. It also showed the effect of gas-liquid interfacial (*a*). The main reason would be the higher gas liquid interfacial area obtained in Taylor flow in a microfluidic reactor ensure higher oxygen for the local free radicals to facilitate the selective product formation.[5] Therefore, regardless of the reactor, batch or microfluidic, interfacial area greatly affect the conversion and selectivity.

4.5 Conclusions

An comparison study of tetralin oxidation in a microfluidic reactor and batch reactor has been conducted to evaluate conversion rate and oxidation product selectivity with variables like gas-liquid interfacial area (*a*), length of gas bubble (L_G), length of liquid slug (L_S), two-phase superficial velocity (U_{TP}) and tetralin flowrate to the reactor (Q). Key findings were:

a) Liquid phase oxidation in a microfluidic reactor is advantageous to manipulate conversion rate and product selectivity.
b) Gas-liquid interfacial area (*a*) was the most important parameter that affect the conversion rate and oxidation product selectivity.

c) Gas-liquid interfacial area (a) influenced the conversion and selectivity regardless of the reactor type, batch or microfluidic. In case of Taylor flow in a microfluidic reactor.

4.6 Nomenclatures

a	gas-liquid interfacial area, (m^2/m^3)
CR	Conversion rate, mol/s
D_A	diffusivity of oxygen in tetralin (m^2/s)
d_H	hydraulic diameter; $d_H = 2[wh/(w+h)]$, (m)
FID	flame ionization detector
GC	gas chromatography
h	depth of the reactor, (m)
k_L	mass transfer coefficient; $k_L = D_A/\delta$, (m/s)
$k_L a$	overall mass transfer coefficient, (s^{-1})
L_G	length of gas bubble, (m)
L_S	length of liquid slug, (m)
Q	tetralin flow rate to the reactor, μL/min.
S_G	surface area of gas bubble, (m^2)
U_G	superficial gas bubble velocity, (m/s)
U_L	superficial liquid slug velocity, (m/s)
U_{TP}	two phase superficial velocity, (m/s)
V_G	volume of gas bubble, (m^3)
V_L	volume of liquid slug, (m^3)
w	width of the reactor, (m)
We	Weber number; $We = D_h U_{TP}^2 \rho_L/\sigma_L$

Greek letters

δ	thickness of liquid film, (m)
ε_G	volume fraction of gas bubble
ρ_G	density of gas, (kg/m^3)
ρ_l	density of liquid, (kg/m^3)

G	gas
L	liquid
TP	two-phase

4.7 Literature Cited

1. G. Centi, F. Cavani, F. Trifiro, Selective Oxidation by Heterogenous Catalysis, Kluwer/Plenum, New York, 2001. doi:10.1007/s13398-014-0173-7.2.

2. A.K. Suresh, M.M. Sharma, T. Sridhar, Engineering aspects of industrial liquid-phase air oxidation of hydrocarbons, Ind. Eng. Chem. Res. 39 (2000) 3958–3997. doi:10.1021/ie0002733.

3. M.G. Clerici, O.A. Kholdeeva, Liquid Phase Oxidation via Heterogeneous Catalysis, John Wiley & Sons, Inc., Hoboken, New Jersey, 2013. doi:10.1002/9781118356760.

4. I. Hermans, J. Peeters, P.A. Jacobs, Autoxidation of hydrocarbons: From chemistry to catalysis, Top. Catal. 50 (2008) 124–132. doi:10.1007/s11244-008-9099-7.

5. M.N. Siddiquee, A. de Klerk, N. Nazemifard, Application of microfluidics to control product selectivity during non-catalytic oxidation of naphthenic-aromatic hydrocarbons, React. Chem. Eng. 1 (2016) 418–435. doi:10.1039/C6RE00010J.

6. A. De Klerk, Continuous-Mode Thermal Oxidation of Fischer-Tropsch Waxes, Ind. Eng. Chem. Res. 42 (2003) 6545–6548. doi:10.1021/ie030293f.

7. V. Govindan, A.K. Suresh, Modeling liquid-phase cyclohexane oxidation, Ind. Eng. Chem. Res. 46 (2007) 6891–6898. doi:10.1021/ie070365t.

8. M.N. Siddiquee, A. de Klerk, In Situ Measurement of Liquid Phase Oxygen during Oxidation, Ind. Eng. Chem. Res. 55 (2016) 6607–6618. doi:10.1021/acs.iecr.6b00949.

9. N.M. Emanuel, E. Denisov, Z.K. Maizus, Liquid-Phase Oxidation of Hydrocarbons, Plenum Press, New York, 1967.

10. H.P.L. Gemoets, Y. Su, M. Shang, V. Hessel, R. Luque, T. Noël, Liquid phase oxidation 30 chemistry in continuous-flow microreactors, Chem. Soc. Rev. 45 (2016) 83–117. doi:10.1039/C5CS00447K.

11. P. Sobieszuk, J. Aubin, R. Pohorecki, Hydrodynamics and mass transfer in gas-liquid flows in microreactors, Chem. Eng. Technol. 35 (2012) 1346–1358. doi:10.1002/ceat.201100643.

12. A. Günther, S.A. Khan, M. Thalmann, F. Trachsel, K.F. Jensen, Transport and reaction in microscale segmented gas–liquid flow, Lab Chip. 4 (2004) 278–286. doi:10.1039/B403982C.

13. K.A. Triplett, S.M. Ghiaasiaan, S.I. Abdel-Khalik, D.L. Sadowski, Gas–liquid two-phase flow in microchannels Part I: two-phase flow patterns, Int. J. Multiph. Flow. 25 (1999) 377–394. doi:10.1016/S0301-9322(98)00054-8.

14. C. Yao, Z. Dong, Y. Zhao, G. Chen, An online method to measure mass transfer of slug fl ow in a microchannel, Chem. Eng. Sci. 112 (2014) 15–24. doi:10.1016/j.ces.2014.03.016.

15. J. Yue, L. Luo, Y. Gonthier, G. Chen, Q. Yuan, An experimental study of air – water Taylor flow and mass transfer inside square microchannels, Chem. Eng. Sci. 64 (2009) 3697–3708. doi:10.1016/j.ces.2009.05.026.

16. D.M. Fries, F. Trachsel, P.R. Von Rohr, International Journal of Multiphase Flow Segmented gas – liquid flow characterization in rectangular microchannels, Int. J. Multiph. Flow. 34 (2008) 1108– 1118. doi:10.1016/j.ijmultiphaseflow.2008.07.002.

17. J. Yun, Q. Lei, S. Zhang, S. Shen, K. Yao, Slug flow characteristics of gas-miscible liquids in a rectangular microchannel with cross and T-shaped junctions, Chem. Eng. Sci. 65 (2010) 5256–5263. doi:10.1016/j.ces.2010.06.031.

18. R. Jevtic, P.A. Ramachandran, M.P. Dudukovic, Capillary reactor for cyclohexane oxidation with oxygen, Chem. Eng. Res. Des. 88 (2010) 255–262. doi:10.1016/i.cherd.2009.12.008.

19. A. Leclerc, M. Alam, D. Schweich, P. Pouteau, C. De Bellefon, Gas – liquid selective oxidations with oxygen under explosive conditions in a micro-structured reactor, Lab Chip. 8 (2008) 814– 817. doi:10.1039/b717985e.

20. J. Fischer, T. Lange, R. Boehling, A. Rehfinger, E. Klemm, Uncatalyzed selective oxidation of liquid cyclohexane with air in a microcapillary reactor, Chem. Eng. Sci. 65 (2010) 4866–4872. doi:10.1016/j.ces.2010.05.028.

21. L. Vanoye, A. Aloui, M. Pablos, R. Philippe, A. Percheron, A. Favre-Reguillon, C. De Bellefon, A Safe and Efficient Flow Oxidation of Aldehydes with O 2, Org. Lett. 15 (2013) 5978–5981. doi:10.1021/ol401273k.

22. M. Hamano, K.D. Nagy, K.F. Jensen, Continuous flow metal-free oxidation of picolines using air, Chem. Commun. 48 (2012) 2086–2088. doi:10.1039/c2cc17123f. [23] X. Yan, S. Xiaogang, Simple Linear Regression, in: Linear Regres. Anal. Theory Comput., World Scientific, 2009: pp. 9–39.

23. Gemoets HPL, Su Y, Shang M, Hessel V, Luque R, Noël T (2016) Liquid phase oxidation chemistry in continuous flow microreactor. *Chem Soc Rev* 45:83–117.

Chapter 5: Conclusion

5.1 Introduction

Liquid phase oxidation is an industrially important process to produce many chemicals, for instance, petrochemicals and pharmaceuticals. However, the key challenge of this free radical oxidation process involving initiation, propagation, and termination is to control the product selectivity. Currently, the industry follows a low-conversion process to control the selectivity. Microfluidic reactors have the advantage of improved heat and mass transfer due to the higher surface area-to-volume ratio, better mixing because of small radial diffusion and internal circulation in liquid slug in case of Taylor flow, well-defined flow properties, exact control of gas-liquid ratio and enhanced safety for using pure oxygen. All these characteristics make the microfluidic reactors suitable for the study of liquid phase oxidation. The focus of the thesis is to study the role of oxygen availability, to compare the microfluidic reactor performance with semi-batch reactor, to study the effect of microfluidic reactor configuration (size and shape) and to study the effect of temperature on liquid phase oxidation of naphthenic-aromatic hydrocarbon. The understanding from the study can be applied in design and operation of industrial units to control the conversion and product selectivity of a complex free radical system.

5.2 Significance, Major Conclusions and Key Insights

The important conclusions derived from the research in the thesis are provided as following.

(a) Liquid phase oxidation in a microfluidic reactor is advantageous to manipulate conversion rate and product selectivity.

(b) Reactor dimensions and volume changed the reactor hydrodynamics and influenced the oxygen availability in different ways and affected the conversion and product selectivity differently. It was observed that reactor with smaller size had higher oxidation conversion and suppressed the addition product selectivity, whereas large reactor had moderate conversion and enhanced ketone-to-alcohol product selectivity.

(c) The most important parameter that ensured oxygen availability was the gas-liquid interfacial area. The contributor to get higher oxygen availability could either be smaller reactor dimension and volume or increased length of the liquid film surrounding the gas bubble.

(d) The oxygen availability increased the concentration of oxygen centered free radical ($RO^{\cdot}$ or $ROO^{\cdot}$) and produced more oxygen containing functional groups, and decreased the concentration of stable carbon centered free radical ($R^{\cdot}$) of naphthenic-aromatic compounds. It reduced the risk of addition product formation via hydrogen disproportion. The higher ketone formation over alcohol was due to the reaction of oxygen with oxygen center free radicals ($RO^{\cdot}$ or $ROO^{\cdot}$) and/or with alcohol (R-OH) formed during the oxidation.

(e) Gas-liquid interfacial area influenced the oxidation conversion and selectivity regardless of the reactor type, semi-batch or microfluidic.

(f) The study demonstrated how engineering could be used to control the chemistry. The understanding from the study could be used in design and operation of liquid phase oxidation to produce fine chemicals and pharmaceuticals.

5.3 Future Work

A list of suggestions of future work are provided here for further research in the field.

- Direct measurement of hydrodynamic properties during liquid phase oxidation in a microfluidic reactor. Current research, as observed in Chapter 3 and Chapter 4, shows a significant impact of gas-liquid interfacial on oxidation product conversion and selectivity. However, the correlation used to calculate the hydrodynamic properties such as thin film thickness and gas-liquid interfacial area introduce large error bars. Therefore, it is suggested to achieve direct measurement of those properties using high-resolution microscope or in-channel sensor to improve measurement accuracy.
- Effect of oxygenate on liquid phase naphthenic-aromatic hydrocarbon oxidation. Oxygenate such as ketone and alcohol could be produced as intermediate or final products according to specific reaction path. This work would help understand how different concentrations of oxygenate could impact the reaction path, oxidation product conversion, and selectivity.

- Effect of changing surface wettability of reactor channel from hydrophilic to hydrophobic. Current research uses glass microfluidic reactors to conduct liquid phase hydrocarbon oxidation. Liquid hydrocarbon flows near the channel wall surrounding the oxygen bubble. Changing the surface wettability would change the gas-liquid interfacial and thus impact the product conversion and selectivity. Polydimethylsiloxane (PDMS) reactor could be used to understand the wettability effect on liquid phase hydrocarbon oxidation.
- Investigation on oxidation of diluted bitumen using microfluidic reactor. In the study of indan oxidation in a microfluidic reactor, it shows that microfluidic reactor has the potential to control product selectivity while surpassing formation of addition product. Due to the complex nature of bitumen, oxidation product of bitumen is usually composed of wide range of products. The additional work would provide understanding of how microfluidic reactor could help improve oxidation product selectivity of bitumen while minimizing unwanted addition product. The high viscosity bitumen should be diluted with toluene or benzene to allow flows in a microfluidic reactor.

5.4 Publications and Presentations

A list of publications and presentations provided in the following is related to the work done in the current research.

1. Siddiquee M. N., Sivaramakrishnan K., **Wu Y.**, De Klerk. A and Nazemifard N. A statistical approach dealing with multicollinearity among predictors in microfluidic reactor operation to control liquid-phase oxidation selectivity. *React. Chem. Eng.*, **2018**, 3, 972-990.

2. **Wu Y.**, Siddiquee M. N., De Klerk. A and Nazemifard N. Microfluidics to investigate temperature effect on liquid phase oxidation of naphthenic-aromatic hydrocarbons. [Presented at the 68th Canadian Chemical Engineering Conference (CSChE), **2018,** Toronto, ON, Canada]

3. Siddiquee M. N., **Wu Y.**, and Nazemifard N. Comparative study of liquid-phase autoxidation of indan in microfluidic reactors. The 23rd International Conference on Miniaturized Systems for Chemistry and Life Sciences (MicroTAS), **2019,** Basel, Switzerland. (Poster)

4. Siddiquee M. N., **Wu Y.**, De Klerk. A and Nazemifard N. The impact of microfluidic reactor configuration on hydrodynamics, conversion, and selectivity during indan oxidation. (*Accepted by Journal of Flow Chemistry*)

Bibliography

- Gemoets HPL, Su Y, Shang M, Hessel V, Luque R, Noël T (2016) Liquid phase oxidation chemistry in continuous flow microreactor. Chem Soc Rev 45:83–117.
- Hone CA, Kappe CO (2019) The Use of Molecular Oxygen for Liquid Phase Aerobic Oxidations in Continuous Flow. Top Curr Chem 2: 377.
- Vanoye L, Aloui A, Pablos M, Philippe R, Percheron A, Favre-Réguillon A, de Bellefon C (2013) A safe and efficient flow oxidation of aldehydes with O2. Org Lett 15:5978–5981.
- Siddiquee MN, Sivaramakrishnan K, Wu Y, De Klerk A, Nazemifard N (2018) A statistical approach dealing with multicollinearity among predictors in microfluidic reactor operation to control liquid-phase oxidation selectivity. React Chem Eng 3:972–990.
- Sharma S, Yaminia, Das P (2019) Hydrogenation of nitroarenes to anilines in a flow reactor using polystyrene supported rhodium in a catalyst-cartridge. (Cart-Rh@PS) New J Chem 43: 1764–1769.
- Ifran M, Glasnov TN, Kappe CO (2011) Heterogeneous catalytic hydrogenation reactions in continuous-flow reactors. Chem Sus Chem 4, 300 – 316.
- Cantillo, D, Kappe, CO (2017) Halogenation of organic compounds using continuous flow and microreactor technology. React Chem Eng 2:7–19.
- Karande R, Schmid A, Buehler K (2016) Applications of Multiphasic Microreactors for Biocatalytic Reactions. Org Process Res Dev 20:361-370.
- L. Kiwi-Minsker and A. Renken, Microstructured reactors for catalytic reactions, Catal. Today, 2005, 110, 2–14.
- J. J. Lerou, A. L. Tonkovich, L. Silva, S. Perry and J. McDaniel, Microchannel reactor architecture enables greener processes, Chem. Eng. Sci. 2010, 65, 380–385.
- D. Wilms, J. Klos and H. Frey, Microstructured reactors for polymer synthesis: a renaissance of continuous flow processes for Tailor-Made macromolecules? Macromol. Chem. Phys., 2008, 209, 343–356.
- G. Chen, Q. Yuan, H. Li and S. Li, CO selective oxidation in a microchannel reactor for PEM fuel cell, Chem. Eng. J., 2004, 101, 101–106.
- Suresh AK, Sharma MM, Sridhar T (2000) Engineering aspects of industrial liquid-phase air oxidation of hydrocarbon. Ind Eng Chem Res 39:3958–3997.

- De Klerk A (2003) Continuous- mode thermal oxidation of Fischer-Tropsch waxes. Ind Eng Chem Res 42:6545–6548.
- Siddiquee MN, De Klerk A (2016) In situ measurement of liquid Phase oxygen during oxidation. Ind Eng Chem Res 55:6607–6618.
- Dimitratos N, Lopez-Sanchez JA, Hutchings GJ (2014) Supported metal nanoparticles in liquid-phase oxidation reactions. In: Duprez D, Cavani F (Eds) Handbook of Advanced Methods and Processes in Oxidation Catalysis: From Laboratory to Industry, Imperial College Press, London 631–678.
- Snead DR, Jamison TF (2015) A three-minute synthesis and purification of ibuprofen: pushing the limits of continuous-flow processing. Angew Chem Int Ed 54:1521–3773.
- Gutmann B, Cantillo D, Kappe CO (2015) Continuous-flow technology—A tool for the safe manufacturing of active pharmaceutical ingredients Angew Chem Int Ed 54:6688–6729.
- C. D. Pina, E. Falletta and M. Rossi, Liquid phase oxidation of organic compounds by supported metal-based catalysts with a focus on gold. In Liquid Phase Oxidation via Heterogeneous Catalysis: Organic Synthesis and Industrial Applications, First Edition; M. G. Clerici and O. A. Kholdeeva, Eds.; Wiley: Hoboken, 2013, 221–262.
- G. Centi and S. Perathoner, Selective oxidation— industrial. In Encyclopedia of Catalysis; Wiley, 2002.
- Hermans, J. Peeters and P. A. Jacobs, Autoxidation of Hydrocarbons: From Chemistry to Catalysis, Top Catal. 2008, 50, 124–132.
- N. M. Sánchez and A. de Klerk, Autoxidation of aromatics, App. Petro. Res., 2018, 8, 55–78.
- M. N. Siddiquee, A. de Klerk and N. Nazemifard, Application of microfluidics to enhance gas-liquid mass transfer during selective oxidation of hydrocarbons. React. Chem. Eng., 2016, 1, 418–435.
- N. M. Emanuel, E. T. Denisov, and Z. K. Maizus, Liquidphase oxidation of hydrocarbons; Plenum Press: New York, 1967.
- de Klerk, Continuous- mode thermal oxidation of Fischer-Tropsch waxes, Ind. Eng. Chem. Res., 2003, 42, 6545–6548.
- P. V. Danckwerts, Gas-Liquid Reactions; McGraw-Hill: New York, 1970.

- F. Kaštánek, J. Zaharadnǐk, J. Kratochvǐl and J. Čermák, Chemical Reactors for Gas-Liquid Systems, 1st ed.; Ellis Horwood: West Sussex, 1993.
- E. L. Cussler. Diffusion: Mass Transfer in Fluid Systems, 3rd ed.; Cambridge University Press: Cambridge, 2009.
- L. K. Doraiswamy and D. Üner, Chemical Reaction Engineering, Beyond the Fundamentals; CRC Press: Boca Raton, 2014.
- K. Suresh, T. Sridhar and O. E. Potter, Autocatalytic oxidation of cyclohexane− mass transfer and chemical reaction. AIChE J., 1988, 34(1), 81–93.
- M. N. Siddiquee, K. Sivaramakrishnan, Y. Wu, A. de Klerk and N. Nazemifard, A statistical approach dealing with multicollinearity among predictors in microfluidic reactor operation to control liquid-phase oxidation selectivity. React. Chem. Eng., 2018, 3,972–990.
- P. Tabeling, Introduction to Microfluidics. Oxford, U.K., OUP Oxford, 2005.
- K. F. Jensen, "Silicon-based microchemical systems: Characteristics and applications." Mrs Bulletin 31(2): 101-107, 2006.
- G. M. Whitesides, E. Ostuni, S. Takayama, X. Jiang and D. E. Ingber. "Soft Lithography in Biology and Biochemistry." Annual Review of Biomedical Engineering 3(1): 335-373, 2001.
- R. Gupta, D. F. Fletcher and B. S. Haynes, "Taylor Flow in Microchannels: A Review of Experimental and Computational Work." The Journal of Computational Multiphase Flows 2(1): 1-31, 2010.
- K. A. Triplett, S. M. Ghiaasiaan, S. I. Abdel-Khalik and D. L. Sadowski, "Gas-liquid two-phase flow in microchannels part I: Two-phase flow patterns." International Journal of Multiphase Flow 25(3): 377-394, 1999.
- H. Song, J. D. Tice and R. F. Ismagilov, "A Microfluidic System for Controlling Reaction Networks in Time." Angewandte Chemie International Edition 42(7): 768-772, 2003.
- R. Jevtic, P. A. Ramachandran and M. P. Dudukovic. Capillary reactor for cyclohexane oxidation with oxygen, Chem. Eng. Res. Des., 2010, 88, 255–62.
- U. Neuenschwander and K. F. Jensen, Olefin autoxidation in flow, Ind. Eng. Chem. Res., 2014, 53(2), 601–608.
- Gemoets HPL, Su Y, Shang M, Hessel V, Luque R, Noël T (2016) Liquid phase oxidation chemistry in continuous flow microreactor. *Chem Soc Rev* 45:83–117.

- Hone CA, Kappe CO (2019) The Use of Molecular Oxygen for Liquid Phase Aerobic Oxidations in Continuous Flow. Top Curr Chem 2: 377.
- Vanoye L, Aloui A, Pablos M, Philippe R, Percheron A, Favre-Réguillon A, de Bellefon C (2013) A safe and efficient flow oxidation of aldehydes with O_2. Org Lett 15:5978–5981.
- Siddiquee MN, Sivaramakrishnan K, Wu Y, De Klerk A, Nazemifard N (2018) A statistical approach dealing with multicollinearity among predictors in microfluidic reactor operation to control liquid-phase oxidation selectivity. React Chem Eng 3:972–990.
- Sharma S, Yaminia, Das P (2019) Hydrogenation of nitroarenes to anilines in a flow reactor using polystyrene supported rhodium in a catalyst-cartridge. (Cart-Rh@PS) New J Chem 43: 1764–1769.
- Ifran M, Glasnov TN, Kappe CO (2011) Heterogeneous catalytic hydrogenation reactions in continuous-flow reactors. Chem Sus Chem 4, 300 – 316.
- Cantillo, D, Kappe, CO (2017) Halogenation of organic compounds using continuous flow and microreactor technology. React Chem Eng 2:7–19.
- Karande R, Schmid A, Buehler K (2016) Applications of Multiphasic Microreactors for Biocatalytic Reactions. Org Process Res Dev *20:361-370.*
- Siddiquee MN, De Klerk A, Nazemifard N (2016) Application of microfluidics to enhance gas-liquid mass transfer during selective oxidation of hydrocarbons. React Chem Eng 1:418–435.
- Hartman RL, McMullen JP, Jensen KF (2011) Deciding whether to go with the flow – evaluating the merits of flow reactors for synthesis. Angew Chemie Int Ed 50:7502–7519.
- Leclerc A, Alame M, Schweich D, Pouteau P, Delattreb C, de Bellefon C (2008) Gas–liquid selective oxidations with oxygen under explosive conditions in a micro-structured reactor. Lab Chip 8:814–817.
- Suresh AK, Sharma MM, Sridhar T (2000) Engineering aspects of industrial liquid-phase air oxidation of hydrocarbon. Ind Eng Chem Res 39:3958–3997.
- De Klerk A (2003) Continuous- mode thermal oxidation of Fischer-Tropsch waxes. Ind Eng Chem Res 42:6545–6548.
- Siddiquee MN, De Klerk A (2016) *In situ* measurement of liquid Phase oxygen during oxidation. Ind Eng Chem Res 55:6607–6618.

- Dimitratos N, Lopez-Sanchez JA, Hutchings GJ (2014) Supported metal nanoparticles in liquid-phase oxidation reactions. In: Duprez D, Cavani F (Eds) Handbook of Advanced Methods and Processes in Oxidation Catalysis: From Laboratory to Industry, Imperial College Press, London 631–678.
- Snead DR, Jamison TF (2015) A three-minute synthesis and purification of ibuprofen: pushing the limits of continuous-flow processing. Angew Chem Int Ed 54:1521–3773.
- Gutmann B, Cantillo D, Kappe CO (2015) Continuous-flow technology—A tool for the safe manufacturing of active pharmaceutical ingredients *Angew Chem Int Ed 54:*6688–6729.
- Hobbs CC, Drew EH, Van't Hof HA, Mesich FG, Onore MJ (1972) Mass transfer rate-limitation effects in liquid-phase oxidation. Ind Eng Chem Prod Res Develop 11:220–225.
- Siddiquee MN, De Klerk A (2014) Hydrocarbon addition reactions during low temperature autoxidation of oilsands bitumen. Energy Fuels 28:6848–6859.
- Siddiquee MN, De Klerk A (2015) Heterocyclic addition reactions during low temperature autoxidation. Energy Fuels 29*:*4236–4244.
- Yun J, Lei Q, Zhang S, Shen S, Yao K (2010) Slug flow characteristics of gas-miscible liquids in a rectangular microchannel with cross and T-shaped junctions. Chem Eng Sci 65:5256–5263.
- Emanuel MN, Denisov ET, Maizus ZK (1967) Liquid-phase oxidation of hydrocarbons. Plenum Press, New York.
- Sheldon RA, Kochi JK (1981) Metal-Catalyzed Oxidations of Organic Compounds. Academic Press, New York.
- Twigg GH (1954) The mechanism of liquid-phase oxidation. Chem Eng Sci Suppl 8:5–16.
- Jiayu L, Wanghua C, Liping C, Yingtao T, Xin S (2012) Thermal decomposition analysis and safety study on di-tert-butyl peroxide. Procedia Eng 43:312–317.
- Tolman CA, Druliner JD, Nappa MJ, Herron N (1989) Alkane oxidation studies in du Pont's central research department. In: Hill CL (ed) Activation and Functionalization of Alkanes, Wiley, New York.
- Dietz WA (1967) Response factors for gas chromatographic analyses. J Chromatogr Sci 5: 68-71.
- Diaz M, Vega A, Coca J (1987) Correlation for the estimation of gas-liquid diffusivity. Chem Eng Com 52: 271-281.

- Vandu CO, Liu H, Krishna R (2005) Mass transfer from Taylor bubbles rising in single capillaries. Chem Eng Sci 60: 6430-6437.
- G. Centi, F. Cavani, F. Trifiro, Selective Oxidation by Heterogenous Catalysis, Kluwer/Plenum, New York, 2001. doi:10.1007/s13398-014-0173-7.2.
- A.K. Suresh, M.M. Sharma, T. Sridhar, Engineering aspects of industrial liquid-phase air oxidation of hydrocarbons, Ind. Eng. Chem. Res. 39 (2000) 3958–3997. doi:10.1021/ie0002733.
- M.G. Clerici, O.A. Kholdeeva, Liquid Phase Oxidation via Heterogeneous Catalysis, John Wiley & Sons, Inc., Hoboken, New Jersey, 2013. doi:10.1002/9781118356760.
- Hermans, J. Peeters, P.A. Jacobs, Autoxidation of hydrocarbons: From chemistry to catalysis, Top. Catal. 50 (2008) 124–132. doi:10.1007/s11244-008-9099-7.
- M.N. Siddiquee, A. de Klerk, N. Nazemifard, Application of microfluidics to control product selectivity during non-catalytic oxidation of naphthenic-aromatic hydrocarbons, React. Chem. Eng. 1 (2016) 418–435. doi:10.1039/C6RE00010J.
- De Klerk, Continuous-Mode Thermal Oxidation of Fischer-Tropsch Waxes, Ind. Eng. Chem. Res. 42 (2003) 6545–6548. doi:10.1021/ie030293f.
- V. Govindan, A.K. Suresh, Modeling liquid-phase cyclohexane oxidation, Ind. Eng. Chem. Res. 46 (2007) 6891–6898. doi:10.1021/ie070365t.
- M.N. Siddiquee, A. de Klerk, In Situ Measurement of Liquid Phase Oxygen during Oxidation, Ind. Eng. Chem. Res. 55 (2016) 6607–6618. doi:10.1021/acs.iecr.6b00949.
- N.M. Emanuel, E. Denisov, Z.K. Maizus, Liquid-Phase Oxidation of Hydrocarbons, Plenum Press, New York, 1967.
- H.P.L. Gemoets, Y. Su, M. Shang, V. Hessel, R. Luque, T. Noël, Liquid phase oxidation 30 chemistry in continuous-flow microreactors, Chem. Soc. Rev. 45 (2016) 83–117. doi:10.1039/C5CS00447K.
- P. Sobieszuk, J. Aubin, R. Pohorecki, Hydrodynamics and mass transfer in gas-liquid flows in microreactors, Chem. Eng. Technol. 35 (2012) 1346–1358. doi:10.1002/ceat.201100643.
- Günther, S.A. Khan, M. Thalmann, F. Trachsel, K.F. Jensen, Transport and reaction in microscale segmented gas–liquid flow, Lab Chip. 4 (2004) 278–286. doi:10.1039/B403982C.

- K.A. Triplett, S.M. Ghiaasiaan, S.I. Abdel-Khalik, D.L. Sadowski, Gas–liquid two-phase flow in microchannels Part I: two-phase flow patterns, Int. J. Multiph. Flow. 25 (1999) 377–394. doi:10.1016/S0301-9322(98)00054-8.
- Yao, Z. Dong, Y. Zhao, G. Chen, An online method to measure mass transfer of slug fl ow in a microchannel, Chem. Eng. Sci. 112 (2014) 15–24. doi:10.1016/j.ces.2014.03.016.
- J. Yue, L. Luo, Y. Gonthier, G. Chen, Q. Yuan, An experimental study of air – water Taylor flow and mass transfer inside square microchannels, Chem. Eng. Sci. 64 (2009) 3697–3708. doi:10.1016/j.ces.2009.05.026.
- D.M. Fries, F. Trachsel, P.R. Von Rohr, International Journal of Multiphase Flow Segmented gas – liquid flow characterization in rectangular microchannels, Int. J. Multiph. Flow. 34 (2008) 1108– 1118. doi:10.1016/j.ijmultiphaseflow.2008.07.002.
- J. Yun, Q. Lei, S. Zhang, S. Shen, K. Yao, Slug flow characteristics of gas-miscible liquids in a rectangular microchannel with cross and T-shaped junctions, Chem. Eng. Sci. 65 (2010) 5256– 5263. doi:10.1016/j.ces.2010.06.031.
- R. Jevtic, P.A. Ramachandran, M.P. Dudukovic, Capillary reactor for cyclohexane oxidation with oxygen, Chem. Eng. Res. Des. 88 (2010) 255–262. doi:10.1016/i.cherd.2009.12.008.
- Leclerc, M. Alam, D. Schweich, P. Pouteau, C. De Bellefon, Gas – liquid selective oxidations with oxygen under explosive conditions in a micro-structured reactor, Lab Chip. 8 (2008) 814–817. doi:10.1039/b717985e.
- J. Fischer, T. Lange, R. Boehling, A. Rehfinger, E. Klemm, Uncatalyzed selective oxidation of liquid cyclohexane with air in a microcapillary reactor, Chem. Eng. Sci. 65 (2010) 4866–4872. doi:10.1016/j.ces.2010.05.028.
- L. Vanoye, A. Aloui, M. Pablos, R. Philippe, A. Percheron, A. Favre-Reguillon, C. De Bellefon, A Safe and Efficient Flow Oxidation of Aldehydes with O 2, Org. Lett. 15 (2013) 5978–5981. doi:10.1021/ol401273k.
- M. Hamano, K.D. Nagy, K.F. Jensen, Continuous flow metal-free oxidation of picolines using air, Chem. Commun. 48 (2012) 2086–2088. doi:10.1039/c2cc17123f. [23] X. Yan, S. Xiaogang, Simple Linear Regression, in: Linear Regres. Anal. Theory Comput., World Scientific, 2009: pp. 9–39.
- Gemoets HPL, Su Y, Shang M, Hessel V, Luque R, Noël T (2016) Liquid phase oxidation chemistry in continuous flow microreactor. *Chem Soc Rev* 45:83–117.

Appendix A

The measurement of length of gas bubble, liquid slug and velocity is taken in the MATLAB 2018b version (**Code 1**) based on captured images.

```
clc
clear
close all

image_folder = 'D:\Software_Coding\MATLAB\2 microliter per min'; %  Enter name of folder from which you want to upload pictures with full path
filenames = dir(fullfile(image_folder, '*.jpg')) ; % read all images with specified extention, its jpg in our case
total_images = numel(filenames) ;  % count total number of photos present in that folder

A=imread(fullfile(image_folder, filenames(1).name)); % active to calculate slug size
% B=imread(fullfile(image_folder, filenames(5).name)); % active to calculate velocity
% C=imfuse(slugimageread,B); % imfuse two images (image quality dependent)
imtool(A) % make adjustment of calculating slug size or velocity
```

Code 1. Matlab 2018b code to load captured images of Taylor flow in microfluidic reactors

Appendix B

The analysis of GC data is processed in the MATLAB 2018b version (**Code 2**). The code returns composition of primary, secondary and addition product generated during liquid phase oxidation. In addition, the code provides results of conversion and product selectivity (ketone to alcohol ratio).

```
clc
clear
close all


format bank
tic

% Locate Path

source_dir =
'C:\Users\Umbar\Desktop\Tom_Microfluidics\Tom_Batch_Indan\GC\Batch\Tom_Bat_5%indan
ol';

source_files = dir(fullfile(source_dir, '*.xls'));
%
file_counter = length(source_files);

% Title Matrix
Report_title = {'Sample Name','Conversion Reactant Side','Conversion Product Side
wt%','Ketone-to-alcohol ratio','Produced Primary product wt%','Produced Secondary product
wt%','Produced Addition product wt%','Produced Indanone wt%','Produced Indanol
wt%','Produced Indan-1,2-dione wt%','Produced 1,3-Indandione wt%','Produced Addition
Product','Indan Peak Area', 'Indanone Peak Area', 'Indanol Peak Area', 'Indandione12 Peak Area',
'Indandione13 Peak Area','Addition Peak Area','Converted Indan Peak Area', 'Produced Indanone
Peak Area', 'Produce Indanol Peak Area', 'Produced Indandione12 Peak Area', 'Produced
Indandione13 Peak Area','Produced Addition Peak Area'};

% Title Output in Excel File as Summary
Export_filename = 'summary_report_trial.xlsx';
sheet = 1;
Title_xlRange = 'A1';
xlswrite(Export_filename,Report_title,sheet,Title_xlRange)


% Title length Compound Matrix
```

```
title_length=length(Report_title)-1; % Leave first column for sample name cell

Summary_Matrix=zeros(file_counter,title_length);

Sample_Name_Matrix=num2cell(zeros(file_counter,1));

% Original Compound peak area

INDAN_original=5797.079209;

INDANONE_original=2.759307838; INDANOL_original=311.0371071;
INDANDIONE12_original=0; INDANDIONE13_original=0; AdditionProduct_original=0;

Product_original=[INDANONE_original INDANOL_original INDANDIONE12_original
INDANDIONE13_original];

% RRF Pre-calculated using GC

CHCL3_RRF=0.06; HCB_RRF=0.31; INDAN_RRF=0.88; INDANOL_RRF=0.79;
INDANONE_RRF=0.83; INDANDIONE13_RRF=0.58; INDANDIONE12_RRF=0.67;
ADDITION_RRF=0.58;

RRF=[INDAN_RRF INDANONE_RRF INDANOL_RRF INDANDIONE12_RRF
INDANDIONE13_RRF ADDITION_RRF];


for total_exp=1:file_counter

% Identify Experiment Name

select_excel=fullfile(source_dir, source_files(total_exp).name);
select_sample_sheet='Sheet1';
select_sample_position='b26';
[~, Sample_Name]=xlsread(select_excel,select_sample_sheet,select_sample_position);
Sample_Name_Matrix(total_exp,:)=Sample_Name;


% Import Data Set

select_data_sheet='IntResults1';
select_data_range='e1:f50';
Selected_peak=xlsread(select_excel,select_data_sheet,select_data_range);

% Number of file

counter1 = length(Selected_peak);
```

```
% Initial Parameters

CHCL3=0; HCB=0; INDAN=0; INDANOL=0; INDANONE=0; INDANDIONE12=0;
INDANDIONE13=0;AdditionProduct=0;

% initial assessment without RRF

for i=1:counter1

   if Selected_peak(i,1)<2.25 && Selected_peak(i,1)>2.14

      CHCL3=Selected_peak(i,2)+CHCL3;

   elseif Selected_peak(i,1)<7.7 && Selected_peak(i,1)>7.6

      HCB=Selected_peak(i,2)+HCB;

   elseif Selected_peak(i,1)<4.0 && Selected_peak(i,1)>3.3

      INDAN=Selected_peak(i,2)+INDAN;

   elseif Selected_peak(i,1)<5.5 && Selected_peak(i,1)>5.1

      INDANOL=Selected_peak(i,2)+INDANOL;

   elseif Selected_peak(i,1)<6.3 && Selected_peak(i,1)>6.0

      INDANONE=Selected_peak(i,2)+INDANONE;

   elseif Selected_peak(i,1)<7.2 && Selected_peak(i,1)>6.9

      INDANDIONE13=Selected_peak(i,2)+INDANDIONE13;

   elseif Selected_peak(i,1)<8.2 && Selected_peak(i,1)>7.9

      INDANDIONE12=Selected_peak(i,2)+INDANDIONE12;

   elseif Selected_peak(i,1)>8.5

      AdditionProduct=Selected_peak(i,2)+AdditionProduct;

   end
end

% Result
```

```
% Raw Peak Area of each compound
OXIDIZED_INDAN_PRODUCT=[INDAN,INDANONE,INDANOL,INDANDIONE12,INDA
NDIONE13,AdditionProduct];

% Actual Peak Area with RRF

OXIDIZED_INDAN_PRODUCT_ACTUAL=OXIDIZED_INDAN_PRODUCT./RRF;


% Produced Peak Area of each compound
HCB_ACTUAL=HCB/HCB_RRF;
CHCL3_ACTUAL=CHCL3/CHCL3_RRF;
INDAN_RAW=INDAN/INDAN_RRF;
INDAN_ACTUAL=INDAN_RAW-INDAN_original;
INDANONE_ACTUAL=INDANONE/INDANONE_RRF-INDANONE_original;
INDANOL_ACTUAL=INDANOL/INDANOL_RRF-INDANOL_original;
INDANDIONE12_ACTUAL=INDANDIONE12/INDANDIONE12_RRF-
INDANDIONE12_original;
INDANDIONE13_ACTUAL=INDANDIONE13/INDANDIONE13_RRF-
INDANDIONE13_original;
Addition_Product=AdditionProduct/ADDITION_RRF-AdditionProduct_original;

% k-to-a ratio
ketone_to_alcohol_selectivity=INDANONE_ACTUAL/INDANOL_ACTUAL;

% Product selectivity
Primary_Product=INDANONE_ACTUAL+INDANOL_ACTUAL;
Secondary_Product=INDANDIONE12_ACTUAL+INDANDIONE13_ACTUAL;
Produced_Product_Total_Peak_Area=Primary_Product+Secondary_Product+Addition_Product;
Produced_Product_peak=[INDANONE_ACTUAL,INDANOL_ACTUAL,INDANDIONE12_A
CTUAL,INDANDIONE13_ACTUAL,Addition_Product];
Produced_Product_weight_percentage=Produced_Product_peak/Produced_Product_Total_Peak_
Area*100;
Produced_Primary_Percentage=Primary_Product/Produced_Product_Total_Peak_Area*100;
Produced_Secondary_Percentage=Secondary_Product/Produced_Product_Total_Peak_Area*100
;
Produced_Addition_Percentage=Addition_Product/Produced_Product_Total_Peak_Area*100;
Produced_Product_Selectivity=[Produced_Primary_Percentage,Produced_Secondary_Percentag
e,Produced_Addition_Percentage];

% Conversion Calculation
Indan_Conversion_Product_side=Produced_Product_Total_Peak_Area/(Produced_Product_Tota
l_Peak_Area+INDAN_RAW)*100;
Indan_Conversion_Reactant_side=-
INDAN_ACTUAL/(Produced_Product_Total_Peak_Area+INDAN_RAW)*100;
```

```
Indanone_Conversion=INDANONE_ACTUAL/(Produced_Product_Total_Peak_Area+INDAN
_RAW)*100;
Indanol_Conversion=INDANOL_ACTUAL/(Produced_Product_Total_Peak_Area+INDAN_R
AW)*100;
Indandione12_Conversion=INDANDIONE12_ACTUAL/(Produced_Product_Total_Peak_Area
+INDAN_RAW)*100;
Indandione13_Conversion=INDANDIONE13_ACTUAL/(Produced_Product_Total_Peak_Area
+INDAN_RAW)*100;
Product_Conversion=[Indanone_Conversion Indanol_Conversion Indandione12_Conversion
Indandione13_Conversion];

% Data Output in Matlab as Summary

fprintf('Indan_Conversion = %i \n', Indan_Conversion_Product_side)
fprintf('ketone_to_alcohol_selectivity = %i \n', ketone_to_alcohol_selectivity)
fprintf('primary product selectivity = %i \n', Produced_Product_Selectivity(1))
fprintf('secondary product selectivity = %i \n', Produced_Product_Selectivity(2))
fprintf('addition product selectivity = %i \n', Produced_Product_Selectivity(3))

% Product Output in Summary Matrix

Summary_Matrix(total_exp,:) = [Indan_Conversion_Reactant_side,
Indan_Conversion_Product_side, ketone_to_alcohol_selectivity, Produced_Product_Selectivity,
Produced_Product_weight_percentage, OXIDIZED_INDAN_PRODUCT_ACTUAL,
INDAN_ACTUAL, Produced_Product_peak];

end


% Product Output in Excel File as Summary

Data_obtained = num2cell(Summary_Matrix);
Complete_data_obtained=[Sample_Name_Matrix,Data_obtained];
sheet = 1;
xlRange = 'a2';
xlswrite(Export_filename,Complete_data_obtained,sheet,xlRange)
%
toc
```

Code 2. Sample Matlab code to batch analyze GC data